Defect Passivation of Perovskite Films for Highly Efficient and Stable Solar Cells

Mahdi Malekshahi Byranvand* and Michael Saliba*

Perovskite solar cells (PSCs) have been introduced as an attractive photovoltaic technology over the past decade due to their low-cost processing, earth-abundant raw materials, and high power conversion efficiencies (PCEs) of up to 25.2%. However, the relatively high density of defects within the bulk, grain boundaries, and surface of polycrystalline perovskite films acts as recombination centers and facilitates ion migration, lowering the theoretical PCE ceiling, often leading to inferior device stability. Therefore, understanding the defect sources and developing passivation methods are key factors for reaching higher PCEs and stabilities in perovskite photovoltaics. Herein, various passivation methods, including bulk and surface treatment of perovskite films, are explored. In the bulk treatment, the passivating agents should be directly added to the perovskite precursor. However, in the surface treatment method, the surface of perovskite films can be treated by inducing passivating agents during the intermediate phase or after annealing steps, denoted here as in-film or surface posttreatment. In addition, different kinds of passivating agents are categorized based on their functional groups. Finally, the outline directions to minimize the defects in perovskite films are highlighted.

1. Introduction

Perovskite solar cells (PSCs) have attracted tremendous attention as an alternative to silicon-based photovoltaics due to their lower cost and low-temperature processing, even being able to be deposited on flexible substrates using widely available solution deposition techniques.[1–3] Currently, the power conversion efficiency (PCE) of single-junction PSCs has reached 25.2%[4,5]

Dr. M. M. Byranvand, Prof. M. Saliba
Institute for Photovoltaics (IPV)
University of Stuttgart
Pfaffenwaldring 47, 70569 Stuttgart, Germany
E-mail: mahdi.malekshahi@ipv.uni-stuttgart.de;
michael.saliba@ipv.uni-stuttgart.de

Dr. M. M. Byranvand, Prof. M. Saliba
Helmholtz Young Investigator Group FRONTRUNNER
IEK5-Photovoltaik, Forschungszentrum Jülich
52425 Jülich, Germany

The ORCID identification number(s) for the author(s) of this article can be found under https://doi.org/10.1002/solr.202100295.

by optimizing the composition,[6–8] morphology,[9–11] and interfaces[12–15] of perovskite films. This excellent efficiency has been achieved due to the unique properties of perovskite materials, such as the high absorption coefficient, long diffusion length, and outstanding carrier mobility.[16,17] The remarkable efficiency rise has put PSCs into a prominent position among emerging PVs such as organic photovoltaics (OPVs),[18,19] quantum dot solar cells (QDSCs),[20,21] and dye-sensitized solar cells (DSCs).[22–29] Moreover, bandgap tunability of perovskite materials from 1.2 to 3.0 eV makes PSCs attractive as top cells in tandem structure with well-established solar cells such as crystalline silicon (c-Si) and copper indium gallium selenide (CIGS), overcoming the Shockley–Queisser efficiency limit of 33.7% in single-junction solar cells.[30–32]

However, further performance improvement of PSCs depends on well understanding the optoelectronic properties of perovskite films. Ideally, a perfect solar cell should work similarly to an ideal light-emitting device, which means the rate of charge recombination should be equal to the rate of charge generation, i.e., radiative recombination (**Figure 1**a).[33]

However, unlike well-controlled manufacturing of crystalline silicon semiconductors, the crystal-growth kinetic of perovskite is generally fast and produces polycrystalline films, which forms a wide range of structural defects. The defects are the primary source of nonradiative recombination in perovskite films and affect photovoltaic parameters negatively.[34–37] The open-circuit voltage (V_{OC}) is highly dependent on the density of defects compared to other photovoltaic parameters.[38]

The V_{OC} is derived from splitting quasi-Fermi levels of electron and hole carriers in a photoexcited perovskite film. Defects in perovskite structure recombine some parts of charge carriers nonradiatively, reducing the steady-state charge density. As a result, the splitting of quasi-Fermi levels will be diminished, decreasing the V_{OC} of PSCs subsequently (Figure 1a). Therefore, there is always a difference between the perovskite bandgap and measured V_{OC}, known as V_{OC} deficit. Nevertheless, defects affect the fill factor (FF) of PSCs as well, decreasing the overall PCE detrimentally.[39,40] In addition, defects also contribute to hysteresis in the current–voltage (J–V) characteristics of PSCs.[41,42]
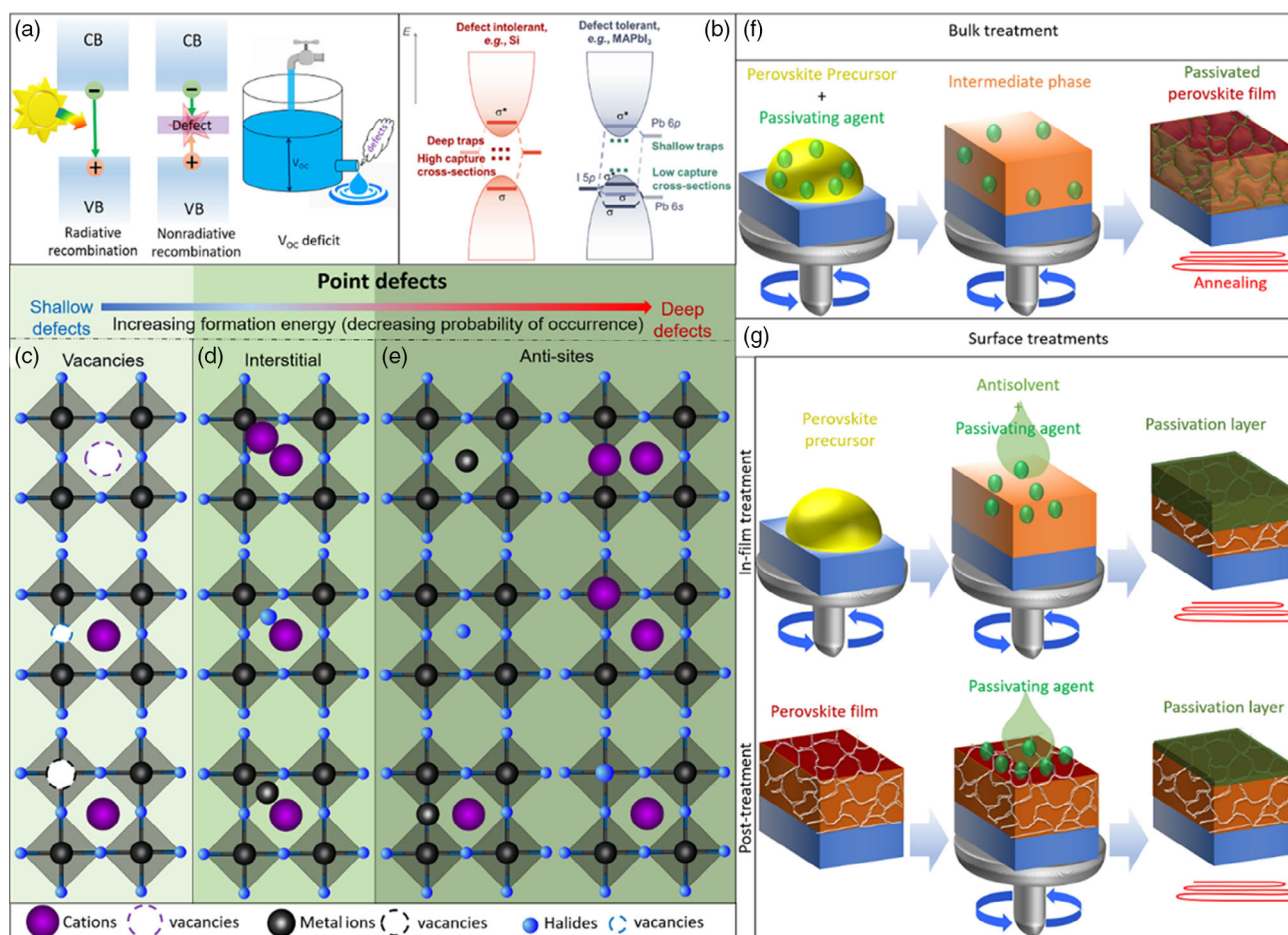
Figure 1. a) Schematic illustration of radiative and nonradiative recombination, as well as the effect of defects on V_{OC} in PSCs. b) Molecular orbital structures of deep- (left side) and shallow-level (right side) defects in defect-intolerant materials (e.g., silicon) and defect-tolerant materials (e.g., MAPbI$_3$), respectively. Reproduced with permission.[57] Copyright 2021, John Wiley and Sons. Various types of point defects, including c) vacancies, d) interstitials, and e) antisite defects in the perovskite structure. Schematic illustration of perovskite film passivation methods: f) bulk treatment and g) surface treatments (in-film and posttreatment).

On the other hand, the instability of PSCs is another issue that needs serious consideration because the best-reported stability of 1 year for PSCs[43] still is inferior compared to 25 years for silicon solar cells.[44] Although the moisture and oxygen instability can be minimized by improving the perovskite interfaces[45–48] and device encapsulation,[49–51] the thermal and photostability are directly related to the intrinsic stability of perovskite films.[52] To respond to these challenges, passivation of perovskite films has been introduced as an efficient approach to reduce the density of defects, improving the efficiency and stability of PSCs simultaneously.[53,54] This Review describes different types of defects in perovskite films and their passivation mechanisms to minimize the nonradiative recombination. We categorize defect passivation methods to bulk and surface treatments. Various passivating agent materials based on their functional groups are also explored. Moreover, we discuss the effect of defect passivation on photovoltaic parameters and the stability of PSCs. Finally, a perspective direction for further developments in defect passivation is presented.

2. Defects in Perovskite Films

The general performance of solar cells is highly dependent on the presence of impurities and defects within the semiconducting material. In an idealized perovskite crystal structure, each ion would be located on its equilibrium site. However, due to the polycrystalline nature of organic–inorganic perovskites, the generation of a wide range of structural defects at the bulk, grain boundaries (GBs), and surface is frequently observed.

Generally, defects can be categorized into deep and shallow levels.[55] In traditional semiconductors such as Si with high formation energies, usually, the defects are located at a deep energy level, i.e., within the bandgap (see Figure 1b, left). However, these kinds of defects are uncommon in perovskite films due to the high formation energy. In contrast, defects in perovskite films are usually shallow-level due to the low formation energy. To explain this, the electronic structure of perovskite materials should be considered. Figure 1b (right side) shows the electronic structure of MAPbI$_3$ as the most common organic–inorganic perovskite. The hybridization of the 6s and 5p orbitals

from Pb and I, which forms a pair of bonding and antibonding states close to the valence band (VB). However, the p-orbital hybridization, i.e., $6p$ from Pb and $5p$ from I, leads to a bonding state close to the VB and an antibonding state close to the conduction band. Therefore, the original atomic orbitals will be located around the band edges. As the primary estimation, defect states form close to this orbital and are resonant within the bands or shallow within the bandgap. As a result, perovskite films with higher defect densities than Si or GaAs semiconductors show low nonradiative recombination rates due to their shallow-level defects.[56] However, due to the ionic nature and volatile organic components in perovskite materials, the ions can easily migrate to or evaporate from the defect points during the device performing condition, increasing the defect densities and charge recombination.

An organic–inorganic perovskite crystal structure with formula ABX_3 consisting of B (central metal ions: Pb^{2+}, Sn^{2+}) and X (halides atoms: Cl^-, Br^-, or I^-) forms BX_6^{4-} corner-sharing octahedra, which define a cuboctahedral cavity occupied by A cations (MA^+; $CH_3NH_3^+$, FA^+; $HC(NH_2)_2^+$). However, in the actual situation, defects change the perovskite crystal in different ways. Figure 1c–e shows the different types of point defects, including the vacancies, interstitial and anti-site defects, which are the most critical defects in the atomic level of perovskite structure. In addition, other types of more complicated defects such as Schottky defects and Frenkel defects can also happen.[57]

Although all types of mentioned defects potentially can occur, considering the formation energies, the vacancies have been assigned as the most common defects in perovskite films, including halide vacancies (mostly iodide) and cation vacancies (mostly MA^+ or FA^+).

The halide vacancies lead to the formation of undercoordinated positively charged metal ions, i.e., Pb^{2+} or Sn^{2+}, which can form other types of defects by reduction and oxidation of these ions to Pb^0 and Sn^{4+}, respectively. In contrast, the cation vacancies create other negatively charged defects such as Pb—I antisites (PbI_3^-), with undercoordinated I^- ions. Moreover, due to the ionic nature of perovskite materials, some of the cations and anions (MA^+ and I^-) can migrate within the perovskite film when applying an electric field, photon illumination, or temperature. Normally, the GBs are the primary migration channel in perovskite films, imposing challenges for PSCs such as J–V hysteresis,[58] phase segregation,[59] or the reaction of migrated ions with other function layers in PSCs,[60] i.e., the electron transport layer (ETL), perovskite, hole transport layer (HTL), or even the metal back contact. Therefore, developing passivation methods for suppressing the defects in perovskite films is an important direction.

Various methods have been established for the passivation of perovskite films. One of the most common passivation methods is the bulk treatment of perovskite films by directly adding the passivating agent to the perovskite precursor (Figure 1f). Surface treatment of the perovskite films is another often reported passivation method. As shown in Figure 1g (top part), the surface of perovskite films can be treated during the intermediate phase formation, e.g., by adding the passivating agent to the antisolvent, named an in-film surface treatment. Moreover, the surface of perovskite films can be treated by the passivating agent after the crystallization step, named a surface posttreatment (Figure 1g, bottom part).

However, it should be considered that most of the passivation methods lead to modified morphologies and an altered perovskite film crystallization, which significantly influences the PSCs' efficiency and, importantly, their stability. Here, we review the passivation of different kinds of defects in perovskite films by various methods.

3. Halide Vacancy Passivation

One of the possible negative results of halide vacancies is the undercoordinated central metals (M^{2+}), i.e., Pb^{2+} or Sn^{2+} ions, located in the bulk or surface of perovskite films.[61,62] Nevertheless, the M^{2+} ions in perovskite films can create other types of defects such as Pb^0 and Sn^{4+} by reduction or oxidation reactions.[63,64] Therefore, the passivation of undercoordinated M^{2+} ions not only suppresses the nonradiative recombination, but also prevents forming new defects. Materials with free lone electron pairs; i.e., Lewis bases can coordinate with the free orbits of M^{2+} ions and passivate halide vacancies.[65,66] Moreover, halides or other similar anions can be directly replaced with halide vacancies.[67] In this part, we review the most important strategies of halide vacancy passivation.

3.1. Small Molecules

The small molecules with free lone-pair electrons in their structure, i.e., the Lewis base characteristic, can coordinate with undercoordinated M^{2+} ions, i.e., Pb^{2+} or Sn^{4+}, passivating the halide vacancies. So far, many small molecules with O, N, or S functional groups have been successfully used for this purpose (**Figure 2**a).[68–71] However, these small molecules can be added directly to the liquid perovskite precursor (bulk treatment) or deposited onto the perovskite film (surface treatment).

As one of the first reports on the bulk treatment of perovskite films, the Seok[9] and Park[72] groups demonstrated, separately, the critical role of dimethyl sulfoxide (DMSO) as a cosolvent of the perovskite precursor for achieving highly efficient PSCs (Figure 2b). They demonstrated that the free electron pairs of the oxygen atoms in the DMSO structure coordinate to undercoordinated Pb^{2+} ions and form a Lewis acid–base adduct of PbI_2–DMSO. This results in a high-quality perovskite film, suppressing nonradiative recombination. It shows that even in the initial step of the perovskite crystallization, the free Pb^{2+} ions need to be passivated using a cosolvent with Lewis base characteristic. However, even in the presence of a DMSO cosolvent, perovskite films tend to show some intrinsic Pb^{2+} defects after DMSO evaporation during the perovskite crystallization.[73] Therefore, adding nonvolatile Lewis base materials to the perovskite precursor could benefit the passivation of Pb^{2+} defects. In this regard, Yang and co-workers[74] demonstrated that adding small amounts of CH_4N_2O (urea) as a nonvolatile Lewis base to the perovskite precursor can form a stronger PbI_2–DMSO–urea adduct compared to the conventional PbI_2–DMSO adduct, resulting in better crystal growth with fewer defects (Figure 2c). Likewise, they showed that urea was precipitated at the perovskite GBs, removing the trap states in these regions and facilitating charge transport by enhancing the quasi-Fermi level and thereby improving the V_{OC}.
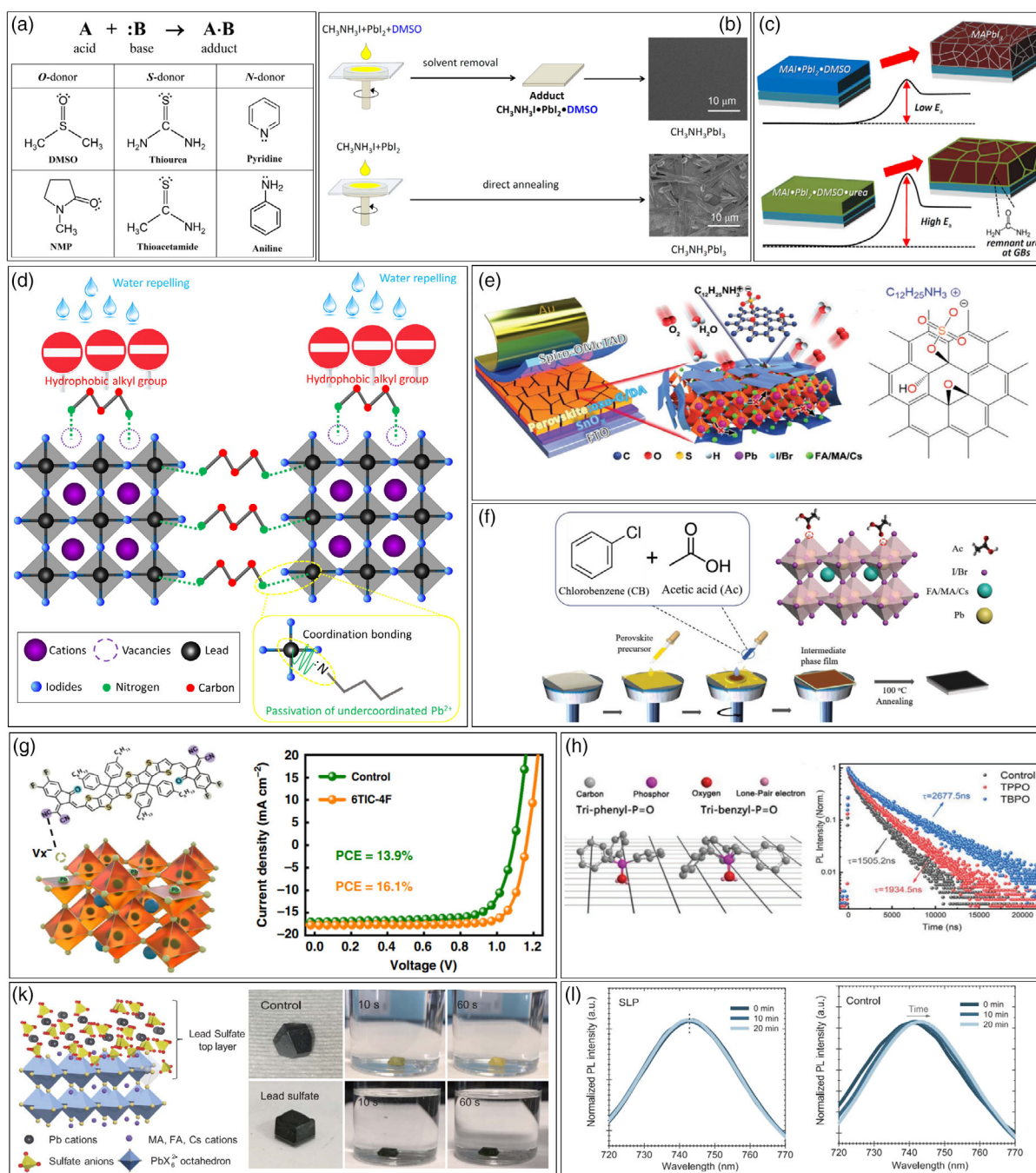
Figure 2. a) The Lewis acid–base interaction forms an adduct and various Lewis base molecules with different functional groups. Reproduced with permission.[73] Copyright 2016, American Chemical Society. b) Schematic illustration of the effect of DMSO on the fabrication of the perovskite films. Reproduced with permission.[73] Copyright 2016, American Chemical Society. c) Schematic of film crystallization in the presence of urea. Reproduced with permission.[74] Copyright 2017, Elsevier. d) Schematic of defect passivation by BAA incorporation in perovskite films. e) Schematic of passivation of PSC with oxo-G/DA nanosheets. Reproduced with permission.[71] Copyright 2019, John Wiley and Sons. f) Schematic of acetic acid (Ac)-assisted perovskite passivation strategy. Reproduced with permission.[277] Copyright 2020, John Wiley and Sons. g) Illustration of the passivation mechanism of the 6TIC-4F molecule with perovskite and the J–V curves of champion PSCs. Reproduced with permission.[79] Copyright 2020, Springer Nature. h) TPPO and TBPO molecular structures and their corresponding TRPL data. Reproduced with permission.[80] Copyright 2020, John Wiley and Sons. (k) Schematic of lead sulfate overlayer on the perovskite surface and the stability test. Reproduced with permission.[91] Copyright 2019, The Authors, some rights reserved; exclusive licensee American Association for the Advancement of Science. No claim to original U.S. Government Works. l) Normalized PL spectra of SLP-treated and control perovskite films after illuminating for 0, 10, and 20 min. Reproduced with permission.[31] Copyright 2020, The Authors, some rights reserved; exclusive licensee American Association for the Advancement of Science. No claim to original U.S. Government Works.

Moreover, the Huang group[70] demonstrated that adding a small amount of bilateral alkylamine molecules, i.e., 1,3-diaminopropane (DAP), to the perovskite precursor not only passivates the perovskite grains, but also improves the morphology and stability of the perovskite films. The bilateral $-NH_2$ groups in DAP structure can form coordination bonds with neighboring undercoordinated Pb^{2+} ions and link them together. Moreover, the linked hydrophobic carbon chain forms a moisture barrier in perovskite grains (see schematic in Figure 2d). The time-resolved photoluminescence (TRPL) and transient photovoltage (TPV) characterizations of passivated perovskite films showed a longer carrier lifetime, achieving a lower V_{oc} deficit (discrepancy between V_{OC} and bandgap) of 0.35 V.

Abate and co-workers recently incorporated 2D nanosheets of oxo-functionalized graphene/dodecylamine (oxo-G/DA) into perovskite films to improve the efficiency and stability of PSCs.[71] They showed that the lone-pair electrons of the functional group of oxo-G/DA structure, i.e., oxygen atoms, can form a coordination bond with free Pb^{2+} ions during the crystallization process (Figure 2e). The open-circuit photovoltage decay measurement confirmed the longer charge lifetime of passivated oxo-G/DA compared to the control film, which indicates that the oxo-G/DA nanosheets suppress electron–hole recombination, leading to a hysteresis-free PCE of 21.1% and improved long-term stability.

The antisolvent deposition method is a well-known method for achieving high-quality and compact perovskite films.[11,75,76] In this method, the antisolvent plays a crucial role in forming the intermediate phases that significantly affect the final perovskite film quality. Many works report on adding small molecules with a Lewis base functional group to the antisolvent as an in-film treatment method for the passivation of undercoordinated M^{2+} ions.[77–80] Here, the small molecules penetrate into the intermediate phase of the perovskite, passivating the surface and the GBs during the crystallization. In this regard, Ho-Baillie and co-workers[81] added small amounts of acetic acid (Ac) to chlorobenzene (CB), also an antisolvent, to fabricate highly crystalline perovskite films with excellent optoelectronic properties (Figure 2f). Their characterizations showed that the electron-rich carbonyl group (C=O) in the Ac molecular structure acts as a Lewis base and donates its pair electron to the undercoordinated Pb^{2+} ions, thereby passivating the defects and leading to a high PCE of 23.0% with negligible hysteresis.

As another example, recently, the Jen group[79] introduced 6TIC-4F molecules with the electron-donating core terthieno[3,2-b]thiophene (6T) and two electron-withdrawing units 2-(5,6-difluoro-3-oxo-2,3-dihydro-1H-inden-1-ylidene) malononitrile (IC-2F), which can be dissolved in CB to passivate these kinds of defects at the surface/GBs of all-inorganic perovskite films. Their theoretical and experimental studies revealed that the numerous nitrogen atoms (nitrile (C−N) groups) in the 6TIC-4F molecular structure provide lone-pair electrons to direct coordination with the Pb^{2+} ions through the formation of Lewis adducts. This leads to an improved V_{oc} from 1.10 to 1.16 V and PCE from 13.9% to 16.1%, respectively (Figure 2g). Similarly, Meng and co-workers[80] used tribenzylphosphine oxide (TBPO) and triphenylphosphine oxide (TPPO) small molecules for the in-film treatment of perovskite films. The coordination bond was formed between TBPO and TPPO with Pb^{2+} ions (P = O→Pb) on the surface of perovskite films, suppressing

the nonradiative recombination. As a result, a PCE of 22.1% with a V_{OC} of 1140 mV and environment stability (sustaining 92% of initial efficiency after 250 h maximum-power-point tracking) were achieved for TBPO-passivated PSCs (Figure 2h).

Indeed, posttreatment of perovskite films with Lewis base small molecules was introduced, for the first time, by the Snaith group in 2014.[82] They used thiophene and pyridine with sulfur and nitrogen functional groups, respectively, for passivating the undercoordinated Pb^{2+} ions on the surface of perovskite film, which led to significantly reduced nonradiative recombination. To date, various small molecules with different functional groups such as $-N$,[83,84] $-S$,[85,86] $-C = O$,[87] $-C \equiv N$,[87] $-O$,[85] $-S-N$,[88] and $P = O$[65,89] have been used for the passivation of these defects. For instance, Hillhouse et al.[90] calculated that the surface passivation of perovskite films using n-trioctylphosphine oxide (TOPO) molecules with the P = O functional group could improve the PCE to 27.9% compared to nonpassivated PSCs with PCE at 24.3%, which was attributed to V_{OC} and FF improvements. In another report, Huang and co-workers[91] treated the film surface with SO_4^{2-} ions to passivate the undercoordinated Pb^{2+} ions, forming an inorganic wide-bandgap overlayer of lead sulfate on top of the main perovskite film. Their optoelectronic studies confirmed the improvement of the charge lifetime of the passivated perovskite film (Figure 2k). The passivated PSC showed a higher V_{OC} than the nonpassivated sample, which was attributed to lower trap densities. In contrast, the water resistance was increased for lead-sulfate-passivated perovskite (Figure 2k). In another report from this research group, it was observed that[92] the trap density near the surface of a perovskite single crystal is approximately tenfold higher than in the bulk, which confirms the importance of surface passivation in perovskite materials.

However, in most solution-proceed posttreatment of perovskite films with small molecules, the thickness of the passivation layer is not controllable. Very recently, the Sargent group[31] passivated perovskite films with a monolayer of 1-butanethiol molecules to fabricate highly efficient monolithic perovskite-based tandem solar cells. Due to the self-limiting passivant (SLP) nature of this molecule, it can be self-assembled as a monolayer on the surface of the perovskite film. The strong coordination between sulfur atoms from 1-butanethiol molecules and Pb^{2+} ions leads to a higher charge carrier lifetime and a suppressed photo phase segregation compared to nonpassivated film (Figure 2l). The monolithic SLP-passivated perovskite–silicon tandem solar cell showed a certified PCE of 25.7%.

In summary, small molecules with Lewis base function groups can coordinate with undercoordinated Pb^{2+} ions in the bulk and surface of perovskite films, passivating the halide vacancy defects. We also summarize the most significant small molecules as passivating agents for passivation of the halide vacancies with different methods (**Table 1**).

3.2. Polymers

The long-chain polymers with Lewis base functional groups can also coordinate with undercoordinated metal ions, passivating the halide vacancies in the bulk and surface of perovskite films. Compared to small molecules, the main advantage of the polymers as a passivation agent is their stronger cross-link

Table 1. Summarization of halide vacancy passivation utilizing small molecules: passivation methods, passivating agents, device structures, perovskites, and photovoltaic parameters.

Small molecules	Method	Passivating agent	Device structure	V_{OC} [V]	FF	J_{SC} [mA cm^{-2}]	PCE [%]	Ref.
	Bulk treatment	DMSO	FTO/c-TiO$_2$/m-TiO$_2$/MAPb(I$_{1-x}$Br$_x$)$_3$/Spiro-OMeTAD/Au	1.06	0.75	19.9	15.9	[75]
		DMSO	FTO/c-TiO$_2$/m-TiO$_2$/MAPbI$_3$/Spiro-OMeTAD/Au	1.08	0.76	23.8	19.7	[72]
		Urea	FTO/SnO$_2$/MAPbI3/Spiro-OMeTAD/Au	1.10	0.75	21.7	17.8	[288]
		Propylene carbonate (PC)	ITO/PTAA/MAPbI$_3$ single crystal/C60/bathocuproine (BCP)/Cu	1.14	0.81	23.6	21.9	[289]
		Hexafluoro-2-propanol (HFP)	ITO/PEDOT:PSS/FASnI$_3$/C60/BCP/Ag	0.53	0.73	17.3	6.8	[290]
		Bilateral alkylamine (BAA)	ITO/PTAA/MAPbI$_3$ /C60/BCP/Cu	1.18	0.81	22.5	21.7	[70]
		Nitrogen-doped reduced graphene oxide	FTO/c-TiO$_2$/m-TiO$_2$/double-cation perovskite/Spiro-OMeTAD/Au	1.15	0.74	21.8	18.7	[291]
		Oxo-functionalized graphene	FTO/SnO$_2$/triple-cation perovskite/Spiro-OMeTAD/Au	1.13	0.81	23.1	21.1	[71]
		Trioctylphosphine oxide	ITO/SnO$_2$/CsPbI$_3$/PDCBT/MoOX/Au	1.17	0.73	16.4	14.0	[69]
		ITIC-Th	FTO/c-TiO$_2$/double-cation perovskite/Spiro-OMeTAD/Au	1.13	0.75	22.4	19.2	[68]
	Surface in-film treatment	Acetic acid	FTO/c-TiO$_2$/m-TiO$_2$/triple-cation perovskite/Spiro-OMeTAD/Au	1.19	0.79	23.2	22	[277]
		Donor–π–acceptor (D–π–A) molecules	FTO /NiO$_x$/MAPbI$_3$/PCBM/BCP/Ag	1.14	0.78	22.6	20.4	[77]
		Conjugated molecules with rhodanine moieties	ITO/HTL/double-cation perovskite/PCBM/ZnO/Ag	1.13	0.80	22.4	20.3	[78]
		π-conjugated 6TIC-4F	ITO/NiO$_x$/CsPbI$_x$Br$_{3-x}$/ZnO/C60/Ag	1.16	0.78	17.7	16.1	[79]
		Tribenzylphosphine oxide (TBPO)	FTO/c-TiO$_2$/PCBA/ triple-cation perovskite /Spiro-OMeTAD/Au	1.14	0.80	23.9	21.7	[80]
	Surface post treatment	Thiophene or pyridine	FTO/c-TiO$_2$/ MAPbI$_{3x}$Cl$_x$/Spiro-OMeTAD/Au	1.02	0.72	24.1	16.5	[82]
		Pyridine	FTO/c-TiO$_2$/MAPbI$_3$(Cl)/Spiro-OMeTAD/Au	1.00	79.3	18.3	14.5	[83]
		Benzylamine	FTO/c-TiO$_2$/FAPbI$_3$/Spiro-OMeTAD/Au	1.12	0.73	23.6	19.2	[84]
		TPP–SMeTAD	ITO/TPP–SMeTAD/MAPbI$_3$/PCBM/ZnO NPs/Al	1.07	0.77	20.1	16.6	[85]
		π-Conjugated IDIC	ITO/PTAA/MAPbI$_3$/IDIC/C60/BCP/Cu	1.03	0.67	19.3	13.5	[87]
		rGO–4FPH	ITO/c-TiO$_2$/MAPbI$_{3-x}$Cl$_3$/Spiro-OMeTAD/Au	1.03	0.78	20.1	18.7	[292]
		Lead sulfate	ITO/PTAA/triple-cation perovskite /C60/BCP/Cu	1.16	0.80	22.6	21.1	[91]
		PCBB–S–N	ITO/PTAA/ MAPbI$_3$/PCBM/Al	1.12	0.79	23.8	21.0	[88]
		2-Mercaptopyridine	ITO/SnO$_2$/MAPbI$_3$/Spiro-OMeTAD/Au	1.16	0.77	22.61	20.2	[293]
		Pentaerythritoltetrakis(3 mercaptopropionate)	ITO/SnO$_2$/triple-cation perovskite/Spiro-OMeTAD/Au	1.16	0.78	23.5	21.4	[86]
		1-Butanethiol	Tandem perovskite-silicon	1.70	0.77	19.8	26.0	[31]
		Tris(pentafluoropheny) phosphine	ITO/SnO$_2$/triple-cation perovskite/Spiro-OMeTAD/Au	1. 16	0.76	23.9	21.0	[89]

interactions with perovskite grains, improving the stability and suppressing the ion migration in PSCs. Many polymers with different functional groups, such as amine (—NH$_2$), carboxyl (—C(═O)OH)), carbonyl (—C═O), and cyanide (—C≡N), have been used for bulk and surface passivation of perovskite films.[93–110] Given the electron-donating properties of different functional groups, different coordination bond strengths with undercoordinated metal ions can be formed.

Regarding the perovskite bulk treatment, the Yang group explored the chemical interactions of various polymers such as branched polyethyleneimine (b-PEI), poly(4-vinylpyridine) (PVP), and polyacrylic acid (PAA) with perovskite films.[111] The lone electron pairs on the N or O atoms of these polymers form coordination bonds, with different bonding strengths with the undercoordinated Pb^{2+} ions. However, the relatively viscous perovskite–polymer mixed precursor solution confines their application for bulk treatment of perovskite films. To address this challenge, they proposed a mesoporous PbI$_2$-scaffold-facilitated method for enabling the interdiffusion polymers in perovskite film (**Figure 3**a). The PVP-passivated PSC showed the lowest V_{OC} deficit of 0.47 V among all the polymers used in this work, suggesting a significant suppression of nonradiative charge recombination (Figure 3a). Additionally, the improved moisture stability was attributed to preventing water access into the perovskite and reducing ion migration due to the cross-linked perovskite grains by the PVP polymer.

As an additional bulk treatment method, monomers have been mixed into the perovskite precursor. Consequently, the monomers start polymerization in the perovskite film after or during the perovskite crystallization. For instance, Li et al. added
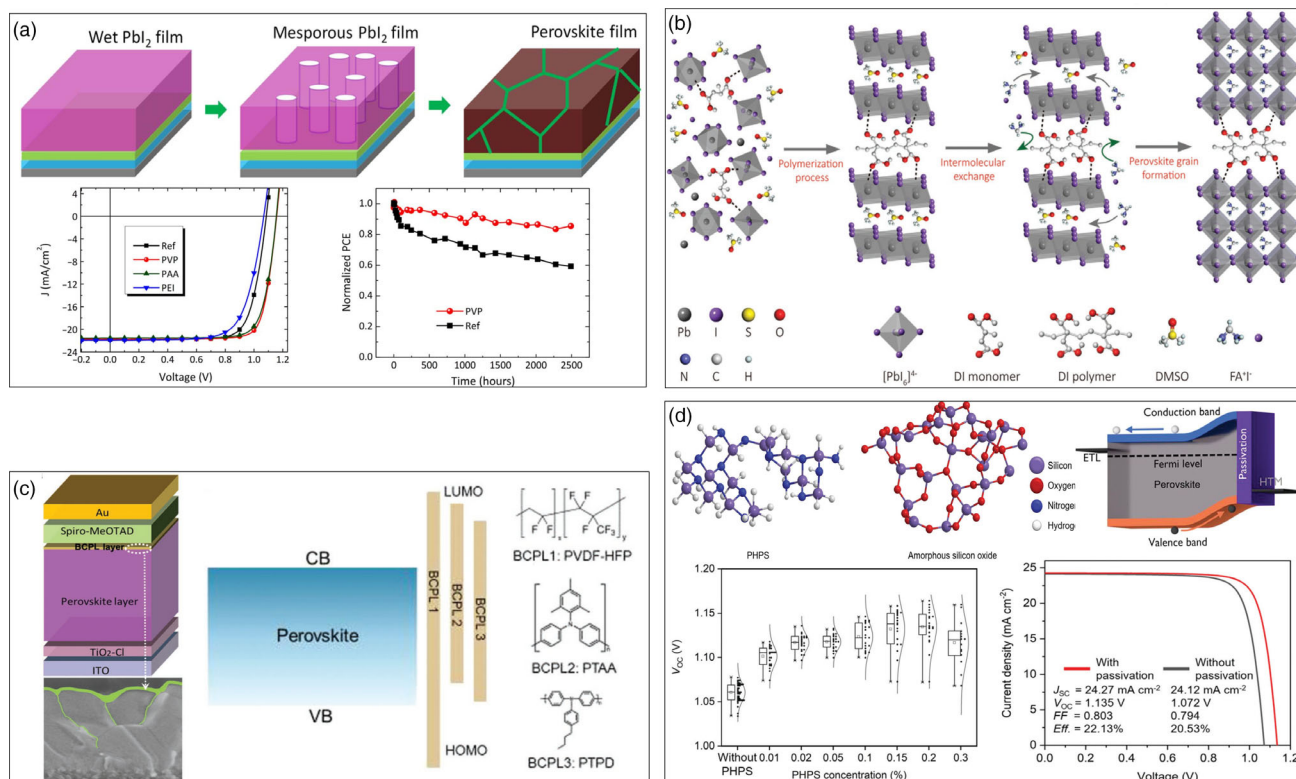
Figure 3. a) Schematic of incorporating the polymer into the perovskite films, *J–V* characteristics of different polymers, and stability test. Reproduced with permission.[94] Copyright 2017, The Authors, some rights reserved; exclusive licensee American Association for the Advancement of Science. No claim to original U.S. Government Works. Distributed under a Creative Commons Attribution NonCommercial License 4.0 (CC BY-NC). b) Illustration of the mechanism of polymerization of polymerization-assisted grain growth (PAGG) in perovskite film. Reproduced with permission.[96] Copyright 2020, John Wiley and Sons. c) The passivated PSC structure, the energy-level alignments of different polymers with perovskite, and the chemical structure of passivation agents. Reproduced with permission.[278] Copyright 2019, John Wiley and Sons. d) The chemical structures of PHPS and amorphous silicon oxide, the band-bending effect of induced passivation, *V*oc distribution as a function of PHPS concentration, and champion *J–V* curves. Reproduced with permission.[110] Copyright 2020, the Royal Society of Chemistry.

a 2-cyanoacrylate (E2CA) monomer to the perovskite precursor to polymerize it after perovskite film formation. They showed that the —CN and —C=O functional groups in the E2CA molecular structure coordinate to undercoordinated Pb^{2+} ions during the perovskite crystallization.[112] Interestingly, by exposing the passivated perovskite films to the ambient atmosphere, the E2CA monomers in the perovskite GBs spontaneously polymerized to a hydrophobic polymer, enhancing the moisture-resisting properties of PSCs. Moreover, the Yang group[96] added a dimethyl itaconate (DI) monomer with C=O and C=C functional groups into the PbI_2 solution. The C=O groups coordinate with Pb^{2+} ions, and the C=C groups start the polymerization process during the PbI_2 annealing (Figure 3b). Finally, the bulkier polymers are anchored on the GBs after perovskite film formation. As a result, the undercoordinated Pb^{2+} ions are effectively passivated, and a PCE of 23.0% is achieved.

In 2016, the Graetzel group introduced an in-film treatment method for the passivation of perovskite film.[113] They added poly(methyl methacrylate) (PMMA) polymer to the antisolvent as a template of the intermediate phase to control nucleation and crystal growth. They demonstrated that the C=O functional group of PMMA forms an adduct with Pb^{2+} ions. The C=O→PbI_2 adduct was shown to be beneficial for increasing the perovskite grain size,

reducing the GBs, improving the V_{oc} and FF, and achieving a certified PCE of 21%. Various polymers with different Lewis base functional groups have been successfully introduced since using this method to passivate the halide vacancies defects as well as improving device stability.[99–102,114–116] Beyond insulating polymers, many semiconducting polymers have been used for the in-film treatment of perovskite films to improve the electronic contact at the perovskite/HTL or ETL interfaces.[99–102,116] Recently, the Sargent group[103] used the same approach to compare the passivation effect of an insulating polymer (PVDF-HFP, i.e., BCPL1) with different semiconductor polymers (poly[bis(4-phenyl)(2,4,6-trimethylphenyl) amine] (PTAA) and poly(4-butylphenyldiphenylamine) (PTPD), i.e., BCPL2 and BCPL3) (Figure 3c). The optoelectronic characterizations showed that BCPL1 substantially increases the charge carrier lifetime, although it was reduced for BCPL2 and BCPL3 compared to the control film. They suggested that the insulating BCPL1 polymer only passivates defects on the surface of the perovskite film by coordination of the fluorine terminal groups with Pb^{2+} ions, improving the V_{OC} of fabricated PSCs. However, they observed a short carrier lifetime for BCPL2 and BCPL3 polymers, proposing efficient charge transfer due to their proper band alignment, leading to a simultaneous V_{OC} and FF improvement.

As already mentioned, posttreatment of perovskite films is also an efficient passivation approach. In this regard, many groups tried to deposit an ultrathin polymer layer on the surface of perovskite films. For example, PVP,[117,118] PMMA,[107,119,120] PEO,[115] and P3HT[121] with the nitrogen (—N), ester (—C(=O)OCH₃)), oxygen (—O), and sulfur (—S) functional groups, respectively, have been reported for the successful passivation of undercoordinated Pb^{2+} ions. Again, apart from the defect passivation role, an efficient polymer passivator should play a role in charge extraction at the perovskite/HTL or ETL interfaces. Very recently, the Nazeeruddin group[110] introduced a successful passivation strategy using perhydropoly(silazane) (PHPS) as a saturated inorganic polymer. In this strategy, two critical points were highlighted. First, the PHPS with the —O^{2-}—Si^{4+} functional group can form chemical bonds with Pb^{2+} ions, i.e., coordination of $Pb^{2+} \leftarrow O^{2-}$—$Si^{4+}$, and passivate the defects on the surface of perovskite film (Figure 3d). Second, this chemical reaction causes band bending between the surface and bulk of the perovskite film, enhancing the hole extraction from the absorber bulk to the HTL. Using this strategy, the V_{OC} increased from 1.07 up to 1.13 V, leading to a PCE of 22.13% for passivated PSCs with 0.2 vol% PHPS. As a side benefit of this inorganic passivation, the light and moisture stability of fabricated PSCs were improved (Figure 3d).

In summary, polymers with Lewis base function groups can coordinate with undercoordinated Pb^{2+} in perovskite structure and passivate the halide vacancy defects. The main advantage of polymers as passivating agents is making stronger cross-link interactions with perovskite grains and improving the stability of PSCs consequently. However, monomers can be added to the perovskite precursor as the passivating agent instead of polymers to overcome the high viscosity of the perovskite precursor in the bulk treatment method. Although insulating polymers have successfully improved the V_{oc} of PSCs, it is necessary to develop new polymers with semiconducting properties to improve the V_{oc}, FF, and J_{sc} simultaneously.

3.3. Halide Replacements

According to the perovskite coordination chemistry, PbI_6^{4-} is the ideal iodoplumbate with fully coordinated Pb^{2+} ions without halide vacancies.[122] However, under perovskite processing or operational conditions, for example, due to some of the volatile components in the perovskite structure, the formation of undercoordinated Pb^{2+} ions in perovskite films is practically unavoidable. Apart from the small molecules or polymers with Lewis base characteristic, the halide vacancies can be directly replaced by additional treatment with halides or other anions with similar ionic radius to halides. In this part, we explore the possibilities for anion replacements for the passivation of the halide vacancies.

3.3.1. Iodide

Iodide is the most common halide in perovskite materials that can leave the crystal structure along with the volatile organic cation components such as MA^+ or FA^+, in MAI or FAI forms. Considering the bulk treatment method, hydriodic acid (HI) has been added to the perovskite precursor solution to replace

the iodide vacancies and convert the undercoordinated Pb^{2+} ions into a favorable PbI_4^{4-} complex.[123,124] However, controlling the precise stoichiometry in this approach is very important.[125] In this regard, Abdi-Jalebi et al.[67] added a small amount of potassium iodide (KI) to the perovskite precursor to introduce excess iodide-compensating halide vacancies (**Figure 4**a). Both the nonradiative losses and photoinduced ion migration were mitigated by decorating perovskite film surfaces and grain boundaries with passivating potassium halide layers.

Very recently, Wang et al.[126] used the in-film treatment method by adding some iodine to the antisolvent to simultaneously passivate the halide vacancies and improve the perovskite crystallization. They showed that the added I^- ions in the antisolvent penetrate the MAI–PbI_2–$DMSO$ colloids during solvent extraction. The I^- ion molecules shared their four lone electron pairs with multiple Pb^{2+} ions simultaneously, leading to halide vacancy passivation (Figure 4b).

Posttreatment of perovskite films has been frequently used for iodide replacement, passivating the halide vacancies consequently. In this regard, the You group[127] treated the surface of a perovskite film with a solution of phenethylammonium iodide (PEAI) molecules without postannealing. It should be noted that before this report, PEAI had been used frequently for creating 2D perovskite, which will be discussed subsequently.[128–133] However, the surface characterization showed that the PEAI crystal itself was recrystallized on the surface of the perovskite film, and the 2D perovskite phase was not observed at this low-temperature treatment regime. They demonstrated that the Pb:I ratio in the PEAI-passivated perovskite film increased dramatically, indicating the PEAI forms abundant iodide on the perovskite surface to passivate halide vacancies (Figure 4c). As a result, the optimized PEAI-passivated PSC (20 mM PEAI concentration) showed an efficiency of 23.56% with a high V_{oc} of 1.16 V, which is 94.4% of the Shockley–Queisser limit V_{oc} (1.25 V) for a perovskite with a bandgap of 1.53 eV (Figure 4c).

3.3.2. Chloride

The relatively easily breakable Pb—I chemical bonding in the perovskite structure is one of the main reasons for halide vacancies. Recent reports have shown that chloride (Cl^-) as an additive to the perovskite structure can assist in halide vacancy passivation and improve the perovskite crystal growth as well.[134,135]

Methylammonium chloride (MACl), as one of the most common chloride sources, has been frequently used for bulk treatment of perovskite films, thus improving the film quality and defect passivation.[136–138] Kim et al.[139] demonstrated that adding 40 mol% MACl to the perovskite precursor can dramatically increase the perovskite grain size, as well as increasing the charge carrier lifetime, which is attributed to the strong suppression of nonradiative recombination due to efficient passivation of halide vacancies and perovskite grain enlargement (Figure 4d). Therefore, the MACl-passivated PSC showed a high PCE of 24.02%. Recently, the Huang group[61] observed that the MACl excess not only significantly improves the perovskite morphology, but also reduces the density of shallow traps at the perovskite GBs. They also highlighted that using an extra additive salt along with MACl, i.e., MAH_2PO_2, is necessary for achieving
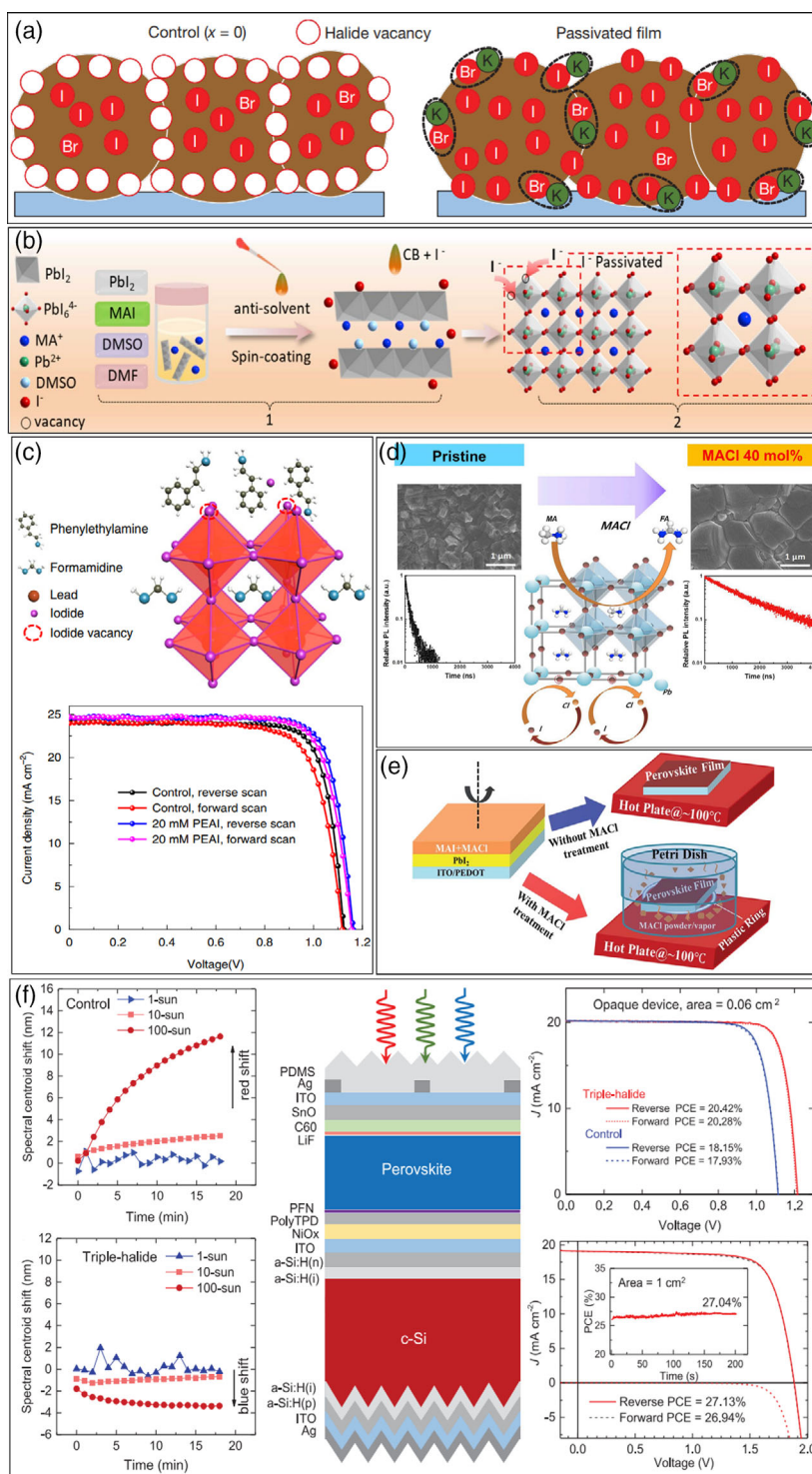
Figure 4. a) Schematic of halide vacancy management in the presence of KI. Reproduced with permission.[67] Copyright 2018, Springer Nature. b) In-film perovskite film passivation mechanism by adding iodine (I₂) to antisolvent. Reproduced with permission.[126] Copyright 2019, Elsevier. c) The possible perovskite passivation mechanism by the PEAI molecules and corresponding J–V characteristics. Reproduced with permission.[279] Copyright 2019, Springer Nature. d) The morphology and carrier lifetimes of perovskite films before and after MACl treatment. Reproduced with permission.[139] Copyright 2019, Elsevier. e) Schematic of the experimental approach of perovskite film treatment with MACl vapor. Reproduced with permission.[140] Copyright 2017, the Royal Society of Chemistry. f) The photoinduced phase segregation of perovskite films with and without PbCl₂ treatment, the schematic of the two-terminal monolithic tandem solar cell, and J–V curves of the champion single-junction and tandem solar cells. Reproduced with permission.[151] Copyright 2020, The Authors, some rights reserved; exclusive licensee American Association for the Advancement of Science. No claim to original U.S. Government Works.

better passivation. As a result, the passivated perovskite/silicon monolithic tandem solar cell showed a PCE of 25.4% with a high V_{OC} of 1.80 V with a perovskite bandgap of 1.64 eV.

Apart from the bulk treatment, MACl has been used for in-film and posttreatment of perovskite films. Khadka et al.[140] introduced an in-film solvent-free MACl treatment of a perovskite film by exposing the perovskite intermediate phase to MACl vapor during the annealing step, improving the perovskite crystallinity and the charge carrier lifetime (Figure 4e). In addition, the Han group[141] observed a similar improvement by in-film surface treatment of an FAPbI$_3$ perovskite film with MACL solution.

The posttreatment of perovskite films with MACl has been widely investigated to improve the perovskite surface properties.[138,142,143] Recently, Hwang et al.[144] used this method for reducing the surface defects in band-tail states of a perovskite film to improve the photovoltaic parameters of PSCs. However, the low degree of chloride incorporation in the perovskite structure still remains a major challenge to using MACl extensively.[145] Nevertheless, even using FACl instead of MACl with a higher boiling point, the chloride ions leave the perovskite surface during the annealing step, and further surface treatment with another chlorine source 1-adamantylamine hydrochloride (ADAHCl) is necessary.[146] Cesium chloride (CsCl) as an inorganic chloride source also has been used for the passivation of perovskite films. Although it improves the crystallinity of perovskite films, most of the chlorine ions leave the film during the annealing step, which is in contrast to the halide vacancy passivation purpose.[62,147]

Lead chloride (PbCl$_2$) has been introduced as a more stable source than other organic chlorine sources for more efficient passivation of halide vacancies.[135,148,149] The Sargent group[122] theoretically demonstrated that the partial replacement of I with Cl decreases the Pb—X bond and decreases the Pb—X—Pb distortion angles, suppressing the iodide vacancies by reducing lattice strain. Moreover, they experimentally confirmed that PbCl$_2$ as a Cl source in perovskite film could mitigate the superoxide generation and decrease the defect densities subsequently. Furthermore, the Yan group[150] used the bulk treatment of low-bandgap perovskite film via incorporation of PbCl$_2$ into a perovskite precursor, leading to the enlargement of perovskite grains and decrement of nonradiative recombination. Very recently, the McGehee group[151] introduced a triple-halide wide-bandgap perovskite by adding a small portion of PbCl$_2$ to double-halide alloys (iodide–bromide) to reduce the photoinduced phase segregation[152] (Figure 4f) and minimize the V_{OC} deficits subsequently, achieving highly efficient two-terminal perovskite–silicon tandem solar cells. A triple-halide perovskite film showed a high photocarrier lifetime and charge-carrier mobility due to reduction of the halide vacancy defects by incorporation of Cl$^-$ ions in the I and Br alloy. As a result, the V_{oc} deficit was considerably reduced to ~0.45 V for a triple-halide perovskite with a bandgap of 1.67 eV, leading to PCEs of over 20% for a single-junction PSC (Figure 4f). In addition, a high PCE of 27.13% for a monolithic triple-halide perovskite–silicon tandem solar cell was achieved.

Given that PbCl$_2$ is only dissolvable in highly polar solvents such as DMF and DMSO, it is challenging to use it for in-film

or posttreatment methods because of the solubility of perovskites in these kinds of solvents.

3.3.3. Other Anions

Bromide (Br$^-$) has been introduced as a critical halogen to fabricate wide-bandgap perovskite films. Similar to PEAI's functionality for passivating iodide vacancies,[127] recently, the Snaith group[153] suggested that posttreatment surface treatment of perovskite films with benzylammonium bromide (BenABr) solution can cure the halide vacancies on the surface of the perovskite, evidenced by a more significant fraction of bromide in the elemental composition (**Figure 5**a). As a result, the optoelectronic properties of BenABr-passivated perovskite film (Figure 5a), as well as, device thermal stability, were improved compared to the nonpassivated sample. However, the bromide-rich perovskite films face phase segregation and light instability. Therefore, bromide has been used less than other halogens for the passivation of halide vacancies in perovskite films.

It has been demonstrated that fluoride (F$^-$) can also play a crucial role in the optoelectronic properties of semiconductors because of its high electronegativity and more robust electron-withdrawing nature than that of other halogens. First, Kanatzidis et al.[154] induced fluorine as a dopant in the CsSnI$_{2.95}$F$_{0.05}$ perovskite structure to improve its hole conductivity properties, leading to significant PCE improvement of all-solid-state DSCs. Afterward, the Zhou group[155] added F$^-$ ions to the perovskite precursor as a bulk treatment method for perovskite film passivation. As shown in Figure 5b, the fluoride ion, as the minor ion in the halogen group, can form stronger chemical bonding with the Pb^{2+} cations and hydrogen atoms, leading to passivation of halide vacancies and immobilization of cations in the perovskite film simultaneously. As a result, the nonradiative recombination is effectively suppressed in the fluorine-passivated perovskite film compared to other halides, leading to V_{OC} and FF improvement (Figure 5b). In addition, the fluorine-passivated PSC exhibited significant long-term stability compared to the nonpassivated PSC (Figure 5b). However, Yi et al.[156] demonstrated that in perovskite film bulk treatment with CsF solution, only the Cs cations were doped in perovskite homogeneously, whereas the F$^-$ ions were aggregated on the surface of the film without any incorporation in the crystal structure. In contrast, theoretically, due to the small ionic radius of F$^-$ ions, the tolerance factor of a mixed-halide perovskite (MAPbI$_{(3-x)}$F$_x$) is not in the required range of 0.7–1 for achieving a stable perovskite structure. Therefore, the passivation of the halide vacancies of perovskite films with fluorine ions is still under debate.[157]

Apart from pure fluoride ions, various anions with similar properties to this halogen have been used for the passivation of halide vacancies. For instance, theoretically, tetrafluoroborate (BF$_4$$^-$), with an equal ionic radius (0.218 nm) to that of I$^-$ (0.22 nm), can incorporate into the perovskite structure without disturbing the crystallographic stability on providing a relevant tolerance factor.[157,158] Recently, the Jen group[158] added a small amount of BF$_4$$^-$ into a perovskite precursor to partially replace the halide vacancies and form FA$_{0.83}$MA$_{0.17}$Pb(IBr)$_{3-x}$(BF$_4$)$_x$ perovskite films, improving the V_{OC} and FF. Apart from the
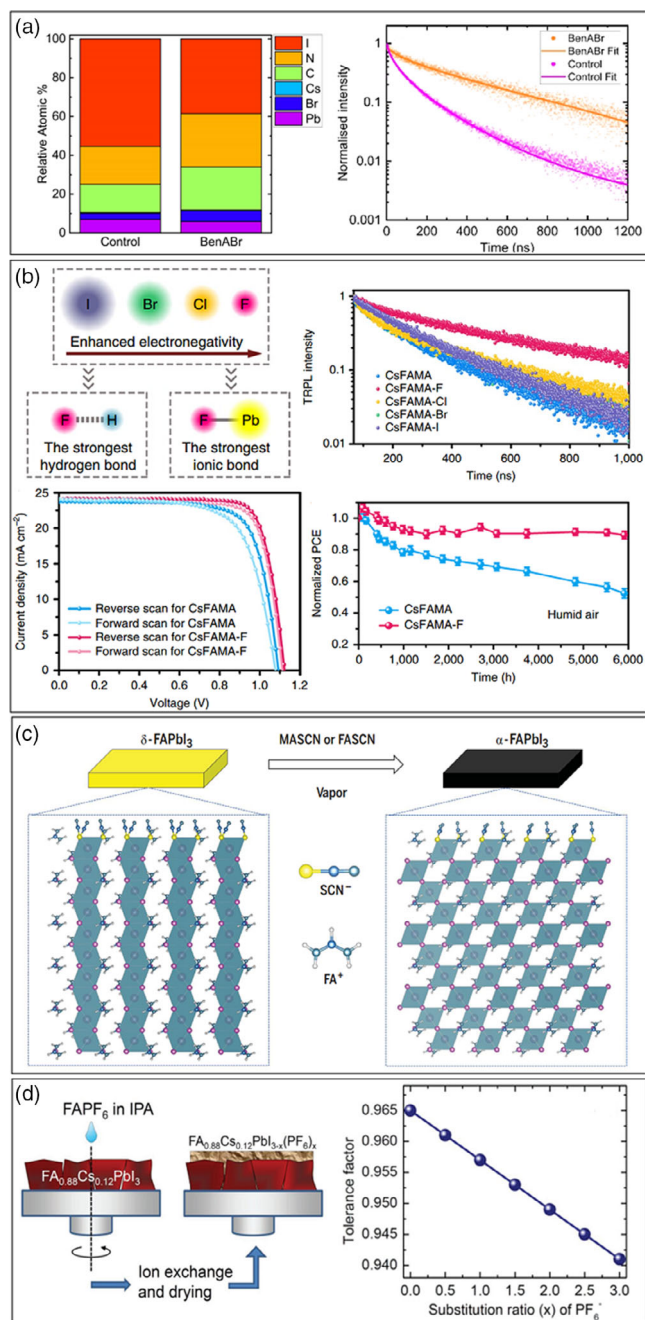
Figure 5. a) The relative atomic composition (extracted from XPS data) and TRPL spectra for the pristine and treated perovskite films with BenABr solution. Reproduced with permission.[153] Copyright 2020, American Chemical Society. b) The schematic of strengthening different chemical bonds and their corresponding TRPL spectra, the champion *J*–*V* curves, and the stability test of pristine NaF-treated PSCs. Reproduced with permission.[155] Copyright 2019, Springer Nature. c) The schematic of perovskite film treatment with the MASCN of FASCN vapor treatment for achieving pure black-phase FAPbI3 perovskite. Reproduced with permission.[160] Copyright 2020, The Authors, some rights reserved; exclusive licensee American Association for the Advancement of Science. No claim to original U.S. Government Works. d) Schematic of ion exchange reaction on the surface of the perovskite film and the calculated GTF according to the ion radii. Reproduced with permission.[161] Copyright 2018, John Wiley and Sons.

BF_4^- ions, pseudohalide materials with a similar ionic radius to iodide have been reported for the passivation of perovskite films. For example, Jiang et al.[159] replaced iodide vacancies with thiocyanate (SCN^-) ions. Compared to the I^- ions, the lone-pair electrons from the S and N atoms in the SCN^- structure can interact with Pb^{2+} ions more strongly, proposing the SCN^- ions as a suitable candidate for halide replacement in perovskite films.

Furthermore, very recently, the Graetzel group[160] used SCN^- ions for stabilizing a black-phase $FAPbI_3$ perovskite film by exposing the perovskite intermediate phase to MASCN or FASCN vapors (in-film treatment method). They emphasized that strong coordination between SCN^- ions and Pb^{2+} ions suppresses the yellow δ-phase, and once the pure α-$FAPbI_3$ is formed, its back-conversion to the δ-phase is prevented by a high energy barrier (Figure 5c). Inspired by the successful halide vacancy passivation utilizing pseudohalides, the Park group[161] used $FAPF_6$ solution for posttreatment surface treatment of a $FA_{0.88}Cs_{0.12}PbI_3$ perovskite film (Figure 5d), which leads to a partial replacement of iodide ions with PF_6^- ions. As shown in Figure 5d, the calculated Goldschmidt tolerance factor (GTF) for different PF_6^- replacement ratios are located in the range of 0.7–1, which is required for stable perovskite materials. Therefore, the replaced PF_6^- ions reduced the defect density and enhanced the carrier lifetime, improving the FF, V_{OC}, and PCE from 17.8% to 19.3% as a consequence.

In summary, we can conclude that halide replacement is a vital strategy to passivate halide vacancies directly. Various halides such as iodine, chloride, and bromide, or other anions with a similar ionic radius to halide ions, have been used for this purpose. However, the most challenging part of this strategy is controlling the precise stoichiometry due to the sensitivity of the perovskite bandgap to the halide ratio. Although iodine itself has been frequently used for halide vacancy passivation, due to the easily breakable Pb—I chemical bond in the perovskite structure, Cl^- ions with stronger bonding with Pb^{2+} ions have been introduced as a passivating agent. The Cl^- ions can not only passivate the halide vacancies, but also improve the perovskite film's crystallinity, which is beneficial to achieve high-performance PSCs. However, the low degree of chloride incorporation in the perovskite structure remains a major challenge because most of the chloride ions leave the film during the annealing step. Br^- ions have been used less than other halogens due to the increasing of the risk of phase segregation and light instability. Although fluoride is theoretically the minor ion in the halogen group, it can form a stronger chemical bond with Pb^{2+} cations. It has been demonstrated that F ions cannot be incorporated in the perovskite crystal structure and aggregate on the surface of the perovskite film. In addition to halides, pseudohalide materials such as SCN^- and PF_6^- with a similar ionic radius to iodide have shown excellent potential for the passivation of halide vacancies. However, incorporating pseudohalides into the perovskite crystal structure is still under debate.

3.4. Metal Replacements

In the previous part, we demonstrated that anion replacement could passivate the halide vacancies. However, incorporating anions with smaller sizes can significantly reduce the perovskite

lattice strain. On the other hand, uncontrollable halide replacement can change the perovskite bandgap and thus affect device performance. Parallel to halide replacement, the central metal replacement has also been considered as an efficient approach for reducing halide vacancies. We categorize metal replacement utilizing isovalent (with a similar oxidation state to central metal ions) and heterovalent (with a different oxidation state to central metal ions) metals. It should be noted that most of the reports in this regard used the perovskite bulk treatment method.

Regarding isovalent replacement, various metal, such as alkaline earth metals Sr,[162] Ca,[163,164] Mg,[165,166] and Ba[167,168] and transition metals such as Cd,[122,169] Ni,[170,171] Co,[172] Cu,[173] and lanthanide[174] ions have been incorporated in perovskite films for suppressing the defect states and reducing the nonradiative recombination. As an example of isovalent central metal replacement, the Sargent group[122] showed that the lattice strain in the perovskite structure could accelerate other vacancies in the perovskite structure, which can be suppressed by partial replacement of the I^- or Pb^{2+} with other halides or metals with smaller ionic radii. They demonstrated that the lattice strain could significantly decrease by partially replacing I^- with the smaller monovalent halogen anions, i.e., Cl^-. To further reduce the lattice strain and defect states, they used Cd^{2+} as an isovalent metal dopant to Pb^{2+} but with a smaller ionic radius (95 vs 119 pm) (see **Figure 6**a).

Regarding the heterovalent replacement, Snaith and co-workers[175] showed that adding a small amount of Al^{3+} ions to the perovskite precursor can reduce the microstrain in the polycrystalline structure, reducing the crystal imperfections/structural defects. Considering the smaller ionic radius of Al^{3+} ions than Pb^{2+} ions (53.5 vs 119 pm), substitutional doping within the crystal was not observed. The minimum microstrain of 5.2×10^{-3} was achieved for 0.15 mol% of the Al^{3+} dopant, which is 30% lower than the control perovskite film (Figure 6b). As shown in Figure 6b, the photoluminescence quantum efficiency (PLQE) was increased by raising the excitation power for both doped and control samples, attributed to the filling of the trap states. However, the Al^{3+}-doped samples showed the highest PLQE amount at all light intensities, attributed to fewer fast nonradiative decay channels in the Al^{3+}-doped samples.

Interestingly, Tang et al.[174] observed a similar lattice contraction by adding various lanthanide ions such as Sm^{3+} (0.958 Å), Tb^{3+} (0.923 Å), Ho^{3+} (0.901 Å), Er^{3+} (0.890 Å), and Yb^{3+} (0.868 Å) because of their smaller radius in comparison to 1.190 Å for Pb^{2+} ions, reducing the defect stats. As discussed, the similarity of ionic radius to that of the primary central metals (i.e., Pb^{2+} or Sn^{2+}) is critical here. However, it remains unclear if metal dopants can incorporate substantially in the perovskite lattice. Recently, Abate and co-workers[176] explored the metal doping mechanism in a perovskite structure with Sr^{2+} and Mg^{2+} ions to compare doping elements with similar chemical properties but different ionic radii (Figure 6c). Their DFT calculation predicted that Sr^{2+} with an almost equal radius to Pb^{2+} (118 vs 119 pm) forms very similar average bonds with iodine and incorporates in the perovskite lattice, whereas Mg^{2+} with a smaller radius (72 pm) forms a shorter Mg—I bond and cannot induce into the perovskite lattice. The experimental investigations showed that at a high-doping-level regime (3–10 mol%), a typical concentration used for metal replacements in the
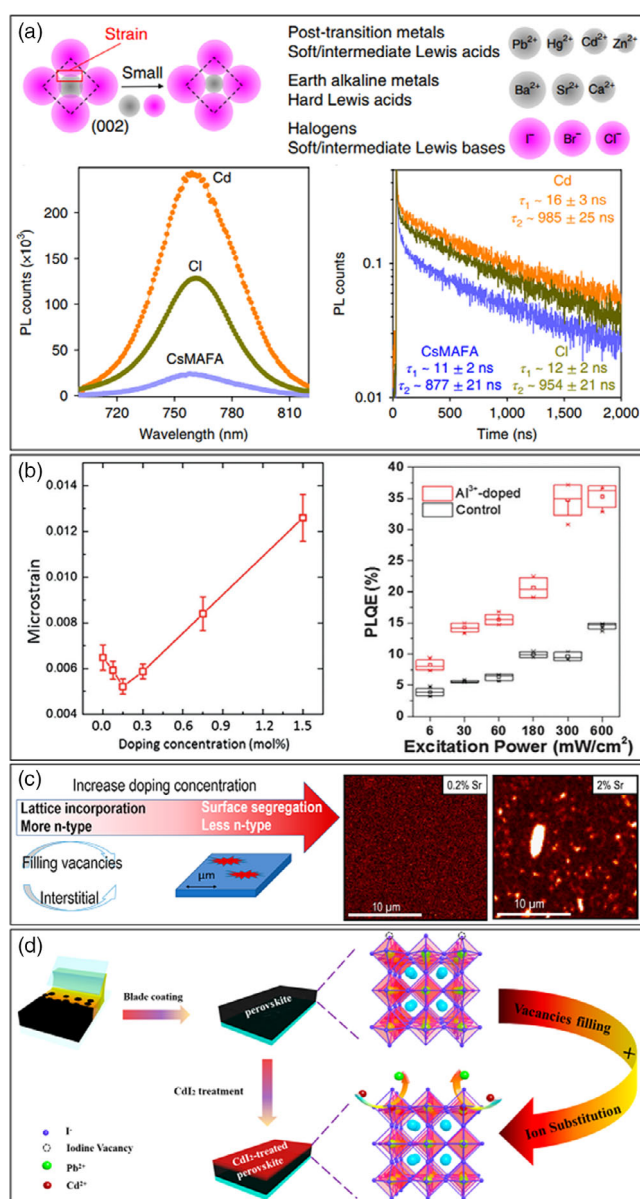

Figure 6. a) Schematic of the reduced strain in the (002) plane by incorporating different candidates and photoluminescence spectra of passivated and nonpassivated perovskite films. Reproduced with permission.[122] Copyright 2018, Springer Nature. b) The calculated microstrain for different Al^{3+} doping concentrations and the PLQE of the control and 0.15 mol% Al^{3+} doped perovskite films as a function of excitation power. Reproduced with permission.[175] Copyright 2016, the Royal Society of Chemistry. c) Schematic of the relationship between the concentration dopants and incorporation in the perovskite lattice, and top-view nXRF maps of 0.2% and 2% Sr-doped $MAPbI_3$ films. Reproduced with permission.[176] Copyright 2020, American Chemical Society. d) The mechanism of passivation of the perovskite film with CdI_2 surface treatment. Reproduced with permission.[280] Copyright 2020, American Chemical Society.

literature, the metal dopants segregate in a secondary phase at the surface of the perovskite, whereas at the superlow-doping-level regime (0.1–1 mol%) the dopants are incorporated into

the perovskite lattice. Top view of nano-X-ray fluorescence (nXRF) elemental concentration maps of the high-concentration Sr doping regime (2 mol%) showed phase segregation as a bright feature (Figure 6c). However, this was not detected in the low-doping regime (0.2 mol%).

Apart from the bulk treatment, very recently, Huang and co-workers[169] used the posttreatment method for surface treatment of a perovskite film with CdI_2 solution, as a result reducing the iodide vacancies and stabilizing iodide ions via the formation of stronger Cd—I ionic bonds compared to Pb—I bonds because of the higher electronegativity difference between Cd and I atoms (Figure 6d). The CdI_2-passivated PSC showed a high PCE of 21.9% with a low V_{oc} deficit of 0.31 V as well as improved the device operational stability (retaining 92% efficiency after constant illumination at 1 sun intensity for 1000 h).

In summary, central metal replacement with isovalent or heterovalent metals can also be considered an efficient approach to passivate halide vacancies by decreasing the lattice strain and suppressing nonradiative recombination. In this approach, the similarity of the ionic radius to that of the central metals (i.e., Pb^{2+} or Sn^{2+}) is critical for achieving an efficient metal replacement. However, the incorporation of the metal dopants in the perovskite lattice remains under investigation. In addition to the ionic radii, controlling the concentration of metal dopants precisely is very important to achieve efficient central metal replacement. Similar to other passivation strategies, bulk and surface treatment of perovskite films can be used for central metal replacement.

3.5. Recovery of Reduced or Oxidized Central Metal Ions

As discussed, the resulting undercoordinated metal ions (Pb^{2+} or Sn^{2+}) from halide vacancies in perovskite films must be passivated. However, Pb^{2+} ions or Sn^{2+} ions can potentially reduce or oxidize to Pb^0 atoms or Sn^{4+} ions, respectively, leading to new nonradiative recombination centers. Therefore, suppressing and recovering the reduced or oxidized M^{2+} ions mitigates the nonradiative recombination more efficiently.

Several efforts have been reported to eliminate the Pb^0 using the bulk treatment method.[63,177,178] For example, recently, Yan and co-workers[179] demonstrated that adding a redox shuttle of a europium ion pair ($Eu^{3+} \leftrightarrow Eu^{2+}$) to a perovskite precursor can selectively recover the Pb^0 as well as I^0 elements in a cyclical transition. This shuttle can transfer electrons from the Pb^0 to I^0 elements, wherein the Eu^{3+} oxidizes Pb^0 to Pb^{2+}, and the formed Eu^{2+} simultaneously reduces I^0 to I^-. Moreover, the passivated perovskite film with Eu^{3+} showed a higher I/Pb ratio than other additives such as Y^{3+} and Fe^{3+}, confirming more efficient ion recovery, lower recombination centers, and higher PCE consequently (**Figure 7**a). Similarly, Yang and co-workers[180] introduced gadolinium fluoride (GdF_3) to a perovskite precursor as a redox shuttle for recovering the Pb^0 defects as well as the growth-assist agent.

On the other hand, oxidation of Sn^{+2} to Sn^{4+} is one of the most common challenges in Sn-based perovskite films, which causes tin vacancies and escalates the halide vacancies in the perovskite structure. This is why many groups tried to suppress this unfavorable oxidation in the Sn-based perovskite films.

Regarding the bulk treatment, first, Mathews et al. demonstrated that adding a small amount of SnF_2 to the perovskite precursor can rather suppress the Sn^{2+}/Sn^{4+} oxidation.[181] Afterward, the Seok group[182] improved the SnF_2 performance by adding pyrazine as a mediator to the perovskite precursor. Recently, Jokar et al.[183] investigated the effect of butylammonium iodide (BAI) and ethylenediammonium diiodide ($EDAI_2$) molecule additives on the quality of $FASnI_3$ perovskite films. They demonstrated that the BAI improves the perovskite crystallinity and the $EDAI_2$ additive decreases the Sn^{2+}/Sn^{4+} oxidation, improving the carrier lifetime and PCE of the passivated PSC (Figure 7b). Wu and co-workers[178] recently suppressed the Sn^{2+} oxidation by adding fluoroaniline isomers to the $FASnI_3$ precursor, achieving a considerable PCE of 10.17%. Afterward, Yan and co-workers[184] introduced hydroxybenzene sulfonic acids as an efficient antioxidant for suppressing the Sn^{2+} oxidation (Figure 7c).

In addition to suppressing Sn^{4+} ions, converting the unfavorable Sn^{4+} to favorable Sn^{2+} in the perovskite precursor has been introduced as another efficient approach to reducing nonradiative recombination. For example, Tan and co-workers[185] added a small amount of metallic tin powder to a Pb–Sn narrow-bandgap perovskite precursor to reduce the Sn^{4+} to Sn^{2+} ions via a comproportionation reaction ($Sn + Sn^{4+} \rightarrow 2Sn^{2+}$). Interestingly, the tin powder in the perovskite precursor becomes a part of the perovskite lattice once oxidized by Sn^{4+} to form Sn^{2+} (red color of the perovskite solution converts to yellow), whereas most of the reported reducing agents are insoluble in the precursor solution (Figure 7d). The tin-powder-passivated perovskite film showed a higher carrier lifetime; thus, the corresponding single-junction and monolithic all-perovskite cells showed a PCE of 21.1% and 24.8%, respectively. Afterward, the same research group reported a PCE record of 25.6% for monolithic all-perovskite tandem solar cells by adding formamidine sulfinic acid (FSA) as an antioxidant along with tin powder to a perovskite precursor.[186] As shown in Figure 7e, the FSA as a zwitterion molecule can passivate both halide vacancies (forming a dative bond with undercoordinated Pb^{2+}/Sn^{2+} using O^- atoms) and cation vacancies (filing the FA/MA vacancy using NH_2^+ fractions). As a result, the surface-anchored FSA neutralizes the oxygen molecules and reduces Sn^{4+} back to Sn^{2+} ions. Moreover, the Wakamiya group[187] converted the Sn^{4+} impurities to Sn^0 nanoparticles (NPs) by adding 1,4-bis(trimethylsilyl)-2,3,5,6-tetramethyl-1,4 dihydropyrazine (TM-DHP) to the perovskite precursor, helping to fabricate a Sn^{4+}-free perovskite film (Figure 7f). A strong photoluminescence and prolonged decay lifetimes were achieved for the Sn^{4+}-free perovskite film with optimum concentration of TM-DHP additive (1 mol%), leading to a high average PCE of 8.9%, compared to 6.6% for the control devices.

In summary, suppressing and recovering the reduced or oxidized M^{2+} ions is another important strategy to mitigate the nonradiative recombination in perovskite films. Adding redox ion pairs to the perovskite precursor can selectively recover the Pb^0 and I^0 elements to Pb^{2+} and I^-, which can be incorporated in the perovskite lattice again. Suppressing the unfavorable oxidation of Sn^{2+} ions to Sn^{4+}, or recovery of Sn^{+4} ions in tin-based perovskites, also has been explored extensively to reduce the nonradiative recombination.
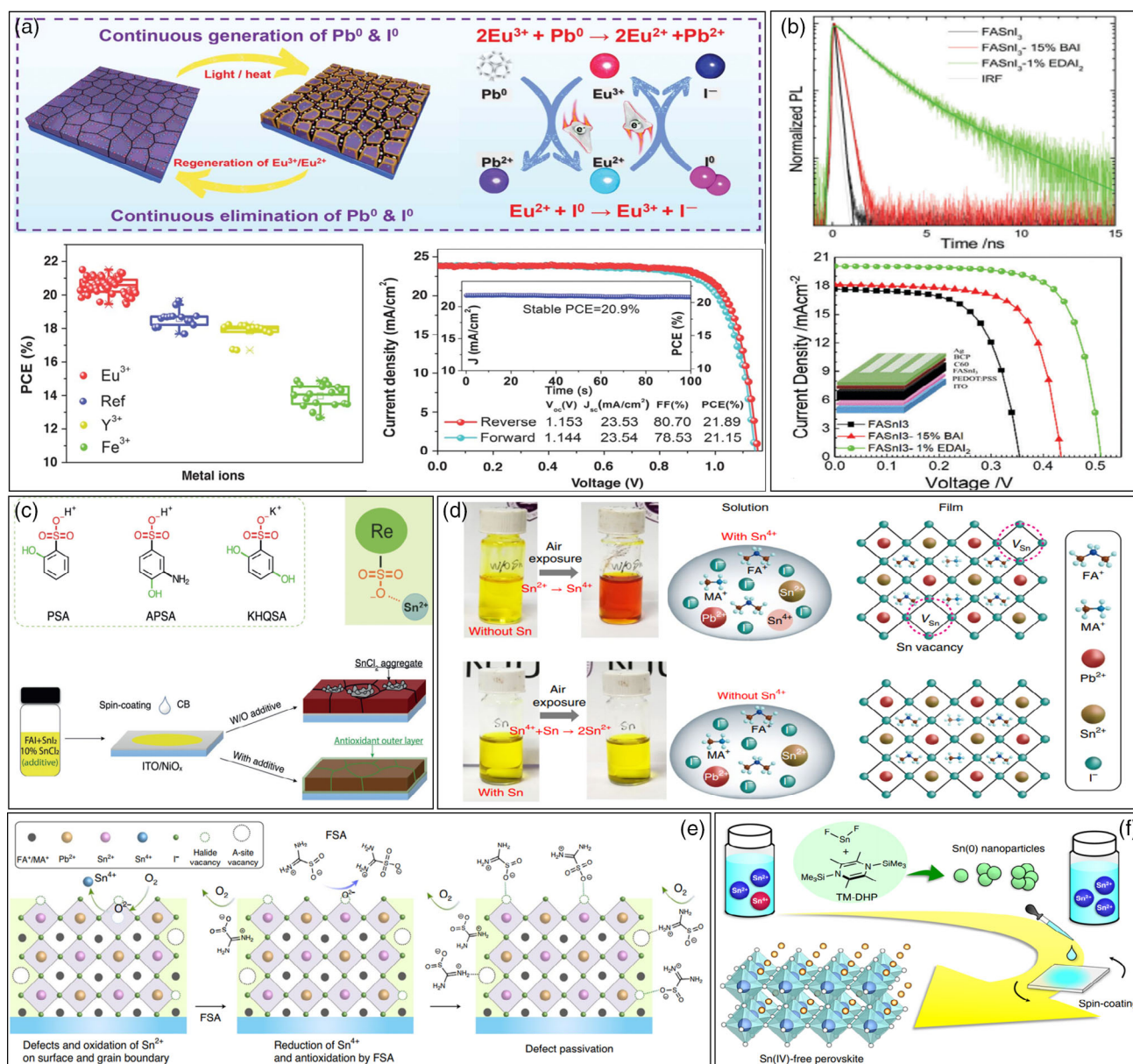
Figure 7. a) The mechanism of Pb⁰ and I⁰ defect passivation: performance data for PSCs with different additives, and the champion J–V curve of PSCs with Eu³⁺ ions. Reproduced with permission.[179] Copyright 2019, The Authors, some rights reserved; exclusive licensee American Association for the Advancement of Science. No claim to original U.S. Government Works. b) The TRPL of pristine and passivated perovskite films with various additives and their corresponding champion J–V curves. Reproduced with permission.[183] Copyright 2018, The Royal Society of Chemistry. c) The molecular structures of different hydroxybenzene sulfonic acids and the perovskite film passivation mechanism. Reproduced with permission.[184] Copyright 2019, John Wiley and Sons. d) Images of the precursor and the mechanism of the Sn vacancy suppression by adding Sn powder to the perovskite precursor. Reproduced with permission.[185] Copyright 2019, Springer Nature. e) The mechanism of antioxidation and defect passivation of perovskite films by FSA antioxidant. Reproduced with permission.[186] Copyright 2020, Springer Nature. f) The mechanism of scavenging the residual Sn⁴⁺ impurities in a perovskite precursor utilizing TM-DHP molecules. Reproduced with permission.[187] Copyright 2020, Springer Nature.

4. Cation Vacancy Passivation

Similar to halide vacancies, cation vacancies can cause defects in the perovskite films and be sources of nonradiative recombination through creating undercoordinated I⁻ and PbI₃⁻ antisites. In contrast to Lewis bases, the organic and inorganic cations with a free orbital, i.e., Lewis acids, can accept free electrons from the dangling undercoordinated halides, eliminating cation vacancies. Nevertheless, besides Lewis acids, organic and inorganic cations can be directly replaced into the cation vacancies. Here, we explore the bulk and surface treatments of perovskite films with different materials for cation vacancy passivation.

4.1. Fullerene-Based Molecules

The fullerene molecule shows an exceptionally high electron affinity because of the ability of rehybridization and its molecular shape, which can receive up to 12 electrons from the other molecules under suitable conditions.[188] Therefore, many fullerene-based molecules have been introduced as a unique Lewis acid for passivating undercoordinated iodide anions and PbI_3^- antisites

in the bulk or surface of perovskite films, forming the Lewis acid–base adduct of fullerene–halide.

Regarding the bulk treatment method, the Sargent group[189] pioneered the passivation of the PbI_3^- antisites by adding the phenyl-C61-butyric acid methyl ester (PCBM) to a perovskite precursor. As shown in **Figure 8**a, they demonstrated that the fullerene group in the PCBM structure acts as a Lewis acid and accepts the free electrons from the PbI_3^- antisites. Therefore,
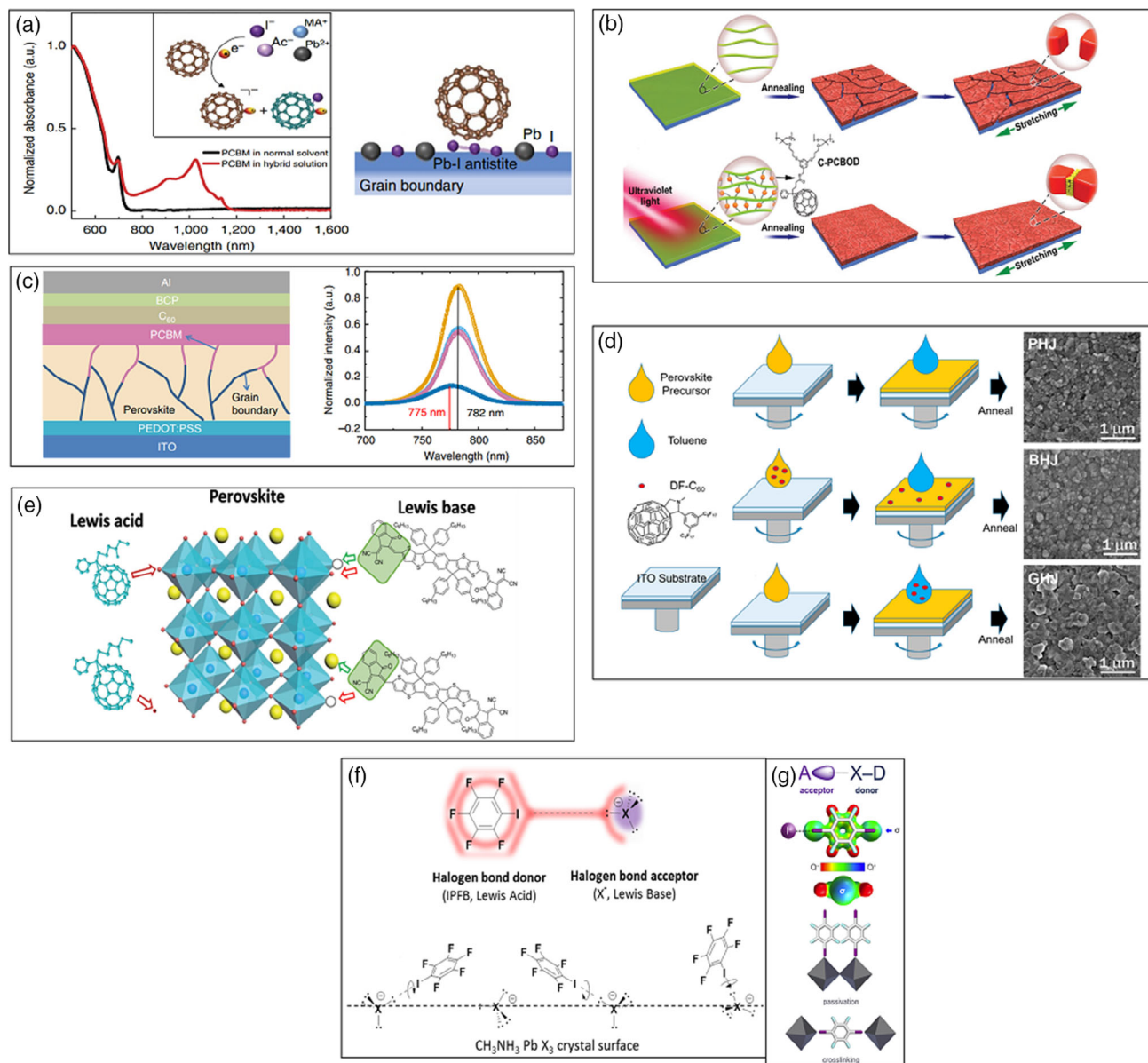

Figure 8. a) UV–vis spectra of the perovskite precursor solution and the schematic of the interaction between PCBM and perovskite ions. Reproduced with permission.[189] Copyright 2015, Springer Nature. b) The operational mechanism of C-PCBOD in the perovskite film. Reproduced with permission.[190] Copyright 2019, John Wiley and Sons. c) Schematic of the PSC structure with an induced PCBM layer and the PL spectra of passivated (blueshift) and nonpassivated (red-shift) perovskite films. Reproduced with permission.[192] Copyright 2014, Springer Nature. d) Schematic of different treatment methods for passivating of perovskite films and their corresponding SEM images. Reproduced with permission.[195] Copyright 2017, American Chemical Society. e) The schematic of interactions between Lewis acid and base functional groups with the perovskite defects. Reproduced with permission.[116] Copyright 2018, John Wiley and Sons. f) Schematic view of IPFB structure and its surface passivation mechanism. Reproduced with permission.[198] Copyright 2014, American Chemical Society. g) Schematic representation of TFDIB structure and its interactions with the perovskite structure. Reproduced with permission.[200] Copyright 2020, American Chemical Society.

after perovskite crystallization, the cation vacancies at the GBs are passivated effectively, suppressing nonradiative recombination and decreasing the J–V hysteresis. After this report, many groups tried to use different fullerene-based-molecule additives. For instance, recently, Abate and co-workers[190] added the [6,6]-phenyl-C61-butyric oxetane dendron ester (C-PCBOD) as a fullerene derivative to a perovskite precursor for not only passivating the perovskite GBs but also improving the mechanical stability of perovskite films. They demonstrated that by exposing the perovskite intermediate phase to UV light, a cross-linked C-PCBOD network around the perovskite grains forms (Figure 8b). This gives the Lewis acid properties of fullerene-based molecules; the C-PCBOD reacts with undercoordinated halides and passivates the cation vacancies. As a result, the trap densities were reduced by 0.25–0.35 eV compared to nonpassivated PSCs, leading to a significantly increased V_{OC} and FF. Very recently, Yao et al.[191] incorporated fullerene molecules into all-inorganic perovskite films to improve their photovoltaic parameters. They demonstrated that the PCBM molecules might react with dangling bonds at the GBs or on the perovskite surface, passivating the defect states in these regions. Kelvin probe force microscopy (KPFM) measurements revealed that distributed PCBM at GBs is beneficial for suppressed ion migration, resulting in reduced J–V hysteresis for the all-inorganic PSCs.

Regarding the posttreatment method, first, Huang and co-workers[192] treated the surface of a perovskite film with PCBM solution (Figure 8c). They showed that inducing of the PCBM interlayer in perovskite GBs reduces the trap densities on the surface and GBs of the perovskite film by two orders of magnitude, leading to hysteresis-free and twice as efficient PSCs. Moreover, the PL emission peak of the passivated perovskite film showed a blueshift, confirming the nonradiative recombination suppression (Figure 8c). Later, the same research group explored the effect of different types of fullerene molecules on the V_{OC} of a wide-bandgap (WBG) perovskite.[193] They showed that using the indene–C60 bisadduct (ICBA) instead of PCBM as an interlayer between the MAPbI₃ perovskite film and ETL increases the V_{OC} by 60 mV, resulting in a stabilized PCE of 18.5%. Moreover, very recently, Ahmad et al.[194] introduced the [6,6]-phenyl-C61 butyric acid n-hexyl ester (PCBC6) as a highly efficient alternative to the commonly used n-type materials, i.e., PCBM and C60, delivering a high PCE of 18.4% for a flexible PSC with an active area of 1 cm². The characterization of the interface of different fullerene derivatives and perovskite films revealed lower nonradiative recombination of PCBC6 due to more effective perovskite surface passivation by the fullerene moiety, leading to a higher V_{OC} than for the C60 and PCBM-based devices.

The Jen group[195] introduced fluoroalkyl-substituted fullerene (DF-C60) molecules into a perovskite film by bulk and in-film surface treatment methods referring to bulk heterojunction (BHJ) and graded heterojunction (GHJ) structures, respectively (Figure 8d). Although the GHJ and BHJ showed the same morphology, the GHJ PSC showed almost double the PCE (15.61%) of the BHJ PSC (7.3%). The graded distribution of DF-C60 molecules was reported as an efficient structure for passivating the defect sites and increasing the surface/bulk recombination resistance, improving the optoelectronic properties as a consequence. In addition, Grätzel and co-workers[196] used a similar

method to incorporate purified α-bis-PCBM into the perovskite film, enhancing the crystallinity and passivating the interface trap states of the GBs. As a result, the charge carrier separation and the charge transport at the perovskite/HTL interface were improved. Moreover, as shown in Figure 8e, Liu and co-workers[116] incorporated PCBM as the Lewis acid and DR3TBDTT as the Lewis base by an in-film treatment, passivating the PbI₃⁻ antisites (cation vacancies) and undercoordinated Pb²⁺ ions (halide vacancies) simultaneously. As a result, the PCE of the passivated PSC was increased up to 19.3%, as well as there being a slight degradation of only ≈13% after 40 days of exposure in 50% relative humidity at room temperature. Moreover, Choi et al.[197] compared the in-film and posttreatment methods for deposition of PCBM on perovskite films. They demonstrated that prepared solar cells via the in-film-deposited PCBM exhibited a higher PCE of 18% than 11% from posttreated PCBM, due to improved electron transfer, and reduced the charge transfer resistance at the interface between the perovskite and PCBM through an increase of the perovskite crystal size and construction of a vertical perovskite–PCBM structure.

4.1.1. Other Molecules

Apart from fullerene-based materials, many small molecules with Lewis acid functionality have been used to passivate the undercoordinated anions resulting from cation vacancies. For example, iodopentafluorobenzene (IPFB), one of the first Lewis acids, was introduced by Abate et al.[198] for surface posttreatment of a perovskite film. As shown in Figure 8f, the highly electronegative fluorine atoms in the IPFB structure can withdraw electron density out of the iodine bond to the aromatic ring, leaving a partial positive charge on this halogen (Lewis acid) that can interact strongly with free halogen anions sites (Lewis base) on the surface of the perovskite film. Another similar example of this kind of Lewis-acid-based molecules has been recent reported by Neher and co-workers.[199] They used self-assembled perfluorinated carbon chains (I-PFCn) with different n (number of carbon) as an interlayer between perovskite and C60 layers by submerging the perovskite film in an I-PFCn solution. Similar to the IPFB molecule,[198] the linear I-terminated I-PFC structure can bind undercoordinated halides, thereby increasing the V_{oc} up to 1.18 V (bandgap of 1.61 eV), the PCE to >21%, and providing thermal device stability (maintaining ≈95% PCE over 3000 h stored in humid air conditions).

Interestingly, the Gratzel group induced a perfluorinated supramolecule, 1,2,4,5-tetrafluoro-3,6-diiodobenzene (TFDIB), into a perovskite film using the in-film treatment method.[200] As shown in Figure 8g, the four highly electronegative fluorine atoms strongly polarize the two iodine atoms in the TFDIB structure. Therefore, the highly polarized halogen atom in the TFDIB structure forms a halogen bond with another halogen atom as a nucleophilic halogen bond acceptor, consequently leading to the passivation of undercoordinated halogen atoms. Furthermore, this strategy (in-film treatment) amplifies the effect of TFDIB molecules by cross-linking the perovskite grains within the perovskite film, leading to more stable PSCs.

In summary, fullerene-based molecules with high electron affinity have shown a great potential for passivating the

undercoordinated iodide anions and the PbI_3^- antisites in the bulk or surface of the perovskite films. These molecules could be directly added to the perovskite precursor or treat the surface of perovskite films, i.e., bulk and surface treatments. In addition to fullerene-based molecules, small molecules with Lewis acid functionality also can be used to react with the undercoordinated anions, passivating the cation vacancies.

4.2. Cation Replacement

Apart from Lewis acid passivation, cation vacancies could be replaced by incorporating cation additives with similar sizes and properties. Notably, the cations additives must be small enough to fit within the voids of the octahedral PbI_6^{4-} units; otherwise, the perovskite lattice would be disordered from 3D3Dto 2D structure. Organic cations with hydrogen bonding capability and inorganic cations with suitable radii have been used for this purpose, which will be reviewed in this part. In every case, we consider applied perovskite treatment methods as well.

4.2.1. Organic Cations

Typically, organic molecules with ammonium ($-NH_3^+$) functional group can replace the cation vacancies in the undercoordinated halides voids with a negative charge through hydrogen bonding. Regarding the GTF, organic cations with a radius up to 2.6 Å are candidates for replacing the MA^+ vacancies without changing the perovskite lattice dimension. Therefore, only a few organic cations have suitable sizes to insert into the perovskite structure and form a stable 3D lattice. However, as mentioned, the bulky ammonium organic cations not only can passivate the cation vacancies but also with the advantage of changing the perovskite crystal phase from 3D to 2D for fabricating more stable PSCs.

Small Organic Molecules: Small organic cations can be added to the perovskite precursor to passivate the cation vacancies, i.e., the bulk treatment method. One of the most frequently used organic cations for this purpose is carbamimidoylazanium ($CH_6N_3^+$), known as guanidinium (GUA or GA), by forming hydrogen bonding with undercoordinated halides within the bulk through or at grain boundaries of the perovskite.[201–204] Considering the bigger GA radius (278 pm) compared to the commonly used MA (217 pm) in the perovskite structure, GTF suggests a full MA replacement with GA cations cannot form a stable 3D perovskite lattice. However, Emsley and co-workers[205] by means of solid-state NMR demonstrated that adding a small amount of GA to perovskite precursor can directly be incorporated into the $MAPbI_3$ and $FAPbI_3$ lattices and forming pure $GA_xMA_{1-x}PbI_3$ or $GA_xFA_{1-x}PbI_3$ phases (**Figure 9**a), albeit the PL signal does not shift accordingly. Indeed, the Yang group demonstrated the passivation effect of GA by partial incorporation to the $MAPbI_3$ perovskite.[206] The passivated PSC showed the V_{OC} improvement of 50 mV, from 1.02 to 1.07 V. As shown in Figure 9b, the PL intensity and carrier lifetime of the GA-passivated perovskite film was increased significantly compared to the pure $MAPbI_3$, confirming the reduced defect density. They suggested that the symmetry of the amine groups in GA enables this molecule to form more hydrogen bonding between the partial negative PbI_6^{4-} units compared to the MA^+ ions, resulting in
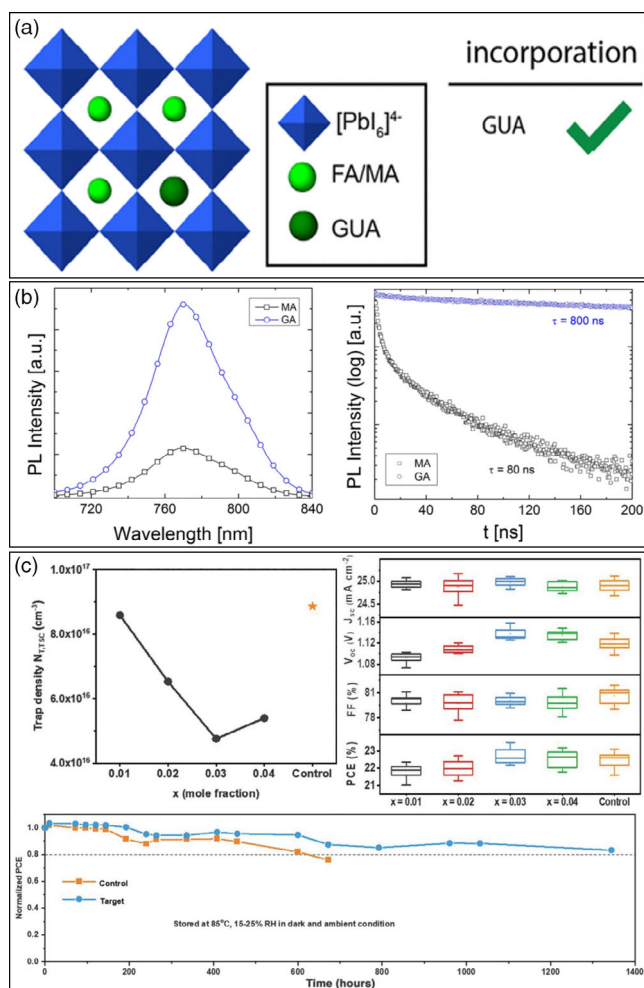

Figure 9. a) Schematic illustration of incorporating a GUA molecule into the $MAPbI_3$ and $FAPbI_3$ lattices. Reproduced with permission.[281] Copyright 2018, American Chemical Society. b) The PL and TRPL spectra of pure MA and GA-passivated perovskite films. Reproduced with permission.[282] Copyright 2016, American Chemical Society. c) Trap density and statistics of PV parameters for deferent MDA-Cs molar ratios and thermal stability test for the target PSC (3:3 molar ratio of MDA-Cs alloy). Reproduced with permission.[208] Copyright 2020, The Authors, some rights reserved; exclusive licensee American Association for the Advancement of Science. No claim to original U.S. Government Works.

more efficient defect passivation. The Seok group[207] introduced a methylenediammonium dichloride ($MDACl_2$) molecule as a new cation to stabilize and passivate the α-$FAPbI_3$ perovskite. Although MDA^+ (262 pm) and FA^+ (256 pm) have a similar ionic radius and molecular configuration, MDA can form a more significant hydrogen bonding with undercoordinated halides, leading to more efficient passivation and stabilization of the α-$FAPbI_3$ phase. As a result, the MDA-passivated perovskite showed higher carrier lifetime and higher PCE than the nonpassivated sample due to reduced nonradiative recombination. Nevertheless, the larger size of MDA^+ than FA^+ can distort Pb—I—Pb bonds by tilting the PbI_6^{4-} octahedral units, which increases the lattice strain. To solve this problem, very recently, the same research group[208] demonstrated that adding

cations with a smaller radius than FA^+, i.e., Cs^+, along with the MDA^+ in an equimolar ratio (3:3) to the $FAPbI_3$ perovskite precursor can form a solid-state alloy in the $FAPbI_3$ lattice, resulting in a significantly reduced lattice strain and defect concentration (Figure 9c). The (MDA-Cs)-passivated PSC showed a certified PCE of 24.4% and superior thermal stability at 85 °C and 15–25% relative humidity for 1300 h (Figure 9c).

Bulky Organic Molecules: 3D/2D Structures: Beyond the small molecules, bulky organic molecules containing ammonium (NH_3^+) with nonconjugated or conjugated aliphatic tails have been used to passivate cation vacancies and stabilize the 3D perovskite by forming a 2D phase. Depending on the used treatment method, the 2D phase could be in the bulk or the surface of the 3D phase (see **Figure 10**a).[209] So far, many ammonium-based bulky organic cations have been used for this purpose (Figure 10b).

Regarding the bulk treatment method, bulky organic molecules can add to the perovskite precursor. First, Mohite and co-workers[210] formed 2D $(BA)_2(MA)_3Pb_4I_{13}$ perovskite films by a hot-casting deposition method. In this perovskite structure, the BA^+ cations act as a spacer between the inorganic PbX_6^{4-} layers. By increasing the number of inorganic layers, the perovskite phase can change from pure 2D to quasi-2D (3D/2D mixed perovskite) or pure 3D. Although pure 2D PSCs have shown superior stability properties, they still suffer from low PCEs. In contrast, 3D perovskites showed high performance but often struggled with low long-term stability. Therefore, the fabrication of 3D/2D perovskite films was suggested to achieve highly efficient and stable PSCs.[183,211,212] For instance, the Snaith group[213] formed a 3D/2D perovskite structure by introducing n-BA to the perovskite precursor. As shown in Figure 10c, the 2D platelets were located at the GBs of highly oriented 3D grains, leading to a clean electronic interface and suppressing the charge trapping at the GBs subsequently (see the TRPL spectra in Figure 10c). Typically, the aliphatic tails of BA^+ cations in the 2D structure have weak van der Waals interaction. Therefore, improving this interaction to stabilize the 2D phase and enhancing the charge transfer in this structure remains a fundamental question. Recently, Huang and co-workers[214] introduced a new bulky organic molecule, 2-(methylthio)ethylamine hydrochloride (MTEACl), instead of BA^+, which forms a strong sulfur–sulfur interaction at the tail parts of this molecule (Figure 10d). As a result, the charge transport and stabilization of the 2D $(MTEA)_2(MA)_4Pb_5I_{16}$ $(n = 5)$ perovskite framework were improved compared to 2D $(BA)_2(MA)_4Pb_5I_{16}$, leading to the PCE improving from 15.94% to 18.06%. This report may provide a direction for fabricating more efficient 3D/2D PSCs by engineering with bulky organic molecules.

Phenylethlammonium (PEA^+) is another frequently used ammonium-based bulky cation that has been added to a perovskite precursor as a bulk treatment method to passivate cation vacancies in perovskite films similarly to the BA^+ cation. Ho-Baillie and co-workers[215] demonstrated that adding PEAI into a perovskite precursor forms a 3D/2D structure at the GBs, improving the carrier lifetimes and V_{OC}. Very recently, the Huang group[216] used PEACl instead of PEAI to improve the optoelectronic properties and crystallinity of the perovskite film simultaneously. As schematically shown in Figure 10e, the PEA^+ cations prefer to either occupy the cation vacancies

at grain surfaces by ionic bonding or interact with undercoordinated I^- ions by hydrogen bonding. In contrast, the Cl^- ions in the PEACl structure enhance the perovskite crystallization. As a result, a blade-coated PEACl-passivated PSC showed a PCE of 22.0% with a small voltage deficit of 0.33 V and significant operational stability (96% of the initial efficiency retained under 1 sun illumination for 500 h).

However, the shape and length of the alkyl chain of bulky organic cations can affect the perovskite crystallization. In a comparative study, the Seok group[217] evaluated octylammonium (OA^+), BA^+, and PEA^+ cations with different alkyl chains as additives in perovskites. They observed that BA^+ and PEA^+ form a 2D structure in a 3D perovskite film. Surprisingly, in contrast to BA^+ and PEA^+, the 2D structure was not detected in the OA^+ case; it was speculated that OA^+ only acts as an encapsulating agent of GBs

Apart from monoammonium bulky organic molecules, multiammonium molecules also have been considered for efficient passivation of the cation vacancies. Very recently, Padture and co-workers[218] demonstrated that the incorporation of 4-(aminomethyl)-piperidinium (4AMP) cations as a diammonium bulky organic cation into a $FASnI_3$ film improves optoelectronic properties and stability of PSCs. As schematically shown in Figure 10f, the optimal concentration of 4AMP forms a nanoscale low-dimensional (LD) perovskite phase around the 3D perovskite GBs, leading to suppressed defects and nonradiative recombination. As a result, a 4AMP-15-passivated PSC showed a maximum performance of 10.9% and 500 h operational stability.

Regarding the surface posttreatment, after successful perovskite film crystallization, a solution of BA^+, PEA^+, or other bulky cations is deposited on the perovskite films. The cations with larger ionic radii than cation vacancies, i.e., MA or FA, can be spatially coordinated with undercoordinated halides to passivate this kind of defect and form a 2D structure. As a recent example, Seok and co-workers[219] demonstrated that charge carrier lifetimes of treated perovskite films with BA, OA, and DA molecules were increased, referring to reduced nonradiative recombination by forming a 2D structure at the perovskite/HTL interface.

Liu and co-workers[220] studied the passivation effect of PEA^+ cations in a $FAPbI_3$ perovskite film. They also compared the passivation properties of PEA^+ to fluorinated PEA^+ (F-PEA^+), BA^+, fluorinated BA^+ (F-BA^+) cations, and a mixture of PEA^+:FA^+ cations (Figure 10g). They demonstrated that the underlying 3D phase templates the growth of the 2D capping layer during the film treatment. This facilities faster charge transfer at the interface of the 2D/3D perovskite with lower charge recombination losses. On the other hand, due to the hydrophobic properties of fluorinated molecules, the passivated PSCs with all fluorinated cations showed higher environmental stability compared to other cations but at the cost of lower PCEs.

As already mentioned, the long-chain cations improve the stability of PSCs, but with the loss of PCE due to reduced charge transport at the 3D/2D interface. To tackle this challenge, recently, the Sargent group[221] introduced 4-vinylbenzylammonium (VBA^+) as a cation with an additional terminal vinyl group in the *para* position of the aromatic phenyl ring compared to the PEA^+ cation. Similar to other cations, the ammonium group of VBA^+ passivates the cation vacancies. In contrast, the vinyl group starts the photochemical cross-linking by exposing the
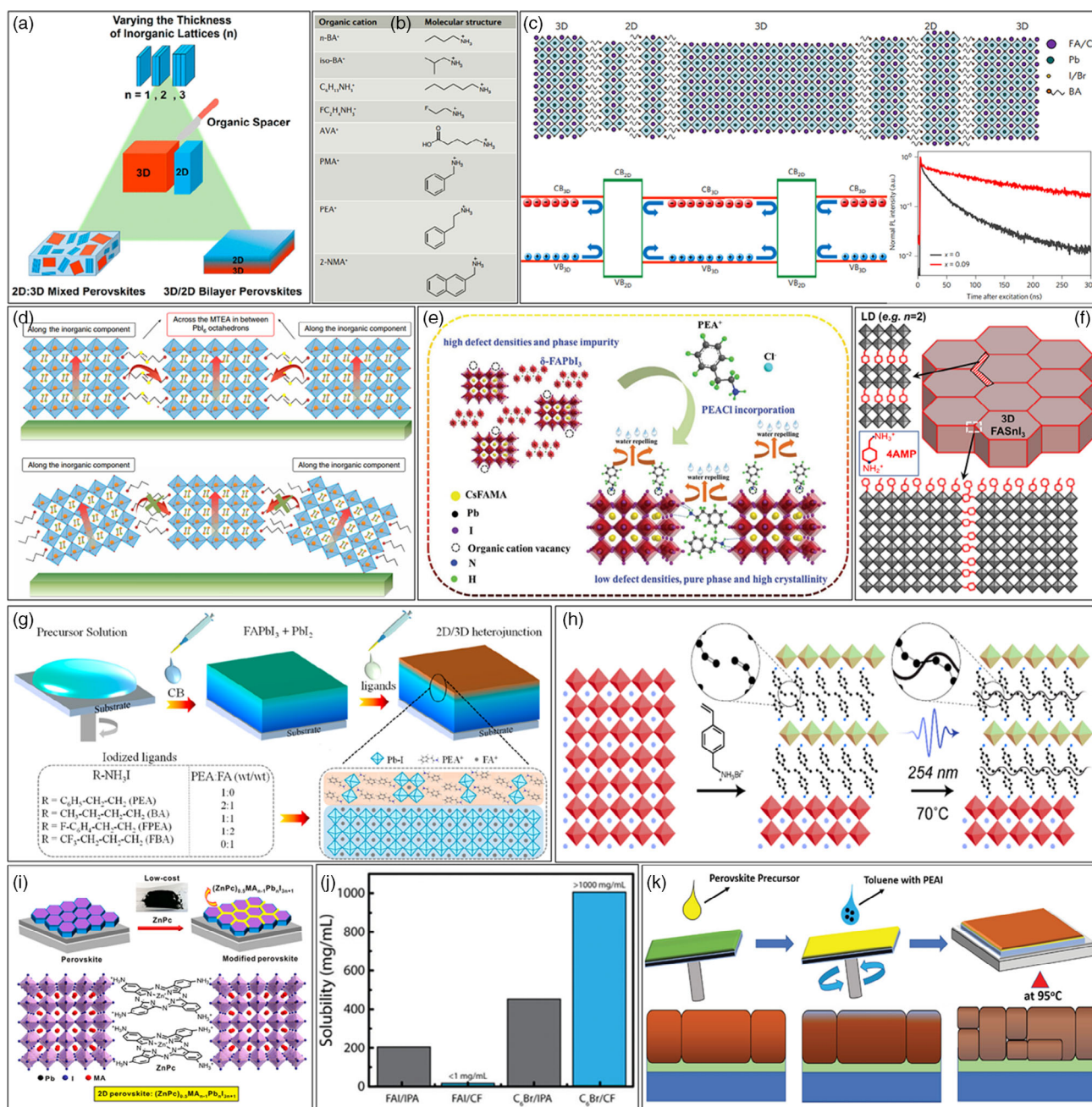
Figure 10. a) Schematic illustration of 3D/2D mixed and 3D/2D bilayer perovskite structures. Reproduced with permission.[209] Copyright 2018, American Chemical Society. b) Most common bulky organic cations. Reproduced with permission.[283] Copyright 2019, Springer Nature. c) Schematic of the proposed self-assembled 2D/3D perovskite film, its electronic band offsets, and the TRPL spectra. Reproduced with permission.[213] Copyright 2017, Springer Nature. d) Schematics of charge transport in passivated 2D perovskite films with MTEA and BA. Reproduced with permission.[284] Copyright 2020, Springer Nature. e) Schematic of the mechanism of defect passivation and improving the moisture stability in a perovskite film through PEACl molecules. Reproduced with permission.[216] Copyright 2020, John Wiley and Sons. f) Schematic illustration of the functionality of 4AMP molecules on grain surfaces (external) and grain boundaries (internal) in a perovskite film. Reproduced with permission.[218] Copyright 2020, American Chemical Society. g) Engineering of the 3D/2D hierarchical structure by post-surface-treatment method. Reproduced with permission.[285] Copyright 2019, American Chemical Society. h) Mechanism of 3D/2D heterostructure formation using the VBABr ligands. Reproduced with permission.[286] Copyright 2019, American Chemical Society. i) Posttreatment perovskite surface treatment with ZnPc and its passivation mechanism. Reproduced with permission.[222] Copyright 2018, American Chemical Society. j) The solubility of FAI and C6Br in CF and IPA solvents. Reproduced with permission.[223] Copyright 2019, The Royal Society of Chemistry. k) Schematic of forming 3D/2D structure by in-film treatment method. Reproduced with permission.[224] Copyright 2017, John Wiley and Sons.

perovskite film to UV light (∼250 nm) (Figure 10h). The UV cross-linked 3D/2D heterostructure showed lower nonradiative recombination than the pure 3D structure, improving the V_{OC} and PCE.

Apart from BA^+ and PEA^+ as the most frequently used cations, many new ammonium-based bulky organic molecules have been used for posttreatment of the perovskite surface (see **Table 2**).

Similar to the bulk treatment method, multiammonium molecules have also been used to pass perovskite films' passivation by the posttreatment method. For example, Tang and co-workers[222] introduced tetra-ammonium zinc phthalocy-anine (ZnPc), which can coordinate the undercoordinated PbI_6^{4-} units on the perovskite surface by forming four hydrogen bonds at the four ammonium end groups of every ZnPc molecule (Figure 10i). Their optoelectronic characterization showed that ZnPc creates a 2D $(ZnPc)_{0.5}MA_{n-1}Pb_nI_{3n+1}$ structure within the perovskite GBs, improving the charge transport properties and thus the PCE.

One of the significant challenges of the posttreatment method is that most bulky molecules are just dissolvable in protic polar solvents, mainly isopropyl alcohol (IPA), which can destroy the perovskite during the surface treatment. To address this challenge, recently, Bawendi and co-workers[223] introduced a new bulky organic molecule, *n*-hexylammonium bromide (C6Br), which is dissolvable in chloroform (CF) solvent. They demonstrated that IPA could dissolve FAI, whereas the solubility of FAI in CF is less than 1 mg mL^{-1} (Figure 10j). As a result, the passivated perovskite film with a CF-based C6Br solution showed very low nonradiative recombination sites, resulting in a V_{OC} deficit of ≈340 mV at a bandgap of ≈1.56 eV and a PCE of 23.4%.

Nevertheless, various bulky organic molecules have been incorporated into perovskite films during the perovskite crystallization (in-film treatment). As schematically shown in Figure 10k, the Yang group[224] developed a new route of in-film growth of a 3D/2D graded perovskite film by adding PEA^+ into the antisolvent. As a result, the 3D/2D PSC showed a higher V_{oc} and FF compared to the pure 3D PSC. Very recently, the Sargent group[225] compared the in-film (PEA^+ to the antisolvent) and the posttreatment (posttreatment with PEA^+ solution) surface treatment on low-bandgap perovskite films, applicable for all-perovskite tandem solar cells.[225] The nonradiative recombination was suppressed more efficiently in the in-film passivation method compared to the posttreatment method due to suppression of the defects not only at the surface but also on the bulk perovskite film, leading to a stabilized PCE of 23.5% for the all-perovskite tandem solar cell. Table 2 summarizes the most significant bulky molecules for passivation of the cation vacancies with different perovskite film treatment methods.

In summary, organic cation additives with hydrogen bonding capability are able to passivate the cation vacancies in perovskite films, suppressing the nonradiative recombination. However, these organic cation sizes are critical to fit within the voids of the octahedral PbI_6^{4-} units and keep the 3D perovskite structure. Moreover, the electron affinity of the organic cations affects their passivation function. The bulky organic cations could also passivate the cation vacancies and stabilize the 3D perovskite by forming a 2D phase. The bulk and surface treatment of perovskite

films with these kinds of cations could create 3D/2D mixed and bilayer perovskite structures, respectively. The optimization of bulky organic cation concentrations is vital to fabricate an efficient 3D/2D structure, improving the efficiency and stability simultaneously. Moreover, the shape and length of the alkyl chain of the bulky organic cations as well as the number of their functional groups, i.e., ammonium group, can affect the 3D/2D structure properties.

4.2.2. Inorganic Cations

In addition to organic cations, inorganic cations have been frequently used for the passivation of cation vacancies through electrostatic interactions with negatively charged defects, i.e., undercoordinated halides or antisite PbI_3^-. The inorganic cations have been frequently used for bulk treatment of perovskite films; however, due to their high-polarity solution, it is impossible to use them for surface treatment because they can dissolve the perovskite films. Therefore, in this part, we focus on the passivation of cation vacancies by the bulk treatment method. However, for incorporating the inorganic cations into the perovskite structure, the crystal stability should be considered. The perovskite crystal structures are highly dependent on the size and interaction of inorganic cations with the octahedral PbI_6^{2-} units. The GTF is a reliable index for predicting crystal stability based on the ionic radii of the inorganic cations. A range of $0.8 < GTF < 1$ is suitable for achieving a photoactive α-phase perovskite (black phase) applicable to PSCs. However, in the ranges of $GTF < 0.8$ and $GTF > 1$, nonperovskite δ-phase orthorhombic (yellow phase) and hexagonal structures will be formed, respectively. **Figure 11**a shows the correlation between the GTF and perovskite structures. First, the Zhu group[226] tried to stabilize the α-phase by solid-state alloying of $FAPbI_3$ (high GTF) and $CsPbI_3$ (low GTF), improving the phase stability.

As mentioned, the cation vacancies mostly form by evaporation of highly volatile organic cations. FA^+, which is thermally more stable than MA^+, has been used frequently as a suitable candidate for cation replacement. Unfortunately, because FA^+ is larger than MA^+, it crosses the viable tolerance factor range. Thus, pure $FAPbI_3$ shows a yellow phase at room temperature. Therefore, one strategy is to add a small amount of MA^+ with a smaller size as the stabilizer in $FAPbI_3$ to achieve a black phase. However, this may entail the risk of cation vacancies due to volatile MA^+. The cesium cation (Cs^+) with an ionic radius of 1.81 Å, considerably smaller than the MA^+ (2.70 Å) and FA^+ (2.79 Å) radii, can be a suitable candidate for stabilizing the crystal phase of $FAPbI_3$ (Figure 11b). In this regard, Saliba and co-workers[227] demonstrated that using Cs^+ along with MA^+ and FA^+ helps to form a high-quality perovskite film with high thermal stability, achieving highly reproducible stabilized PCEs exceeding 21%. Figure 11c shows the XRD data of the triple-cation $Cs_x(MA_{0.17}FA_{0.83})_{(100-x)}Pb(I_{0.83}Br_{0.17})_3$ perovskite with different concentration of Cs^+ in the precursor; $x = 0\%, 5\%, 10\%, 15\%$. The small side peaks at 11.61° and 12.71° in the $x = 0$ samples were assigned as the nonperovskite δ-phase of $FAPbI_3$ and the cubic PbI_2, respectively, indicating an incomplete conversion toward the black phase. However, this undesirable perovskite

Table 2. Summarization of cation vacancy passivation using bulky molecules: passivation methods, passivating agents, device structures, perovskites, and photovoltaic parameters.

| Small molecules	Method	Passivating agent	Device structure	V_{OC} [V]	FF	J_{SC} [mA cm^{-2}]	PCE [%]	Ref.
	Bulk treatment	BAI	FTO/SnO$_2$/PC61BM/triple-cation perovskite/Spiro-OMeTAD/Au	1.14	0.80	22.7	20.6	[294]
		BAI	ITO/PTAA/MAPbI$_3$/C60/BCP/Cu	1.11	0.78	22.4	19.5	[295]
		EDAI$_2$ and BAI	ITO/PEDOT:PSS/FASnI$_3$/C60 /BCP/Ag	0.58	0.72	21.3	8.9	[183]
		PEAI	FTO/c-TiO$_2$/mp-TiO$_2$/double-cation perovskite/Spiro-OMeTAD/Au	0.96	0.74	19.9	14.3	[215]
		PEACl	ITO/PEDOT:PSS/triple-cation perovskite /C60/BCP/Cu	1.18	0.79	23.6	22.0	[216]
		4-(aminomethyl)-piperidinium (4AMP)	FTO/Cu–NiO$_x$/FASnI$_3$/PCBM/BCP/Ag	0.69	0.74	21.1	10.8	[218]
		1,1,1-Trifluoro-ethyl ammonium iodide	FTO/c-TiO$_2$/m-TiO$_2$/MAPbI$_3$/Spiro-OMeTAD/Au	1.06	0.79	21.2	18.0	[296]
		2-Thiophenemethylammonium (ThMA)	FTO/SnO$_2$/double-cation perovskite/SpiroOMeTAD/Au	1.16	0.81	22.8	21.4	[297]
		Octylammonium iodide (OAI)	FTO/b-TiO$_2$/mp-TiO$_2$/MAPbI3/PTAA/Au	1.11	0.81	22.6	20.6	[217]
		Ethane-1,2-diammonium	FTO/c-TiO$_2$/MAPbI$_3$/Spiro-OMeTAD/Au	1.09	0.74	19.1	15.3	[298]
	Surface in-film treatment	PEAI	FTO/NiO/MAPbI3/PCBM (PN4N)/Ag	1.17	0.78	21.8	19.8	[224]
		PEAI	FTO/PEDOT:PSS/Cs$_{0.1}$ MA$_{0.2}$FA$_{0.7}$Pb$_{0.5}$Sn$_{0.5}$ I$_3$/PCBM/PEIE/Ag	0.81	0.79	30.3	19.4	[225]
	Surface post treatment	BAI	ITO/PTTA/MAPbI$_3$/C60/BCP/Cu	1.09	0.77	22.5	18.8	[295]
		OAI	FTO/c-TiO$_2$/ns-TiO$_2$/double-cation perovskite/Spiro-OMeTAD /Au	1.12	0.82	24.0	22.0	[219]
		PEAI	FTO/c-TiO$_2$ /MAPbI$_3$/Spiro-OMeTAD/Au	1.08	0.73	18.6	14.9	[299]
		PEAI	FTO/NiO$_x$/double-cation perovskite/PCBM/PEIE/Ag	1.07	0.73	21.3	17.0	[133]
		PEAI	FTO/c-TiO$_2$/m-TiO$_2$/triple-cation perovskite/Spiro-OMeTAD/Au	1.11	0.73	22.8	18.5	[128]
		PEAI	FTO/c-TiO$_2$/m-TiO$_2$/ triple-cation perovskite/Spiro-OMeTAD/Au	1.14	0.76	22.7	20.0	[130]
		PEAI	FTO/c-TiO$_2$/triple-cation perovskite /carbon back contact	1.04	0.68	21.1	14.9	[300]
		FPEA/FAI (1:1)	FTO/c-TiO$_2$/FAPbI$_3$/Spiro-OMeTAD/Au	1.14	0.76	24.2	21.1	[285]
		PEAI	ITO/PTTA/double-cation perovskite/C60/BCP/Ag	1.25	0.79	19.4	19.0	[301]
		Octyldiammonium iodide (ODAI$_2$)	FTO/c-TiO$_2$/m-TiO$_2$/double-cation perovskite/Spiro-OMeTAD/Au	1.10	0.81	24.2	21.6	[302]
		4-Vinylbenzylammonium (VBA) bromide	ITO/TiO$_2$ NPs/double-cation perovskite/Spiro-OMeTAD/Au	1.15	0.78	22.5	20.2	[286]
		n-Hexyl trimethyl ammonium bromide	FTO/c-TiO$_2$/m-TiO$_2$/double-cation perovskite/P3HT/Au	1.14	0.80	24.9	22.8	[303]
		Azetidinium iodide	FTO/c-TiO$_2$/m-TiO$_2$/triple-cation perovskite / Spiro-OMeTAD/Au	1.14	0.79	24.7	22.3	[304]
		BAI (vapor)	FTO/SnO$_2$/ MAPbI$_3$/Spiro-OMeTAD/Au	1.16	0.80	20.8	19.4	[305]
		Tetra-ammonium zinc phthalocyanine iodide (ZnPcI)	FTO/c-TiO$_2$/m-TiO$_2$/MAPbI$_3$/Spiro-OMeTAD/Au	1.11	0.77	23.5	20.2	[222]
		NH$_3$I(CH$_2$)$_8$NH$_3$I	ITO/PTTA/MAPbI$_3$/PCBM/BCP/Ag	1.11	0.79	19.3	17.0	[306]
		(CF$_3$)$_3$CO(CH$_2$)$_3$NH$_3$I	FTO/b-TiO$_2$/meso-TiO$_2$/double-cation perovskite/Spiro-OMeTAD/Au	1.11	0.79	22.8	20.1	[307]
		Thiazole ammonium iodide	FTO/b-TiO$_2$/double-cation perovskite/spiro-OMeTAD/Au	1.08	0.77	22.8	18.9	[308]
		n-Hexylammonium bromide (C$_6$Br)	FTO/b-TiO$_2$/meso-TiO$_2$/double-cation perovskite/Spiro-OMeTAD/Au	1.16	0.80	23.9	22.3	[309]
		Pentafluorophenylethylammonium (FEA) iodide	FTO/b-TiO$_2$/meso-TiO$_2$/triple-cation perovskite/Spiro-OMeTAD/Au	1.09	0.78	25.7	22.1	[310]
		2-(4-fluorophenyl)ethyl ammonium iodide (FPEAI)	FTO/b-TiO$_2$/meso-TiO$_2$/triple-Cations perovskite/Spiro-OMeTAD/Au	1.12	0.80	22.8	20.5	[311]
		Benzyl ammonium iodide (BnAI)	FTO/c-TiO$_2$/m-TiO$_2$/SnO$_2$/triple-cation perovskite/Spiro-OMeTAD/Au	1.07	0.78	24.4	20.7	[312]
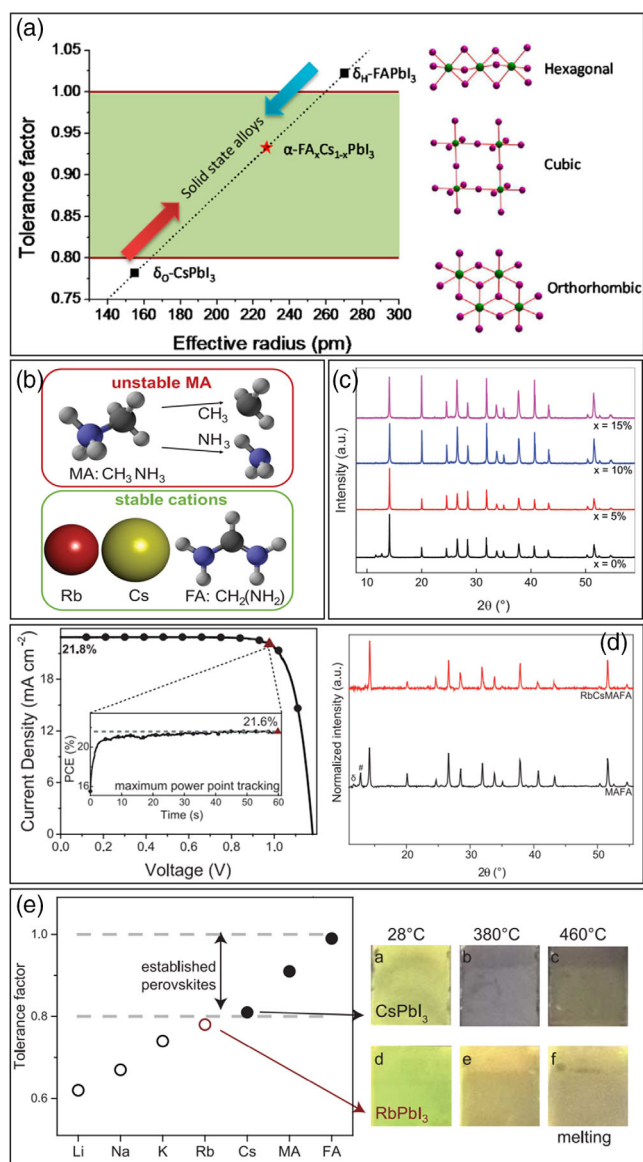
Figure 11. a) Correlations between perovskite crystal stability and G-TF. Reproduced with permission.[226] Copyright 2015, American Chemical Society. b) Various organic and inorganic cations with different shapes and sizes.[287] Copyright 2018, The Authors, some rights reserved; exclusive licensee American Association for the Advancement of Science. No claim to original U.S. Government Works. c) XRD spectra of Cs_xM compounds upon the addition of different amounts of Cs^+. Reproduced with permission.[227] Copyright 2016, the Royal Society of Chemistry. d) Champion *J*–*V* curve of RbCsMAFA solar cell and the XRD data of the MAFA and RbCsMAFA films. e) GTF of perovskite structures with different inorganic cations. Reproduced with permission.[7] Copyright 2016, The American Association for the Advancement of Science.

phase disappeared when adding the optimum amount of Cs^+ ($x = 5\%$). Afterward, the same researchers[228] reported that adding a small amount of Rb^+, only slightly smaller than Cs^+ (152 vs 167 pm), into a triple-cation mixed perovskite (CsMAFA) leads to a stabilized PCE of up to 21.6% and a low V_{OC} deficit of 0.39 V compared to 0.4 V for commercial silicon cells (Figure 11d). As

shown in the XRD data, the residual PbI_2 (12.7°) and yellow-phase peaks (11.7°) were suppressed for the $Rb_5CsMAFA$ as the optimum composition. Moreover, $Rb_5CsMAFA$ showed a higher external PL quantum yield of 3.6% than the CsMAFA sample (2.4%), attributed to low nonradiative recombination losses and passivation of the defect states in this structure. However, apart from Cs^+ or the combination of Cs^+ and Rb^+ cations, other smaller alkaline inorganic cations such as Li^+, Na^+, and K^+ are outside the desired GTF range and can therefore not sustain a stable perovskite black phase (Figure 11e).

In summary, inorganic cations can be used for the passivation of cation vacancies by forming electrostatic interactions with undercoordinated halides or antisite PbI_3^-. However, incorporating the inorganic cations into the perovskite structure depends on their ionic radii and GTF to provide a stable perovskite phase. Mixed cations have been introduced as an efficient strategy to passivate the cation vacancies and stabilize the photoactive perovskite phase.

5. Passivation of Cation and Anion Vacancies Simultaneously (Zwitterions)

So far, all possibilities for passivation of halide vacancies (Section 3) and cation vacancies (Section 4) in perovskite films have been discussed separately. However, due to coexistence of both types of defects in perovskite films, the passivation of one type of these defects keeps the challenge of non-passivated another type of defect. Zwitterions with various functional groups in their molecular structures can passivate the negative and positive charged ionic defects, i.e., halide and cation vacancies. Here, we categorize the application of zwitterions for passivation of perovskite films through bulk and surface (posttreatment and in-film) treatment methods.

Many research groups used zwitterions for bulk passivation of perovskite films.[229–235] Indeed, the butylphosphonic acid 4-ammonium chloride (4-ABPACl) molecule is one of the first zwitterions with $—PO(OH)_2NH_3^+$ terminal groups that have been incorporated into perovskite by the Grätzel group.[229] They proposed that the NH_3^+ groups in the 4-ABPACl structure occupy the cation vacancies by forming an ionic bond. The $PO(OH)_2$ group passivates the undercoordinated iodide ions in the PbI_6^{4-} units by creating a hydrogen bond. This results in simultaneous passivation of the halide and cation vacancies (**Figure 12**a). Afterward, Zhao and co-workers[236] introduced 5-aminovaleric acid (AVA) as a bifunctional molecule for the passivation of perovskite films. They demonstrated that the NH_3^+ groups passivate the cation vacancies and the COO^- groups passivate the halide vacancies by forming ionic bonding with PbI_6^{4-} units and dative bonding with undercoordinated Pb^{2+} ions, respectively. Nevertheless, the bulky carbon chain between cross-linked functional groups in the AVA structure changes the 3D phase of perovskite to a 2D phase, leading to improved device stability (Figure 12b).

Subsequently, the Huang group[237] added a new sulfonic-based zwitterion to the perovskite precursor to not only passivate the perovskite layer, but also improve the perovskite crystallization. As schematically shown in Figure 12c, they proposed that 3-(decyldimethylammonio)-propane-sulfonate inner salt (DPSI)
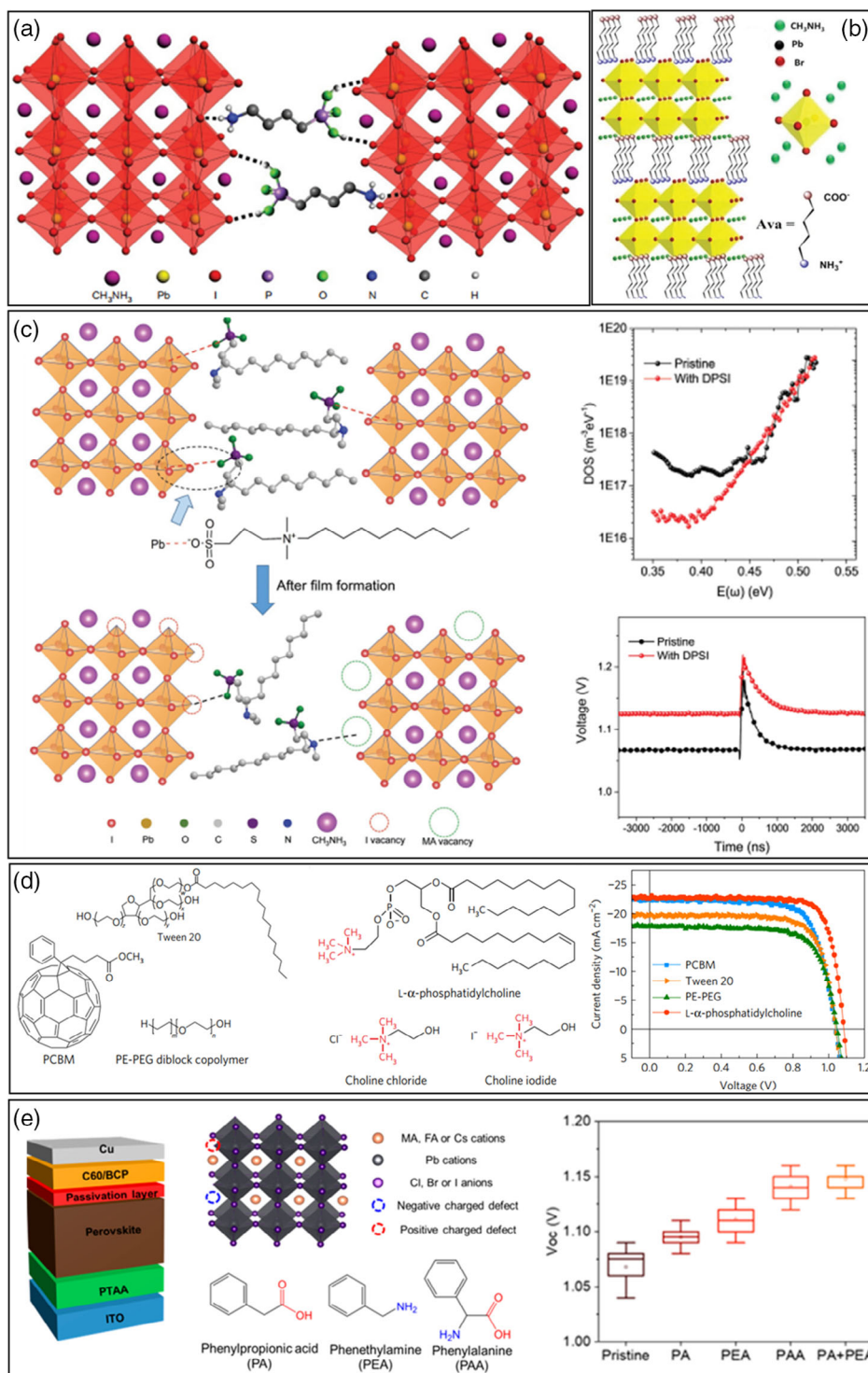
Figure 12. a) Schematic illustration of chemical interaction between the functional groups of the 4-ABPACl molecule and the perovskite. Reproduced with permission.[229] Copyright 2015, Springer Nature. b) The AVA structure and its interaction with the perovskite. Reproduced with permission.[236] Copyright 2017, John Wiley and Sons. c) Schematic illustration of the crystallization and passivation of perovskite in the presence of DPSI molecules, tDOS, and TPV measurements. Reproduced with permission.[237] Copyright 2018, John Wiley and Sons. d) Chemical structures of various passivating agents and the *J–V* characteristics of champion devices. Reproduced with permission.[40] Copyright 2017, Springer Nature. e) Device structure, molecular structures of different passivating agents, and the average V_{OC} of their corresponding devices. Reproduced with permission.[240] Copyright 2019, American Chemical Society.

molecules could form strong chemical bonding with Pb^{2+} cations in the precursor, leading to constraining of the perovskite crystal growth during the crystallization process and improving of the film morphology consequently. In contrast, the trap density of states (tDOS) of the DPSI-passivated perovskite film was six times smaller than that of the nonpassivated film (Figure 12c). Moreover, the transient photovoltage (TPV) lifetime increased from 330 ns for the nonpassivated PSCs to 536 ns for DPSI-passivated PSCs, confirming the improvement of the V_{OC} from 1.07 to 1.13 V.

Regarding the perovskite surface posttreatment, Huang and co-workers[238] demonstrated that various quaternary ammonium halides (QAHs) could efficiently passivate the cation and anion vacancies simultaneously (see the structures of the molecules in Figure 12d). As shown in Figure 12d, the PCE of QAH-passivated PSCs was increased 10–35%, primarily due to an improved V_{OC}, compared to the control devices. Their theoretical and optoelectronic studies showed that the zwitterion structure of QAH molecules with positive and negative electrical charges leads to more efficient defect passivation, resulting in a reduced charge trap density and extended carrier recombination lifetime. Similar to the bulk treatment method, AVA molecules as efficient zwitterions have been used as a surface treatment by the Park group as well.[239] They showed that the formed ultrathin 2D perovskite passivation layer at the interface of a 3D perovskite and the HTL could increase the V_{oc} and FF in the corresponding PSC, which is attributed to enhanced carrier lifetimes and charge extraction by reducing the trap states. Recently, the Huang group[240] systematically engineered various organic molecules with different functional groups and studied their passivating capabilities. As shown in Figure 12e, the passivation layer formed at the perovskite/ETL interface through the surface posttreatment. The phenylalanine (PAA) molecule, with both carboxyl and ammonium groups, passivated both cation and halide vacancy defects simultaneously, leading to a high average V_{OC} of 1.15 V for a perovskite film with a bandgap of 1.57 eV (Figure 11e).

Therefore, all these examples confirm that simultaneously passivating the cation and halide vacancies is an efficient approach for achieving high-quality perovskite films with minimum defect states. Moreover, zwitterions with various functional groups in their molecular structures are a promising candidate to passivate both kinds of cation and anion vacancies in perovskite films simultaneously.

6. Passivation via Insulating Materials

The defects in silicon solar cells can be passivated by depositing an ultrathin layer of electrical insulating materials such as silicon nitride (SiN_x), silicon oxide (SiO_x), or aluminum oxide (Al_2O_3) on the surface of silicon films.[35,241] Considering this, many research groups have tried to use similar passivation strategies for perovskite films. However, this method does not belong to any of the halide or cation vacancy passivation categories.

Mostly, insulating materials have been used primarily for surface posttreatment. However, their incorporation into perovskite film confines charge transfer due to their insulating nature. In

this regard, Koushik et al.[242] used the atomic layer deposition (ALD) technique for depositing an ultrathin Al_2O_3 layer ($\approx$2 nm) on top of a perovskite film as a passivation layer as well as a barrier against moisture ingress (**Figure 13**a). As shown in Figure 13a, such passivated PSCs showed higher PCE and lower J–V hysteresis than the control device, mainly due to V_{OC} and FF improvement from 1.03 to 1.08 V and 69% to 0.77%, respectively. This is attributed to passivating of the trap states and suppressing of the recombination at the perovskite/HTL interface. Moreover, unencapsulated Al_2O_3-passivated PSCs showed significant long-term moisture stability. Insulating polymers are another group of materials that have been reported for surface passivation. First, the Huang group[243] investigated the passivating effect of three solution-processed insulating polymers, including polystyrene (PS), Teflon, and a polyvinylidene–trifluoroethylene copolymer (PVDF–TrFE), on the charge transfer behavior at the perovskite/ETL (C60) interface. As schematically shown in Figure 13b, considering the energy diagram of different layers in the device structure, the insulating polymers act as a tunneling junction at this interface by transporting photogenerated electrons from the perovskite to the C60 layer and blocking the photogenerated holes back into the perovskite layer, resulting in spatial separation of the charge carriers and reduced charge recombination at the interface. Furthermore, due to the super-hydrophobic properties of this kind of polymer, the resistance of the corresponding PSCs to water-caused damage without further encapsulation was dramatically increased (Figure 13b). After this report, many solution-processed insulating polymers such as PMMA,[107,244] poly(ethylene oxide) (PEO),[115] polystyrene,[245] and PVP[246] have been used for surface passivation of perovskite films. However, the uncontrollable thickness and conformal coating of these polymers onto the polycrystalline perovskite films remain the main challenge in this regard. In response to this challenge, very recently, Byranvand et al.[14] developed a chemical vapor deposition (CVD) polymerization as a new solvent-free technique for conformally depositing an ultrathin poly(p-xylylene) (PPX) layer as an insulating polymer onto a perovskite film. As schematically shown in Figure 13c, the radicalized monomer was polymerized on top of the cooled perovskite substrates in the polymerization chamber. The PPX-passivated perovskite film with optimum thickness of 1 nm showed a longer charge carrier lifetime compared to the nonpassivated film, confirming that trap states were suppressed significantly (Figure 13c). As a result, the PPX-passivated PSC showed a higher V_{OC} of 1.11 V and FF of 79.2% compared to the control device with a V_{OC} of 1.08 V and FF of 78.5%, respectively, confirming the passivated defects in the perovskite film.

In summary, the interface of perovskite films can be passivated via insulating materials, suppressing the charge recombination and improving the stability of PSCs. These materials primarily can be used as a nanometric thin layer for surface posttreatment of perovskite films. In most cases, these insulating materials act as a tunnelling junction at perovskite interfaces with the ETL or HTL. Uncontrollable thickness and the nonconformal solution-processed coating are the main challenges of this strategy, which can be solved using solid-state deposition techniques such as ALD and CVD.
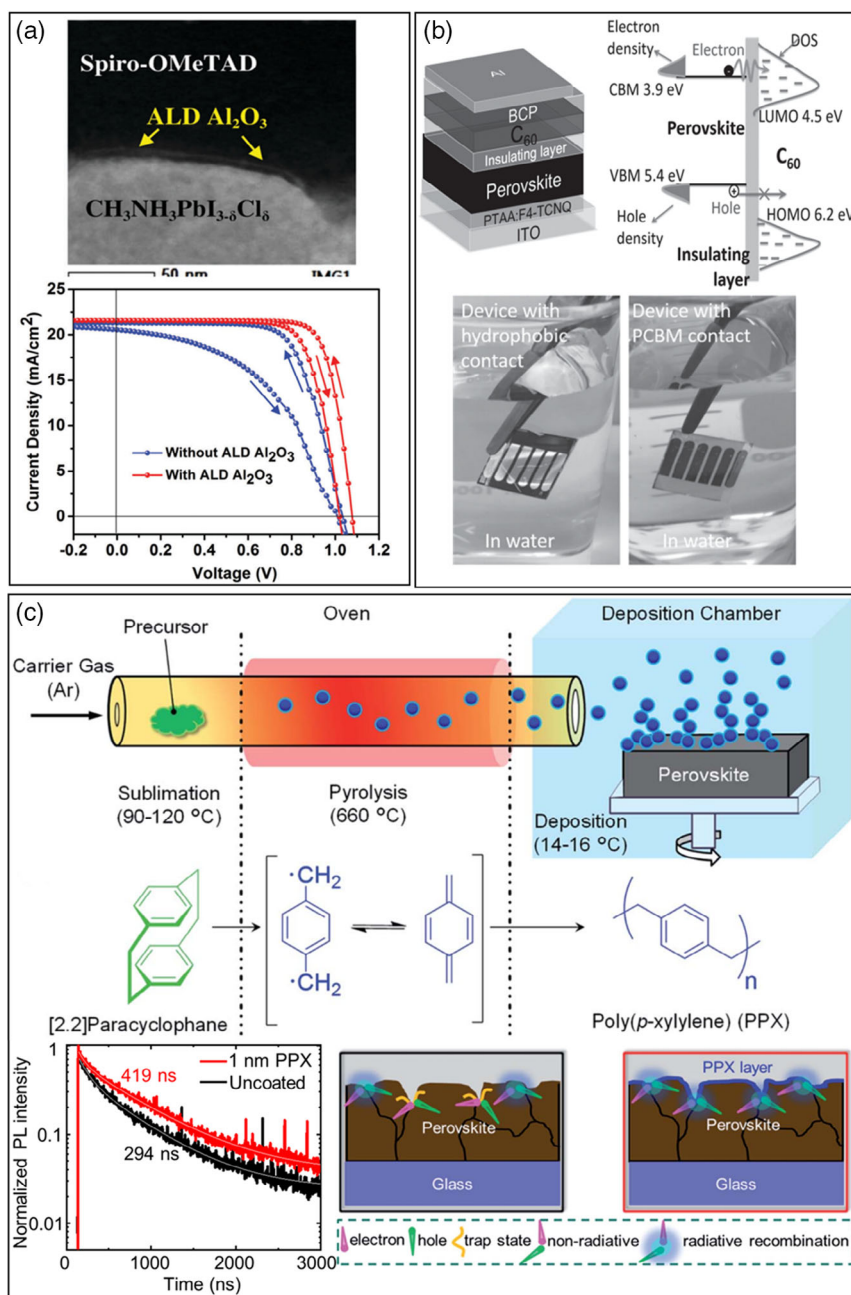
Figure 13. a) High-angle annular dark field TEM image of the perovskite/ALD Al_2O_3 interface and J–V curves of the champion devices with and without the ALD Al_2O_3 interfacial layer. Reproduced with permission.[242] Copyright 2017, The Royal Society of Chemistry. b) The device structure, the mechanism of surface charge recombination blocking by the insulating layer, and pictures of the dipped PSCs with and without an insulating layer in water for 1–2 min. Reproduced with permission.[243] Copyright 2016, John Wiley and Sons. c) Schematic illustration of the CVD polymerization process, TRPL data of the uncoated and 1 nm PPX-coated perovskite film, and schematics of the charge carrier dynamics at the surface of different perovskite films. Reproduced with permission.[14] Copyright 2020, The Royal Society of Chemistry.

7. Passivation via Lead Iodide (PbI₂)

Lead iodide (PbI_2) is the most common insulating material that has been used in small amounts as a self-passivation agent for reducing nonradiative recombination in perovskite films.[247–257] However, uncontrollable inducing of PbI_2 into a perovskite film can confine the charge transfer and stability of PSCs due to its insulating nature and its catalytic role in the perovskite degradation reaction, respectively.[258] Similar to insulating materials (Section 6), PbI_2 passivation belongs to neither the halide nor cation vacancy passivation category.

PbI_2 can induce in the surface or the bulk of perovskite films by different approaches. For example, heating the perovskite films can quickly decompose some parts of the perovskite and

form some excess PbI_2 in the bulk, surface, or GB regions.[248,259] In this regard, Yang and co-workers[250] demonstrated that reannealing the perovskite film releases some of the volatile organic components and forms excess PbI_2 at the perovskite GBs (**Figure 14**a). Their optoelectronic characterization demonstrated that this self-induced PbI_2 excess passivates the perovskite film effectively, resulting in device performance improvement from 0.66% to 12%. This is due to reduced carrier recombination not only in the perovskite film itself, but also at the perovskite/ETL or HTL interfaces due to a favorable energy band alignment (Figure 14a). However, because of the different evaporation rates of the organic components during the reannealing of the perovskite film, controlling the exact amount of excess PbI_2 in this method is challenging.[249,251] In response to this challenge, the Hagfeldt group[260] and Seok group[252] demonstrated that by controlling the molar ratio of PbI_2 in the perovskite film precisely, nonradiative recombination and ion migration could be suppressed.

In addition, Yan and co-workers[261] added lead thiocyanate $(Pb(SCN)_2)$ to the perovskite precursors. This resulted in increased grain size, crystallinity, and an excess of PbI_2 at the perovskite GBs (Figure 14b). They demonstrated that the reaction of SCN^- with $CH_3NH_3^+$ forms a $CH_3NH_3–SCN$ adduct in the perovskite precursor and effects HSCN and CH_3NH_2 gases subsequently, which leads to the mentioned positive effects. As a result, the best PCE with negligible hysteresis was achieved for fabricated PSCs with 5% $Pb(SCN)_2$ due to decreased nonradiative recombination.

However, apart from controlling the PbI_2 molar ratio, the random distribution of excess PbI_2 in the perovskite film still leaves significant room for controlling the location of PbI_2 in it. Ideally, the best place for distributing the excess PbI_2 could be the perovskite GBs. Luo and co-workers[256] demonstrated that using an ionic organic ligand, composed of a hydrophilic "head" and a long-chain hydrophobic "tail," the morphology and distribution of PbI_2 in the perovskite film can be modulated. They demonstrated that adding a specific amount of cetyltrimethylammonium bromide (CTAB) ligand to the perovskite precursor forms vertically distributed 2D PbI_2 nanosheets between the GBs, leading to reduced nonradiative recombination and trap densities (Figure 14c). Recently, Kim and co-workers[262] have proved that using phenethylammonium thiocyanate (PEASCN) as an additive in the perovskite precursor enlarges the perovskite gains and creates only excess PbI_2 at the surface of the perovskite film, while using PEAI as a coadditive with PEASCN forms 2D-phase PbI_2 vertically at the perovskite GBs (Figure 14d).
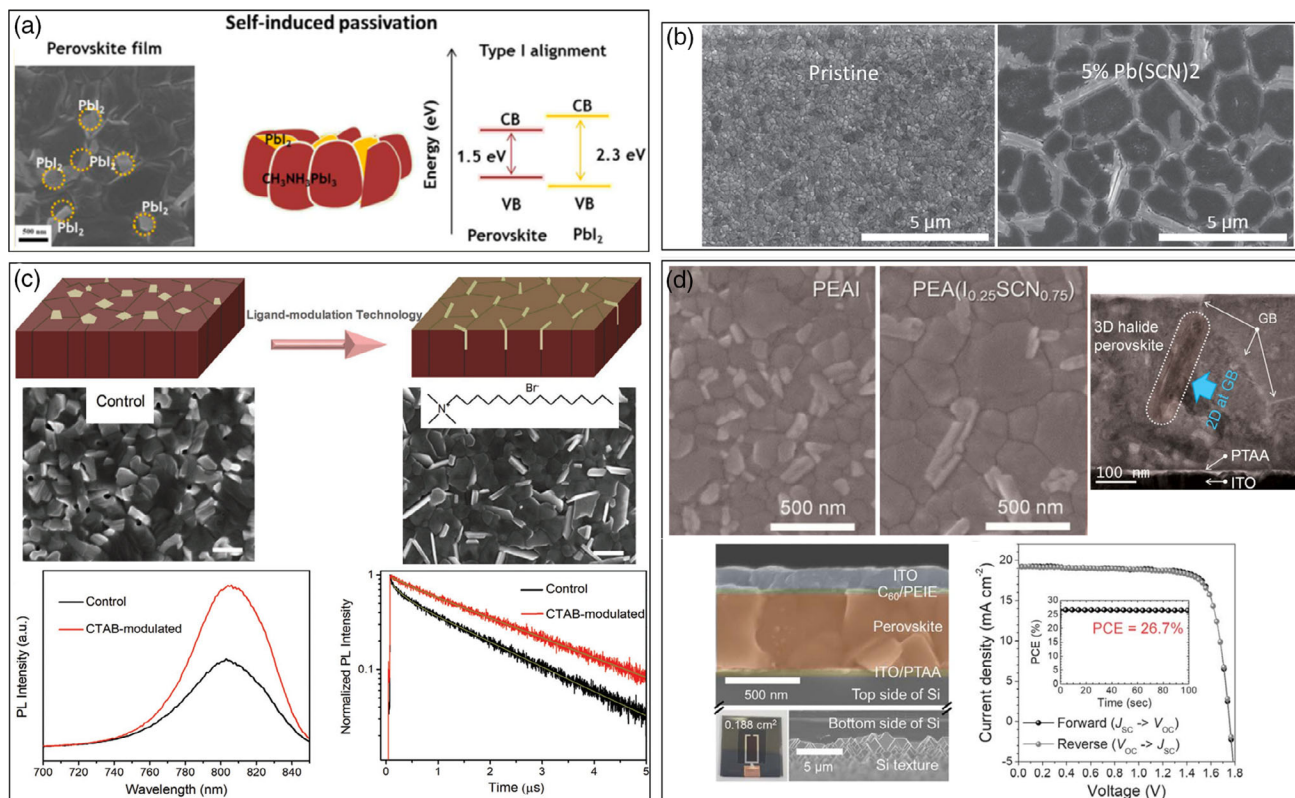

Figure 14. a) Schematic illustration of self-induced PbI_2 in perovskite grains as a passivation agent and their corresponding bandgap diagrams. Reproduced with permission.[250] Copyright 2014, American Chemical Society. b) SEM images of the perovskite film without and with 5% $Pb(SCN)_2$ additive. Reproduced with permission.[254] Copyright 2016, John Wiley and Sons. c) Schematic diagram of the morphology and distribution of modulated PbI_2 in the perovskite film, SEM images, and the PL and TRPL of the perovskite film without and with the CTAB additive. Reproduced with permission.[256] Copyright 2020, John Wiley and Sons. d) Perovskite morphology with PEAI and PEASCN additives, cross-sectional SEM of 2T perovskite/Si tandem device, and the champion J–V curve of a 2T tandem solar cell. Reproduced with permission.[247] Copyright 2020, The American Association for the Advancement of Science.

The highest J_{SC} and V_{OC} were achieved for passivated PSCs with the pure PEASCN and the pure PEAI additives, attributed to larger perovskite grains and passivation of GBs by vertical 2D excess PbI_2, respectively. Finally, the passivated monolithic two-terminal perovskite/Si solar cell showed a high PCE of 26.7%, which was achieved using the mixed additives of PEAS and PEAS (Figure 14d).

In summary, PbI_2 can passivate the bulk or surface of perovskite films by different approaches. The formed PbI_2 can reduce the carrier recombination by providing a favorable energy band alignment at the perovskite/ETL or HTL interfaces. However, controlling the amount and location of PbI_2 in the perovskite films is very important because of its insulating properties.

8. Impact of Defect Passivation on Perovskite Stability

To the best of our knowledge, 1 year stability has been achieved for PSCs under realistic operating conditions,[43] whereas commercial silicon photovoltaic modules have proven to be stable for more than 20 years.[44]

To solve the stability problem, the instability sources in PSCs should be considered. Extrinsic and intrinsic instabilities have been highlighted as the main reasons for the short lifetime of PSCs.[263] Moreover, moisture, oxygen, light, and elevated temperature have been introduced as the acceleration agents for PSC degradation.[264,265] Extrinsic instability is an undeniable challenge for all kinds of photovoltaics, which can be improved by external device modification, i.e., encapsulation.[266,267] However, some parts of the overall instability of PSCs are directly related to the intrinsic stability of perovskite films.[52] Defect states in different parts of perovskite films, i.e., the surface, grain boundaries, and bulk, have been introduced as the main reason for the intrinsic instability of PSCs.[268]

The moisture sensitivity of perovskite films has been well demonstrated.[264,269] Moreover, it has also been found that the defects in perovskite films, especially at the GBs, with a high density of trap states, are the most vulnerable sites for moisture-induced degradation.[270] For example, Ahn et al.[269] demonstrated that defect states at the surface and GBs prompt irreversible degradation of perovskite materials under moisture.

Degradation of PSCs in the presence of oxygen has also been well demonstrated.[271,272] However, the oxygen-induced degradation rate increases under illumination because the resulting superoxide molecules (O_2^-) from the reaction between oxygen and photoexcited electrons induce degradation by forming PbI_2, I_2, H_2O, and CH_3NH_2.[265,271] Therefore, the resulting trapped states from defect states can accelerate the oxygen-induced degradation of PSCs through the formation of O_2^-. It has been demonstrated that PSCs' degradation can accelerate under light illumination in an inert atmosphere.[273,274] Lin et al. found that light-induced degradation is related to excess charge carriers in perovskite interfaces. They observed that HTL- or ETL-covered $MAPbI_3$ films degrade faster than films covered by an insulating layer.[274] Moreover, organic–inorganic hybrid perovskites have shown poor instability at elevated temperatures, which is considered another type of intrinsic instability of PSCs.[274] The volatile organic components in perovskite materials can easily be evaporated at an elevated temperature and create noncoordinated ions, such as halide ions, i.e., cation vacancies, and central metal ions (M^{2+}), i.e., halide vacancies, increasing the defect densities and charge recombination.[275] On the other side, existing defects in the perovskite film increase the thermal instability of PSCs.[276]

Therefore, reducing the trap states by defect passivation of perovskite films enhances the stability of PSCs under moisture, oxygen, and light and elevated temperature. As shown in **Figure 15**a, both cation (A-site) and halide (X-site) vacancies can be passivated by various molecules with Lewis base or acid functional groups, healing of perovskite defects, and forming a
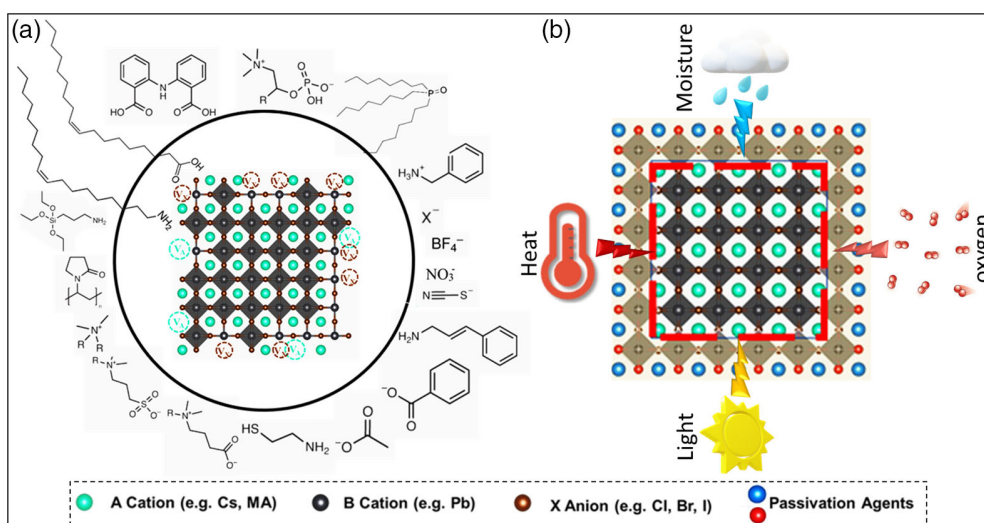

Figure 15. a) Schematic illustration of types of passivating agents used for perovskite film passivation. b) Illustration of perovskite passivated and formation of a well-protected film against organic ligand degradation agents, i.e., moisture, oxygen, light, and temperature. Reproduced with permission.[57] Copyright 2021, John Wiley and Sons.

protective layer at the surface, GBs, or bulk perovskite films, as discussed in Section 3, 4, and 5. Moreover, as discussed in Section 6 and 7, defects in different parts of perovskite films can be passivated using insulating materials such as polymers, metal oxides, and lead iodide, resulting in improved PSC stability.

In summary, an effective passivation strategy can provide a proactive condition for perovskite films to improve their stability against degradation acceleration agents, i.e., moisture, oxygen, light, and temperature (Figure 15b).

9. Conclusion

PSCs have shown great promise to be a part of the future photovoltaic market because of their low-temperature and low-cost processing, as well as the potential for roll-to-roll manufacturing on flexible substrates. Although they showed significant efficiencies of over 25% for the lab-scale solar cells in less than a decade of their invention, which is impressive compared to other well-developed photovoltaics, their efficiency is still below the theoretical Shockley–Queisser limit of about 33% for single-junction solar cells.

Further improvement in efficiency depends on a deeper understanding of the optoelectronic properties of perovskite films. Considering the learned lessons from silicon and OPVs, surface passivation plays a vital role in improving overall performance. However, in PSCs, both bulk and surface passivation should be considered due to the polycrystalline and ionic nature of perovskite films. Therefore, an in-depth understanding of the origin of various defects and their passivation mechanisms matters greatly.

Generally, misplacement or migration of the cations or halide components during the crystallization and application of external stresses such as an electric field, illumination, or temperature are the primary sources of defects in the perovskite films. Following this, we categorize the defects into two big groups of halide (e.g., Cl^-, Br^-, I^-) and cation (e.g., MA^+, FA^+) vacancies. On the one side, the halide vacancies form undercoordinated positively charged central metals (e.g., Pb^{2+} and Sn^{2+}), inducing the Pb^0 and Sn^{4+} well-known recombination centers in perovskite films. On the other side, the cation vacancies lead to negatively charged defects such as undercoordinated halide (e.g., I^-) and Pb–I antisites (PbI_3^-). In addition, we emphasize the passivation of perovskite GBs and interfaces because they are the primary places of ion migration, leading to common challenges in PSCs such as current density–voltage (J–V) hysteresis, phase segregation, and degradation (undermining long-term stability).

The methodology is another crucial aspect of passivation, which classifies different perovskite film treatment approaches with passivating agents. In all parts of this Review, the bulk and surface treatments are investigated as the main approaches for the passivation of different defects. In the bulk treatment, the passivating agents are directly added to the perovskite precursor. This method is seemingly simple. However, it cannot directly passivate the defects on the surface of perovskite films.

On the other hand, surface passivation approaches are classified into in-film and posttreatment methods. In these methods, the passivating agents can be added to antisolvents. For example, it can be introduced in an intermediate step, i.e., in-film treatment, or as a direct deposit on perovskite films after crystallization, i.e., posttreatment. We emphasize that to achieve a defect-free perovskite film, both bulk and surface passivation methods are highly important.

Apart from the methodology, various additives based on their functional groups are divided into Lewis bases and acids for the passivation of cation and halide vacancies. However, because both kinds of defects coexist in the perovskite film simultaneously, we consider the zwitterions, with both base and acid functional groups in their molecular structures, for passivating the negative and positive charged ionic defects, i.e., halide and cation vacancies, simultaneously. In addition, we also consider other passivation methods with insulating materials or lead iodide, which do not belong to any of the halide or cation vacancy passivation categories.

Apart from defect passivation, we describe engineering strategies for the perovskite composition to strengthen interactions between cations and halides, stabilize the perovskite structure, and prevent defect formation.

Despite the dramatic development in a wide range of materials and methods for passivation of perovskite films, we believe the characterization of defects remains challenging. For example, developing precise theoretical models and faster spectroscopic methods to quantify the defects before and after passivation will be very helpful in this regard.

The long-term stability and toxicity of PSCs are two significant obstacles for the entering of this technology into the conventional photovoltaics market. In this Review, the effects of different types of passivation on suppressing of the perovskite degradation are presented. We believe that intelligent defect passivation by designing new and more efficient passivating agents and methods can significantly improve perovskite stability. On the other hand, developing lead-free perovskite materials, e.g., tin, is a vital direction to decrease the toxicity of PSCs. However, it will create the new challenge of tin oxidation from Sn^{2+} to unfavorable Sn^{4+} ions. Therefore, the passivation of tin-based perovskite films should be considered as well. Finally, transferring the lab-scale technology to large-scale processing in terms of perovskite crystallization and passivation will be open challenges for the future of perovskite photovoltaics.

Conflict of Interest

The authors declare no conflict of interest.

[1] A. Kojima, K. Teshima, Y. Shirai, T. Miyasaka, *J. Am. Chem. Soc.* **2009**, *131*, 6050.

[2] J. Y. Kim, J.-W. Lee, H. S. Jung, H. Shin, N.-G. Park, *Chem. Rev.* **2020**, *120*, 7867.

[3] M. Vasilopoulou, A. Fakharuddin, A. G. Coutsolelos, **2020**, https://doi.org/10.1039/c9cs00733d.

[4] https://www.nrel.gov/pv/cell-efficiency.html (accessed: April 2020).

[5] J. J. Yoo, G. Seo, M. R. Chua, T. G. Park, Y. Lu, F. Rotermund, Y.-K. Kim, C. S. Moon, N. J. Jeon, J.-P. Correa-Baena, V. Bulović, S. S. Shin, M. G. Bawendi, J. Seo, *Nature* **2021**, *590*, 587.

[6] M. Saliba, T. Matsui, J.-Y. Seo, K. Domanski, J.-P. Correa-Baena, M. K. Nazeeruddin, S. M. Zakeeruddin, W. Tress, A. Abate, A. Hagfeldt, M. Grätzel, *Energy Environ. Sci.* **2016**, *9*, 1989.

[7] M. Saliba, T. Matsui, K. Domanski, J.-Y. Seo, A. Ummadisingu, S. M. Zakeeruddin, J.-P. Correa-Baena, W. R. Tress, A. Abate, A. Hagfeldt, M. Grätzel, *Science (80-.)*. **2016**, *354*, 206.

[8] S. Shahbazi, M. Malekshahi Byranvand, F. Tajabadi, S. Afshar, N. Taghavinia, *ChemPhysChem* **2016**, *17*, 2389.

[9] N. J. Jeon, J. H. Noh, Y. C. Kim, W. S. Yang, S. Ryu, S. Il Seok, *Nat. Mater.* **2014**, *13*, 897.

[10] N. Ahn, D. Y. Son, I. H. Jang, S. M. Kang, M. Choi, N. G. Park, *J. Am. Chem. Soc.* **2015**, *137*, 8696.

[11] M. M. Byranvand, S. Song, L. Pyeon, G. Kang, G. Y. Lee, T. Park, *Nano Energy* **2017**, *34*, 181.

[12] A. K. Jena, A. Kulkarni, T. Miyasaka, *Chem. Rev.* **2019**, *119*, 3036.

[13] M. M. Byranvand, T. Kim, S. Song, G. Kang, S. U. Ryu, T. Park, *Adv. Energy Mater.* **2018**, *8*, 1702235.

[14] M. Malekshahi Byranvand, F. Behboodi-Sadabad, A. Alrhman Eliwi, V. Trouillet, A. Welle, S. Ternes, I. M. Hossain, M. R. Khan, J. A. Schwenzer, A. Farooq, B. S. Richards, J. Lahann, U. W. Paetzold, *J. Mater. Chem. A* **2020**, *8*, 20122.

[15] H. Taherianfard, G.-W. Kim, F. Ebadi, T. Abzieher, K. Choi, U. W. Paetzold, B. S. Richards, A. Alrhman Eliwi, F. Tajabadi, N. Taghavinia, M. Malekshahi Byranvand, *ACS Appl. Mater. Interfaces* **2019**, *11*, 44802.

[16] M. Saliba, J. P. Correa-Baena, M. Grätzel, A. Hagfeldt, A. Abate, *Angew. Chem., Int. Ed.* **2018**, *57*, 2554.

[17] S. D. Stranks, G. E. Eperon, G. Grancini, C. Menelaou, M. J. P. Alcocer, T. Leijtens, L. M. Herz, A. Petrozza, H. J. Snaith, *Science* **2013**, *342*, 341.

[18] Y.-W. Su, S.-C. Lan, K.-H. Wei, *Mater. Today* **2012**, *15*, 554.

[19] N. Gasparini, A. Salleo, I. McCulloch, D. Baran, *Nat. Rev. Mater.* **2019**, *4*, 229.

[20] A. Sahu, A. Garg, A. Dixit, *Sol. Energy* **2020**, *203*, 210.

[21] M. Malekshahi Byranvand, A. Nemati Kharat, L. Fatholahi, Z. Malekshahi Beiranvand, *Optoelectron. Adv. Mater. Rapid Commun.* **2013**, *7*, 961.

[22] B. O'Regan, M. Grätzel, *Nature* **1991**, *353*, 737.

[23] M. Malekshahi Byranvand, A. Nemati Kharat, N. Taghavinia, A. Dabirian, *ACS Appl. Mater. Interfaces* **2016**, *8*, 16359.

[24] A. Dabirian, M. Malekshahi Byranvand, A. Naqavi, A. Nemati Kharat, N. Taghavinia, *ACS Appl. Mater. Interfaces* **2016**, *8*, 247.

[25] P. Rostami, A. Nemati, M. Malekshahi Byranvand, R. Mohammadpour, H. Faridi, *Mater. Lett.* **2015**, *139*, 433.

[26] M. M. Byranvand, N. Taghavinia, A. N. Kharat, A. Dabirian, *RSC Adv.* **2015**, *5*, 86050.

[27] M. M. Byranvand, A. Dabirian, A. N. Kharat, N. Taghavinia, *RSC Adv.* **2015**, *5*, 33098.

[28] M. M. Byranvand, A. N. Kharat, M. H. Bazargan, *Nano-Micro Lett.* **2012**, *4*, 253.

[29] M. H. Bazargan, M. M. Byranvand, A. N. Kharat, *Int. J. Mater. Res.* **2012**, *103*, 347.

[30] N. G. Park, H. Segawa, *ACS Photonics* **2018**, *5*, 2970.

[31] Y. Hou, E. Aydin, M. De Bastiani, C. Xiao, F. H. Isikgor, D. J. Xue, B. Chen, H. Chen, B. Bahrami, A. H. Chowdhury, A. Johnston, S. W. Baek, Z. Huang, M. Wei, Y. Dong, J. Troughton, R. Jalmood, A. J. Mirabelli, T. G. Allen, E. Van Kerschaver, M. I. Saidaminov, D. Baran, Q. Qiao, K. Zhu, S. De Wolf, E. H. Sargent, *Science (80-.)*. **2020**, *367*, 1135.

[32] A. Al-Ashouri, E. Köhnen, B. Li, A. Magomedov, H. Hempel, P. Caprioglio, J. A. Márquez, A. B. Morales Vilches, E. Kasparavicius, J. A. Smith, N. Phung, D. Menzel, M. Grischek, L. Kegelmann, D. Skroblin, C. Gollwitzer, T. Malinauskas, M. Jošt, G. Matič, B. Rech, R. Schlatmann, M. Topič, L. Korte, A. Abate, B. Stannowski, D. Neher, M. Stolterfoht, T. Unold, V. Getautis, S. Albrecht, *Science (80-.)*. **2020**, *370*, 1300.

[33] A. Abate, F. Giordano, J. C. Baena, J. Decoppet, *Sci. Adv.* **2016**, *5*, 1501170.

[34] B. Chen, P. N. Rudd, S. Yang, Y. Yuan, J. Huang, *Chem. Soc. Rev.* **2019**, *48*, 3842.

[35] E. Aydin, M. De Bastiani, S. De Wolf, *Adv. Mater.* **2019**, *31*, 1900428.

[36] D. Luo, R. Su, W. Zhang, Q. Gong, R. Zhu, *Nat. Rev. Mater.* **2019**, *5*, 44.

[37] L. Fu, H. Li, L. Wang, R. Yin, B. Li, L. Yin, *Energy Environ. Sci.* **2020**, *13*, 4017.

[38] W. Tress, N. Marinova, O. Inganäs, M. K. Nazeeruddin, S. M. Zakeeruddin, M. Graetzel, *Adv. Energy Mater.* **2015**, *5*, 1400812.

[39] Q. Jiang, Y. Zhao, X. Zhang, X. Yang, Y. Chen, Z. Chu, Q. Ye, X. Li, Z. Yin, J. You, *Nat. Photonics* **2019**, *13*, 460.

[40] X. Zheng, B. Chen, J. Dai, Y. Fang, Y. Bai, Y. Lin, H. Wei, X. C. Zeng, J. Huang, *Nat. Energy* **2017**, *2*, 17102.

[41] B. C. O'Regan, P. R. F. Barnes, X. Li, C. Law, E. Palomares, J. M. Marin-Beloqui, *J. Am. Chem. Soc.* **2015**, *137*, 5087.

[42] P. Liu, W. Wang, S. Liu, H. Yang, Z. Shao, *Adv. Energy Mater.* **2019**, *9*, 1803017.

[43] G. Grancini, C. Roldán-Carmona, I. Zimmermann, E. Mosconi, X. Lee, D. Martineau, S. Narbey, F. Oswald, F. De Angelis, M. Graetzel, M. K. Nazeeruddin, *Nat. Commun.* **2017**, *8*, 15684.

[44] L. Meng, J. You, Y. Yang, *Nat. Commun.* **2018**, *9*, 5265.

[45] J. Lee, M. Malekshahi Byranvand, G. Kang, S. Y. Son, S. Song, G.-W. Kim, T. Park, *J. Am. Chem. Soc.* **2017**, *139*, 12175.

[46] G.-W. Kim, G. Kang, M. Malekshahi Byranvand, G.-Y. Lee, T. Park, *ACS Appl. Mater. Interfaces* **2017**, *9*, 27720.

[47] J. Lee, T. H. Lee, M. M. Byranvand, K. Choi, H. Il Kim, S. A. Park, J. Y. Kim, T. Park, *J. Mater. Chem. A* **2018**, *6*, 5538.

[48] A. Khorasani, M. Marandi, R. Khosroshahi, M. Malekshahi Byranvand, M. Dehghani, A. I. Zad, F. Tajabadi, N. Taghavinia, *ACS Appl. Mater. Interfaces* **2019**, *11*, 30838.

[49] R. Cheacharoen, C. C. Boyd, G. F. Burkhard, T. Leijtens, J. A. Raiford, K. A. Bush, S. F. Bent, M. D. McGehee, *Sustain. Energy Fuels* **2018**, *2*, 2398.

[50] F. Matteocci, L. Cinà, E. Lamanna, S. Cacovich, G. Divitini, P. A. Midgley, C. Ducati, A. Di Carlo, *Nano Energy* **2016**, *30*, 162.

[51] R. Schmager, J. Roger, J. A. Schwenzer, F. Schackmar, T. Abzieher, M. Malekshahi Byranvand, B. Abdollahi Nejand, M. Worgull, B. S. Richards, U. W. Paetzold, *Adv. Funct. Mater.* **2020**, *30*, 1907481.

[52] C. C. Boyd, R. Cheacharoen, T. Leijtens, M. D. McGehee, *Chem. Rev.* **2019**, *119*, 3418.

[53] C. Li, H. Li, Z. Zhu, N. Cui, Z. Tan, R. Yang, *Sol. RRL* **2021**, *5*, 2000579.

[54] M. Malekshahi Byranvand, M. Saliba, *Matter* **2021**, *4*, 1758.

[55] W.-J. Yin, T. Shi, Y. Yan, *Appl. Phys. Lett.* **2014**, *104*, 63903.

[56] E. M. Tennyson, T. A. S. Doherty, S. D. Stranks, *Nat. Rev. Mater.* **2019**, *4*, 573.

[57] L. Polavarapu, J. Ye, M. M. Byranvand, C. O. Martínez, R. L. Z. Hoye, M. Saliba, *Angew. Chem., Int. Ed.* **2021**, https://doi.org/10.1002/anie.202102360.

[58] W. Tress, N. Marinova, T. Moehl, S. M. Zakeeruddin, N. Mohammad, M. Grätzel, M. K. Nazeeruddin, M. Grätzel, *Energy Environ. Sci.* **2015**, *8*, 995.

[59] D. J. Slotcavage, H. I. Karunadasa, M. D. McGehee, *ACS Energy Lett.* **2016**, *1*, 1199.

[60] Y. Kato, L. K. Ono, M. V. Lee, S. Wang, S. R. Raga, Y. Qi, *Adv. Mater. Interfaces* **2015**, *2*, 1500195.

[61] B. Chen, Z. Yu, K. Liu, X. Zheng, Y. Liu, J. Shi, D. Spronk, P. N. Rudd, Z. Holman, J. Huang, *Joule* **2019**, *3*, 177.

[62] Q. Li, Y. Zhao, R. Fu, W. Zhou, Y. Zhao, X. Liu, D. Yu, Q. Zhao, *Adv. Mater.* **2018**, *30*, 1803095.

[63] W. Zhang, S. Pathak, N. Sakai, T. Stergiopoulos, P. K. Nayak, N. K. Noel, A. A. Haghighirad, V. M. Burlakov, D. W. deQuilettes, A. Sadhanala, W. Li, L. Wang, D. S. Ginger, R. H. Friend, H. J. Snaith, *Nat. Commun.* **2015**, *6*, 10030.

[64] R. Lindblad, D. Bi, B. Park, J. Oscarsson, M. Gorgoi, H. Siegbahn, M. Odelius, E. M. J. Johansson, H. Rensmo, *J. Phys. Chem. Lett.* **2014**, *5*, 648.

[65] D. W. Dequilettes, S. Koch, S. Burke, R. K. Paranji, A. J. Shropshire, M. E. Ziffer, D. S. Ginger, *ACS Energy Lett.* **2016**, *1*, 438.

[66] S. Wang, A. Wang, X. Deng, L. Xie, A. Xiao, C. Li, Y. Xiang, T. Li, L. Ding, F. Hao, *J. Mater. Chem. A* **2020**, *8*, 12201.

[67] M. Abdi-Jalebi, Z. Andaji-Garmaroudi, S. Cacovich, C. Stavrakas, B. Philippe, J. M. Richter, M. Alsari, E. P. Booker, E. M. Hutter, A. J. Pearson, S. Lilliu, T. J. Savenije, H. Rensmo, G. Divitini, C. Ducati, R. H. Friend, S. D. Stranks, *Nature* **2018**, *555*, 497.

[68] M. Qin, J. Cao, T. Zhang, J. Mai, T. K. Lau, S. Zhou, Y. Zhou, J. Wang, Y. J. Hsu, N. Zhao, J. Xu, X. Zhan, X. Lu, *Adv. Energy Mater.* **2018**, *8*, 1703399.

[69] W. Meng, Y. Hou, A. Karl, E. Gu, X. Tang, A. Osvet, K. Zhang, Y. Zhao, X. Du, J. Garcia Cerrillo, N. Li, C. J. Brabec, *ACS Energy Lett.* **2020**, *5*, 271.

[70] W. Q. Wu, Z. Yang, P. N. Rudd, Y. Shao, X. Dai, H. Wei, J. Zhao, Y. Fang, Q. Wang, Y. Liu, Y. Deng, X. Xiao, Y. Feng, J. Huang, *Sci. Adv.* **2019**, *5*, 8925.

[71] M. Li, W. W. Zuo, Q. Wang, K. L. Wang, M. P. Zhuo, H. Köbler, C. E. Halbig, S. Eigler, Y. G. Yang, X. Y. Gao, Z. K. Wang, Y. Li, A. Abate, *Adv. Energy Mater.* **2020**, *10*, 1902653.

[72] N. Ahn, D. Y. Son, I. H. Jang, S. M. Kang, M. Choi, N. G. Park, *J. Am. Chem. Soc.* **2015**, *137*, 8696.

[73] J. W. Lee, H. S. Kim, N. G. Park, *Acc. Chem. Res.* **2016**, *49*, 311.

[74] J.-W. Lee, S.-H. Bae, Y.-T. Hsieh, N. De Marco, M. Wang, P. Sun, Y. Yang, *Chem* **2017**, *3*, 290.

[75] N. J. Jeon, J. H. Noh, Y. C. Kim, W. S. Yang, S. Ryu, S. Il Seok, *Nat. Mater.* **2014**, *13*, 897.

[76] H. Taherianfard, G.-W. Kim, M. Malekshahi Byranvand, K. Choi, G. Kang, H. Choi, F. Tajabadi, N. Taghavinia, T. Park, *ACS Appl. Energy Mater.* **2020**, *3*, 1506.

[77] T. Wu, Y. Wang, X. Li, Y. Wu, X. Meng, D. Cui, X. Yang, L. Han, *Adv. Energy Mater.* **2019**, *9*, 1803766.

[78] J. C. Yu, S. Badgujar, E. D. Jung, V. K. Singh, D. W. Kim, J. Gierschner, E. Lee, Y. S. Kim, S. Cho, M. S. Kwon, M. H. Song, *Adv. Mater.* **2019**, *31*, 1805554.

[79] J. Wang, J. Zhang, Y. Zhou, H. Liu, Q. Xue, X. Li, C. C. Chueh, H. L. Yip, Z. Zhu, A. K. Y. Jen, *Nat. Commun.* **2020**, *11*, 177.

[80] H. Li, J. Shi, J. Deng, Z. Chen, Y. Li, W. Zhao, J. Wu, H. Wu, Y. Luo, D. Li, Q. Meng, *Adv. Mater.* **2020**, *32*, 1907396.

[81] Y. Li, J. Shi, J. Zheng, J. Bing, J. Yuan, Y. Cho, S. Tang, M. Zhang, Y. Yao, C. F. J. Lau, D. S. Lee, C. Liao, M. A. Green, S. Huang, W. Ma, A. W. Y. Ho-Baillie, *Adv. Sci.* **2020**, *7*, 1903368.

[82] N. K. Noel, A. Abate, S. D. Stranks, E. S. Parrott, V. M. Burlakov, A. Goriely, H. J. Snaith, *ACS Nano* **2014**, *8*, 9815.

[83] D. W. DeQuilettes, S. M. Vorpahl, S. D. Stranks, H. Nagaoka, G. E. Eperon, M. E. Ziffer, H. J. Snaith, D. S. Ginger, *Science (80-.).* **2015**, *348*, 683.

[84] F. Wang, W. Geng, Y. Zhou, H. H. Fang, C. J. Tong, M. A. Loi, L. M. Liu, N. Zhao, *Adv. Mater.* **2016**, *28*, 9986.

[85] H. Chen, W. Fu, C. Huang, Z. Zhang, S. Li, F. Ding, M. Shi, C. Z. Li, A. K. Y. Jen, H. Chen, *Adv. Energy Mater.* **2017**, *7*, 1700012.

[86] Z. Wu, Z. Jiang, Z. Liu, A. Jamshaid, L. K. Ono, Y. Qi, *Adv. Energy Mater.* **2020**, *10*, 1903696.

[87] Y. Lin, L. Shen, J. Dai, Y. Deng, Y. Wu, Y. Bai, X. Zheng, J. Wang, Y. Fang, H. Wei, W. Ma, X. C. Zeng, X. Zhan, J. Huang, *Adv. Mater.* **2017**, *29*, 1.

[88] S. Wang, H. Chen, J. Zhang, G. Xu, W. Chen, R. Xue, M. Zhang, Y. Li, Y. Li, *Adv. Mater.* **2019**, *31*, 1903691.

[89] Z. Yang, J. Dou, S. Kou, J. Dang, Y. Ji, G. Yang, W. Q. Wu, D. Bin Kuang, M. Wang, *Adv. Funct. Mater.* **2020**, *30*, 1910710.

[90] I. L. Braly, D. W. Dequilettes, L. M. Pazos-Outón, S. Burke, M. E. Ziffer, D. S. Ginger, H. W. Hillhouse, *Nat. Photonics* **2018**, *12*, 355.

[91] S. Yang, S. Chen, E. Mosconi, Y. Fang, X. Xiao, C. Wang, Y. Zhou, Z. Yu, J. Zhao, Y. Gao, F. De Angelis, J. Huang, *Science (80-.).* **2019**, *365*, 473.

[92] Z. Ni, C. Bao, Y. Liu, Q. Jiang, W. Q. Wu, S. Chen, X. Dai, B. Chen, B. Hartweg, Z. Yu, Z. Holman, J. Huang, *Science (80-.).* **2020**, *367*, 1352.

[93] F. Gao, Y. Zhao, X. Zhang, J. You, *Adv. Energy Mater.* **2020**, *10*, 1902650.

[94] L. Zuo, H. Guo, D. W. DeQuilettes, S. Jariwala, N. De Marco, S. Dong, R. DeBlock, D. S. Ginger, B. Dunn, M. Wang, Y. Yang, *Sci. Adv.* **2017**, *3*, 1700106.

[95] X. Li, W. Zhang, W. Zhang, H. Q. Wang, J. Fang, *Nano Energy* **2019**, *58*, 825.

[96] Y. Zhao, P. Zhu, M. Wang, S. Huang, Z. Zhao, S. Tan, T.-H. Han, J.-W. Lee, T. Huang, R. Wang, J. Xue, D. Meng, Y. Huang, J. Marian, J. Zhu, Y. Yang, *Adv. Mater.* **2020**, *32*, 1907769.

[97] Y. Zhao, J. Wei, H. Li, Y. Yan, W. Zhou, D. Yu, Q. Zhao, *Nat. Commun.* **2016**, *7*, 10228.

[98] D. Bi, C. Yi, J. Luo, J.-D. Décoppet, F. Zhang, S. M. Zakeeruddin, X. Li, A. Hagfeldt, M. Grätzel, *Nat. Energy* **2016**, *1*, 16142.

[99] L. Meng, C. Sun, R. Wang, W. Huang, Z. Zhao, P. Sun, T. Huang, J. Xue, J. W. Lee, C. Zhu, Y. Huang, Y. Li, Y. Yang, *J. Am. Chem. Soc.* **2018**, *140*, 17255.

[100] P.-L. Qin, G. Yang, Z. Ren, S. H. Cheung, S. K. So, L. Chen, J. Hao, J. Hou, G. Li, *Adv. Mater.* **2018**, *1706126*, 1706126.

[101] F. Li, J. Yuan, X. Ling, Y. Zhang, Y. Yang, S. H. Cheung, C. H. Y. Ho, X. Gao, W. Ma, *Adv. Funct. Mater.* **2018**, *28*, 1706377.

[102] W. Chen, Y. Wang, G. Pang, C. W. Koh, A. B. Djurišić, Y. Wu, B. Tu, F. Z. Liu, R. Chen, H. Y. Woo, X. Guo, Z. He, *Adv. Funct. Mater.* **2019**, *29*, 1808855.

[103] F. Tan, H. Tan, M. I. Saidaminov, M. Wei, M. Liu, A. Mei, P. Li, B. Zhang, C. S. Tan, X. Gong, Y. Zhao, A. R. Kirmani, Z. Huang, J. Z. Fan, R. Quintero-Bermudez, J. Kim, Y. Zhao, O. Voznyy, Y. Gao, F. Zhang, L. J. Richter, Z. H. Lu, W. Zhang, E. H. Sargent, *Adv. Mater.* **2019**, *31*, 1807435.

[104] T. H. Han, J. W. Lee, C. Choi, S. Tan, C. Lee, Y. Zhao, Z. Dai, N. De Marco, S. J. Lee, S. H. Bae, Y. Yuan, H. M. Lee, Y. Huang, Y. Yang, *Nat. Commun.* **2019**, *10*, 520.

[105] M. Kim, S. G. Motti, R. Sorrentino, A. Petrozza, *Energy Environ. Sci.* **2018**, *11*, 2609.

[106] B. Chaudhary, A. Kulkarni, A. K. Jena, M. Ikegami, Y. Udagawa, H. Kunugita, K. Ema, T. Miyasaka, *ChemSusChem* **2017**, *10*, 2473.

[107] J. Peng, J. I. Khan, W. Liu, E. Ugur, T. Duong, Y. Wu, H. Shen, K. Wang, H. Dang, E. Aydin, X. Yang, Y. Wan, K. J. Weber,

K. R. Catchpole, F. Laquai, S. De Wolf, T. P. White, *Adv. Energy Mater.* **2018**, *8*, 1801208.

[108] F. Yang, H. E. Lim, F. Wang, M. Ozaki, A. Shimazaki, J. Liu, N. B. Mohamed, K. Shinokita, Y. Miyauchi, A. Wakamiya, Y. Murata, K. Matsuda, *Adv. Mater. Interfaces* **2018**, *5*, 1701256.

[109] Q. Zeng, X. Zhang, X. Feng, S. Lu, Z. Chen, X. Yong, S. A. T. Redfern, H. Wei, H. Wang, H. Shen, W. Zhang, W. Zheng, H. Zhang, J. S. Tse, B. Yang, *Adv. Mater.* **2018**, *30*, 1.

[110] H. Kanda, N. Shibayama, A. J. Huckaba, Y. Lee, S. Paek, N. Klipfel, C. Roldán-Carmona, V. I. E. Queloz, G. Grancini, Y. Zhang, M. Abuhelaiqa, K. T. Cho, M. Li, M. D. Mensi, S. Kinge, M. K. Nazeeruddin, *Energy Environ. Sci.* **2020**, *13*, 1222.

[111] L. Zuo, H. Guo, D. W. deQuilettes, S. Jariwala, N. De Marco, S. Dong, R. DeBlock, D. S. Ginger, B. Dunn, M. Wang, Y. Yang, *Sci. Adv.* **2017**, *3*, 1700106.

[112] X. Li, W. Zhang, W. Zhang, H.-Q. Wang, J. Fang, *Nano Energy* **2019**, *58*, 825.

[113] D. Bi, C. Yi, J. Luo, J. D. Décoppet, F. Zhang, S. M. Zakeeruddin, X. Li, A. Hagfeldt, M. Grätzel, *Nat. Energy* **2016**, *1*, 16142.

[114] J. Peng, J. I. Khan, W. Liu, E. Ugur, T. Duong, Y. Wu, H. Shen, K. Wang, H. Dang, E. Aydin, X. Yang, Y. Wan, K. J. Weber, K. R. Catchpole, F. Laquai, S. De Wolf, T. P. White, *Adv. Energy Mater.* **2018**, *8*, 1801208.

[115] M. Kim, S. G. Motti, R. Sorrentino, A. Petrozza, *Energy Environ. Sci.* **2018**, *11*, 2609.

[116] T. Niu, J. Lu, R. Munir, J. Li, D. Barrit, X. Zhang, H. Hu, Z. Yang, A. Amassian, K. Zhao, S. (Frank) Liu, *Adv. Mater.* **2018**, *30*, 1706576.

[117] B. Chaudhary, A. Kulkarni, A. K. Jena, M. Ikegami, Y. Udagawa, H. Kunugita, K. Ema, T. Miyasaka, *ChemSusChem* **2017**, *10*, 2473.

[118] M. Yavari, M. Mazloum-Ardakani, S. Gholipour, M. M. Tavakoli, N. Taghavinia, A. Hagfeldt, W. Tress, *ACS Omega* **2018**, *3*, 5038.

[119] F. Wang, A. Shimazaki, F. Yang, K. Kanahashi, K. Matsuki, Y. Miyauchi, T. Takenobu, A. Wakamiya, Y. Murata, K. Matsuda, *J. Phys. Chem. C* **2017**, *121*, 1562.

[120] F. Yang, H. E. Lim, F. Wang, M. Ozaki, A. Shimazaki, J. Liu, N. B. Mohamed, K. Shinokita, Y. Miyauchi, A. Wakamiya, Y. Murata, K. Matsuda, *Adv. Mater. Interfaces* **2018**, *5*, 1701256.

[121] Q. Zeng, X. Zhang, X. Feng, S. Lu, Z. Chen, X. Yong, S. A. T. Redfern, H. Wei, H. Wang, H. Shen, W. Zhang, W. Zheng, H. Zhang, J. S. Tse, B. Yang, *Adv. Mater.* **2018**, *30*, 1.

[122] M. I. Saidaminov, J. Kim, A. Jain, R. Quintero-Bermudez, H. Tan, G. Long, F. Tan, A. Johnston, Y. Zhao, O. Voznyy, E. H. Sargent, *Nat. Energy* **2018**, *3*, 648.

[123] J. H. Heo, D. H. Song, H. J. Han, S. Y. Kim, J. H. Kim, D. Kim, H. W. Shin, T. K. Ahn, C. Wolf, T.-W. Lee, S. H. Im, *Adv. Mater.* **2015**, *27*, 3424.

[124] G. A. H. Wetzelaer, M. Scheepers, A. M. Sempere, C. Momblona, J. Ávila, H. J. Bolink, *Adv. Mater.* **2015**, *27*, 1837.

[125] D.-Y. Son, S.-G. Kim, J.-Y. Seo, S.-H. Lee, H. Shin, D. Lee, N.-G. Park, *J. Am. Chem. Soc.* **2018**, *140*, 1358.

[126] F. Wang, M. Yang, S. Yang, X. Qu, L. Yang, L. Fan, J. Yang, F. Rosei, *Nano Energy* **2020**, *67*, 104224.

[127] Q. Jiang, Y. Zhao, X. Zhang, X. Yang, Y. Chen, Z. Chu, Q. Ye, X. Li, Z. Yin, J. You, *Nat. Photonics* **2019**, *13*, 500.

[128] P. Chen, Y. Bai, S. Wang, M. Lyu, J. H. Yun, L. Wang, *Adv. Funct. Mater.* **2018**, *28*, 1706923.

[129] Y. Cho, A. M. Soufiani, J. S. Yun, J. Kim, D. S. Lee, J. Seidel, X. Deng, M. A. Green, S. Huang, A. W. Y. Ho-Baillie, *Adv. Energy Mater.* **2018**, *8*, 1703392.

[130] K. T. Cho, G. Grancini, Y. Lee, E. Oveisi, J. Ryu, O. Almora, M. Tschumi, P. A. Schouwink, G. Seo, S. Heo, J. Park, J. Jang, S. Paek, G. Garcia-Belmonte, M. K. Nazeeruddin, *Energy Environ. Sci.* **2018**, *11*, 952.

[131] Y. Lin, Y. Bai, Y. Fang, Z. Chen, S. Yang, *J. Phys. Chem. Lett.* **2018**, *9*, 654.

[132] H.-S. Yoo, N.-G. Park, *Sol. Energy Mater. Sol. Cells* **2018**, *179*, 57.

[133] N. Li, Z. Zhu, Q. Dong, J. Li, Z. Yang, C. C. Chueh, A. K. Y. Jen, L. Wang, *Adv. Mater. Interfaces* **2017**, *4*, 1700598.

[134] S. D. Stranks, H. J. Snaith, *Nat. Nanotechnol.* **2015**, *10*, 391.

[135] Y. Tidhar, E. Edri, H. Weissman, D. Zohar, G. Hodes, D. Cahen, B. Rybtchinski, S. Kirmayer, *J. Am. Chem. Soc.* **2014**, *136*, 13249.

[136] Q. Chen, H. Zhou, Y. Fang, A. Z. Stieg, T. Bin Song, H. H. Wang, X. Xu, Y. Liu, S. Lu, J. You, P. Sun, J. McKay, M. S. Goorsky, Y. Yang, *Nat. Commun.* **2015**, *6*, 7269.

[137] F. Xie, C.-C. Chen, Y. Wu, X. Li, M. Cai, X. Liu, X. Yang, L. Han, *Energy Environ. Sci.* **2017**, *10*, 1942.

[138] J. I. Uribe, J. Ciro, J. F. Montoya, J. Osorio, F. Jaramillo, *ACS Appl. Energy Mater.* **2018**, *1*, 1047.

[139] M. Kim, G. H. Kim, T. K. Lee, I. W. Choi, H. W. Choi, Y. Jo, Y. J. Yoon, J. W. Kim, J. Lee, D. Huh, H. Lee, S. K. Kwak, J. Y. Kim, D. S. Kim, *Joule* **2019**, *3*, 2179.

[140] D. B. Khadka, Y. Shirai, M. Yanagida, T. Masuda, K. Miyano, *Sustain. Energy Fuels* **2017**, *1*, 755.

[141] F. Xie, C.-C. Chen, Y. Wu, X. Li, M. Cai, X. Liu, X. Yang, L. Han, *Energy Environ. Sci.* **2017**, *10*, 1942.

[142] Z. Liu, L. Qiu, E. J. Juarez-Perez, Z. Hawash, T. Kim, Y. Jiang, Z. Wu, S. R. Raga, L. K. Ono, S. (Frank) Liu, Y. Qi, *Nat. Commun.* **2018**, *9*, 3880.

[143] T. Leijtens, R. Prasanna, K. A. Bush, G. E. Eperon, J. A. Raiford, A. Gold-Parker, E. J. Wolf, S. A. Swifter, C. C. Boyd, H.-P. Wang, M. F. Toney, S. F. Bent, M. D. McGehee, *Sustain. Energy Fuels* **2018**, *2*, 2450.

[144] T. Hwang, A. J. Yun, B. Lee, J. Kim, Y. Lee, B. Park, *J. Appl. Phys.* **2019**, *126*, 23101.

[145] E. L. Unger, A. R. Bowring, C. J. Tassone, V. Pool, A. Gold-Parker, R. Cheacharoen, K. H. Stone, E. T. Hoke, M. F. Toney, M. D. McGehee, *Chem. Mater.* **2014**, *26*, 7158.

[146] M. M. Tavakoli, P. Yadav, D. Prochowicz, M. Sponseller, A. Osherov, V. Bulović, J. Kong, *Adv. Energy Mater.* **2019**, *9*, 1803587.

[147] D. Prochowicz, R. Runjhun, M. M. Tavakoli, P. Yadav, M. Saski, A. Q. Alanazi, D. J. Kubicki, Z. Kaszkur, S. M. Zakeeruddin, J. Lewiński, M. Grätzel, *Chem. Mater.* **2019**, *31*, 1620.

[148] A. Ren, H. Lai, X. Hao, Z. Tang, H. Xu, B. M. F. Yu Jeco, K. Watanabe, L. Wu, J. Zhang, M. Sugiyama, J. Wu, D. Zhao, *Joule* **2020**, *4*, 1263.

[149] M. M. Lee, J. Teuscher, T. Miyasaka, T. N. Murakami, H. J. Snaith, *Science* **2012**, *338*, 643.

[150] D. Zhao, C. Chen, C. Wang, M. M. Junda, Z. Song, C. R. Grice, Y. Yu, C. Li, B. Subedi, N. J. Podraza, X. Zhao, G. Fang, R. G. Xiong, K. Zhu, Y. Yan, *Nat. Energy* **2018**, *3*, 1093.

[151] J. Xu, C. C. Boyd, Z. J. Yu, A. F. Palmstrom, D. J. Witter, B. W. Larson, R. M. France, J. Werner, S. P. Harvey, E. J. Wolf, W. Weigand, S. Manzoor, M. F. A. M. Van Hest, J. J. Berry, J. M. Luther, Z. C. Holman, M. D. McGehee, *Science (80-.)* **2020**, *367*, 1097.

[152] M. Anaya, G. Lozano, M. E. Calvo, H. Míguez, *Joule* **2017**, *1*, 769.

[153] R. D. J. Oliver, Y.-H. Lin, A. J. Horn, C. Q. Xia, J. H. Warby, M. B. Johnston, A. J. Ramadan, H. J. Snaith, *ACS Energy Lett.* **2020**, *5*, 3336.

[154] I. Chung, B. Lee, J. He, R. P. H. Chang, M. G. Kanatzidis, *Nature* **2012**, *485*, 486.

[155] N. Li, S. Tao, Y. Chen, X. Niu, C. K. Onwudinanti, C. Hu, Z. Qiu, Z. Xu, G. Zheng, L. Wang, Y. Zhang, L. Li, H. Liu, Y. Lun, J. Hong, X. Wang, Y. Liu, H. Xie, Y. Gao, Y. Bai, S. Yang, G. Brocks, Q. Chen, H. Zhou, *Nat. Energy* **2019**, *4*, 408.

[156] X. Yi, Z. Zhang, A. Chang, Y. Mao, Y. Luan, T. Lin, Y. Wei, Y. Zhang, F. Wang, S. Cao, C. Li, J. Wang, *Adv. Energy Mater.* **2019**, *9*, 1.

[157] S. Nagane, U. Bansode, O. Game, S. Chhatre, S. Ogale, *Chem. Commun.* **2014**, *50*, 9741.

[158] J. Chen, Y. Rong, A. Mei, Y. Xiong, T. Liu, Y. Sheng, P. Jiang, L. Hong, Y. Guan, X. Zhu, X. Hou, M. Duan, J. Zhao, X. Li, H. Han, *Adv. Energy Mater.* **2016**, *6*, 1502009.

[159] Q. Jiang, D. Rebollar, J. Gong, E. L. Piacentino, C. Zheng, T. Xu, *Angew. Chem., Int. Ed.* **2015**, *54*, 7617.

[160] H. Lu, Y. Liu, P. Ahlawat, A. Mishra, W. R. Tress, F. T. Eickemeyer, Y. Yang, F. Fu, Z. Wang, C. E. Avalos, B. I. Carlsen, A. Agarwalla, X. Zhang, X. Li, Y. Zhan, S. M. Zakeeruddin, L. Emsley, U. Rothlisberger, L. Zheng, A. Hagfeldt, M. Grätzel, *Science (80-.).* **2020**, *370*, 8985.

[161] J. Chen, S.-G. Kim, N.-G. Park, *Adv. Mater.* **2018**, *30*, 1801948.

[162] T. J. Jacobsson, M. Pazoki, A. Hagfeldt, T. Edvinsson, *J. Phys. Chem. C* **2015**, *119*, 25673.

[163] M. Pazoki, T. J. Jacobsson, A. Hagfeldt, G. Boschloo, T. Edvinsson, *Phys. Rev. B* **2016**, *93*, 144105.

[164] J. Navas, A. Sánchez-Coronilla, J. J. Gallardo, N. Cruz Hernández, J. C. Piñero, R. Alcántara, C. Fernández-Lorenzo, D. M. De Los Santos, T. Aguilar, J. Martín-Calleja, *Nanoscale* **2015**, *7*, 6216.

[165] F. Yang, M. A. Kamarudin, G. Kapil, D. Hirotani, P. Zhang, C. H. Ng, T. Ma, S. Hayase, *ACS Appl. Mater. Interfaces* **2018**, *10*, 24543.

[166] Q. Huang, Y. Zou, S. A. Bourelle, T. Zhai, T. Wu, Y. Tan, Y. Li, J. Li, S. Duhm, T. Song, L. Wang, F. Deschler, B. Sun, *Nanoscale Horizons* **2019**, *4*, 924.

[167] S.-H. Chan, M.-C. Wu, K.-M. Lee, W.-C. Chen, T.-H. Lin, W.-F. Su, *J. Mater. Chem. A* **2017**, *5*, 18044.

[168] S. S. Mali, J. V. Patil, C. K. Hong, *Nano Lett.* **2019**, *19*, 6213.

[169] W. Q. Wu, P. N. Rudd, Z. Ni, C. H. Van Brackle, H. Wei, Q. Wang, B. R. Ecker, Y. Gao, J. Huang, *J. Am. Chem. Soc.* **2020**, *142*, 3989.

[170] L. Chen, L. Wan, X. Li, W. Zhang, S. Fu, Y. Wang, S. Li, H. Q. Wang, W. Song, J. Fang, *Chem. Mater.* **2019**, *31*, 9032.

[171] X. Gong, L. Guan, H. Pan, Q. Sun, X. Zhao, H. Li, H. Pan, Y. Shen, Y. Shao, L. Sun, Z. Cui, L. Ding, M. Wang, *Adv. Funct. Mater.* **2018**, *28*, 1804286.

[172] M. T. Klug, A. Osherov, A. A. Haghighirad, S. D. Stranks, P. R. Brown, S. Bai, J. T.-W. Wang, X. Dang, V. Bulović, H. J. Snaith, A. M. Belcher, *Energy Environ. Sci.* **2017**, *10*, 236.

[173] P. Liu, X. Yang, Y. Chen, H. Xiang, W. Wang, R. Ran, W. Zhou, Z. Shao, *ACS Appl. Mater. Interfaces* **2020**, *12*, 23984.

[174] J. Duan, Y. Zhao, X. Yang, Y. Wang, B. He, Q. Tang, *Adv. Energy Mater.* **2018**, *8*, 1802346.

[175] J. T. W. Wang, Z. Wang, S. Pathak, W. Zhang, D. W. Dequilettes, F. Wisnivesky-Rocca-Rivarola, J. Huang, P. K. Nayak, J. B. Patel, H. A. Mohd Yusof, Y. Vaynzof, R. Zhu, I. Ramirez, J. Zhang, C. Ducati, C. Grovenor, M. B. Johnston, D. S. Ginger, R. J. Nicholas, H. J. Snaith, *Energy Environ. Sci.* **2016**, *9*, 2892.

[176] N. Phung, R. Félix, D. Meggiolaro, A. Al-Ashouri, G. Sousa, E. Silva, C. Hartmann, J. Hidalgo, H. Köbler, E. Mosconi, B. Lai, R. Gunder, M. Li, K. L. Wang, Z. K. Wang, K. Nie, E. Handick, R. G. Wilks, J. A. Marquez, B. Rech, T. Unold, J. P. Correa-Baena, S. Albrecht, F. De Angelis, M. Bär, A. Abate, *J. Am. Chem. Soc.* **2020**, *142*, 2364.

[177] Z. Liu, J. Hu, H. Jiao, L. Li, G. Zheng, Y. Chen, Y. Huang, Q. Zhang, C. Shen, Q. Chen, H. Zhou, *Adv. Mater.* **2017**, *29*, 1.

[178] C. Qin, T. Matsushima, T. Fujihara, C. Adachi, *Adv. Mater.* **2017**, *29*, 1.

[179] L. Wang, H. Zhou, J. Hu, B. Huang, M. Sun, B. Dong, G. Zheng, Y. Huang, Y. Chen, L. Li, Z. Xu, N. Li, Z. Liu, Q. Chen, L.-D. Sun, C.-H. Yan, *Science (80-.).* **2019**, *363*, 265.

[180] Y. Yang, J. Wu, X. Wang, Q. Guo, X. Liu, W. Sun, Y. Wei, Y. Huang, Z. Lan, M. Huang, J. Lin, H. Chen, Z. Wei, *Adv. Mater.* **2020**, *32*, 1.

[181] M. H. Kumar, S. Dharani, W. L. Leong, P. P. Boix, R. R. Prabhakar, T. Baikie, C. Shi, H. Ding, R. Ramesh, M. Asta, M. Graetzel, S. G. Mhaisalkar, N. Mathews, *Adv. Mater.* **2014**, *26*, 7122.

[182] S. J. Lee, S. S. Shin, Y. C. Kim, D. Kim, T. K. Ahn, J. H. Noh, J. Seo, S. Il Seok, *J. Am. Chem. Soc.* **2016**, *138*, 3974.

[183] E. Jokar, C. H. Chien, A. Fathi, M. Rameez, Y. H. Chang, E. W. G. Diau, *Energy Environ. Sci.* **2018**, *11*, 2353.

[184] Q. Tai, X. Guo, G. Tang, P. You, T.-W. Ng, D. Shen, J. Cao, C.-K. Liu, N. Wang, Y. Zhu, C.-S. Lee, F. Yan, *Angew. Chem., Int. Ed.* **2019**, *58*, 806.

[185] R. Lin, K. Xiao, Z. Qin, Q. Han, C. Zhang, M. Wei, M. I. Saidaminov, Y. Gao, J. Xu, M. Xiao, A. Li, J. Zhu, E. H. Sargent, H. Tan, *Nat. Energy* **2019**, *4*, 864.

[186] K. Xiao, R. Lin, Q. Han, Y. Hou, Z. Qin, H. T. Nguyen, J. Wen, M. Wei, V. Yeddu, M. I. Saidaminov, Y. Gao, X. Luo, Y. Wang, H. Gao, C. Zhang, J. Xu, J. Zhu, E. H. Sargent, H. Tan, *Nat. Energy* **2020**, *5*, 870.

[187] T. Nakamura, S. Yakumaru, M. A. Truong, K. Kim, J. Liu, S. Hu, K. Otsuka, R. Hashimoto, R. Murdey, T. Sasamori, H. Do Kim, H. Ohkita, T. Handa, Y. Kanemitsu, A. Wakamiya, *Nat. Commun.* **2020**, *11*, 3008.

[188] R. C. Haddon, R. E. Palmer, H. W. Kroto, P. A. Sermon, H. W. Kroto, A. L. Mackay, G. Turner, D. R. M. Walton, *Philos. Trans. R. Soc. London. Ser. A Phys. Eng. Sci.* **1993**, *343*, 53.

[189] J. Xu, A. Buin, A. H. Ip, W. Li, O. Voznyy, R. Comin, M. Yuan, S. Jeon, Z. Ning, J. J. McDowell, P. Kanjanaboos, J.-P. Sun, X. Lan, L. N. Quan, D. H. Kim, I. G. Hill, P. Maksymovych, E. H. Sargent, *Nat. Commun.* **2015**, *6*, 7081.

[190] M. Li, Y. G. Yang, Z. K. Wang, T. Kang, Q. Wang, S. H. Turren-Cruz, X. Y. Gao, C. S. Hsu, L. S. Liao, A. Abate, *Adv. Mater.* **2019**, *31*, 1901519.

[191] W. Yao, S. Fang, Y. Wang, Z. Hu, L. Huang, X. Liu, T. Jiang, J. Zhang, J. Wang, Y. Zhu, *Appl. Phys. Lett.* **2021**, *118*, 123502.

[192] Y. Shao, Z. Xiao, C. Bi, Y. Yuan, J. Huang, *Nat. Commun.* **2014**, *5*, 5784.

[193] Y. Lin, B. Chen, F. Zhao, X. Zheng, Y. Deng, Y. Shao, Y. Fang, Y. Bai, C. Wang, J. Huang, *Adv. Mater.* **2017**, *29*, 1700607.

[194] T. Ahmad, B. Wilk, E. Radicchi, R. Fuentes Pineda, P. Spinelli, J. Herterich, L. A. Castriotta, S. Dasgupta, E. Mosconi, F. De Angelis, M. Kohlstädt, U. Würfel, A. Di Carlo, K. Wojciechowski, *Adv. Funct. Mater.* **2020**, *30*, 2004357.

[195] A. Rajagopal, P. W. Liang, C. C. Chueh, Z. Yang, A. K. Y. Jen, *ACS Energy Lett.* **2017**, *2*, 2531.

[196] F. Zhang, W. Shi, J. Luo, N. Pellet, C. Yi, X. Li, X. Zhao, T. J. S. Dennis, X. Li, S. Wang, Y. Xiao, S. M. Zakeeruddin, D. Bi, M. Grätzel, *Adv. Mater.* **2017**, *29*, 1606806.

[197] S. R. Ha, W. H. Jeong, Y. Liu, J. T. Oh, S. Y. Bae, S. Lee, J. W. Kim, S. Bandyopadhyay, H. I. Jeong, J. Y. Kim, Y. Kim, M. H. Song, S. H. Park, S. D. Stranks, B. R. Lee, R. H. Friend, H. Choi, *J. Mater. Chem. A* **2020**, *8*, 1326.

[198] A. Abate, M. Saliba, D. J. Hollman, S. D. Stranks, K. Wojciechowski, R. Avolio, G. Grancini, A. Petrozza, H. J. Snaith, *Nano Lett.* **2014**, *14*, 3247.

[199] C. M. Wolff, L. Canil, C. Rehermann, N. Ngoc Linh, F. Zu, M. Ralaiarisoa, P. Caprioglio, L. Fiedler, M. Stolterfoht, S. Kogikoski, I. Bald, N. Koch, E. L. Unger, T. Dittrich, A. Abate, D. Neher, *ACS Nano* **2020**, *14*, 1445.

[200] M. A. Ruiz-Preciado, D. J. Kubicki, A. Hofstetter, L. McGovern, M. H. Futscher, A. Ummadisingu, R. Gershoni-Poranne, S. M. Zakeeruddin, B. Ehrler, L. Emsley, J. V. Milić, M. Grätzel, *J. Am. Chem. Soc.* **2020**, *142*, 1645.

[201] A. D. Jodlowski, C. Roldán-Carmona, G. Grancini, M. Salado, M. Ralaiarisoa, S. Ahmad, N. Koch, L. Camacho, G. De Miguel, M. K. Nazeeruddin, *Nat. Energy* **2017**, *2*, 972.

[202] R. J. Stoddard, A. Rajagopal, R. L. Palmer, I. L. Braly, A. K.-Y. Jen, H. W. Hillhouse, *ACS Energy Lett.* **2018**, *3*, 1261.

[203] N. D. Pham, C. Zhang, V. T. Tiong, S. Zhang, G. Will, A. Bou, J. Bisquert, P. E. Shaw, A. Du, G. J. Wilson, H. Wang, *Adv. Funct. Mater.* **2019**, *29*, 1806479.

[204] S. Wu, Z. Li, J. Zhang, T. Liu, Z. Zhu, A. K. Y. Jen, *Chem. Commun.* **2019**, *55*, 4315.

[205] D. J. Kubicki, D. Prochowicz, A. Hofstetter, M. Saski, P. Yadav, D. Bi, N. Pellet, J. Lewiński, S. M. Zakeeruddin, M. Grätzel, L. Emsley, *J. Am. Chem. Soc.* **2018**, *140*, 3345.

[206] N. De Marco, H. Zhou, Q. Chen, P. Sun, Z. Liu, L. Meng, E. P. Yao, Y. Liu, A. Schiffer, Y. Yang, *Nano Lett.* **2016**, *16*, 1009.

[207] H. Min, M. Kim, S. U. Lee, H. Kim, G. Kim, K. Choi, J. H. Lee, S. Il Seok, *Science (80-.)* **2019**, *366*, 749.

[208] G. Kim, H. Min, K. S. Lee, D. Y. Lee, S. M. Yoon, S. Il Seok, *Science (80-.)* **2020**, *370*, 108.

[209] Y. Chen, S. Yu, Y. Sun, Z. Liang, *J. Phys. Chem. Lett.* **2018**, *9*, 2627.

[210] H. Tsai, W. Nie, J. C. Blancon, C. C. Stoumpos, R. Asadpour, B. Harutyunyan, A. J. Neukirch, R. Verduzco, J. J. Crochet, S. Tretiak, L. Pedesseau, J. Even, M. A. Alam, G. Gupta, J. Lou, P. M. Ajayan, M. J. Bedzyk, M. G. Kanatzidis, A. D. Mohite, *Nature* **2016**, *536*, 312.

[211] Q. Luo, H. Ma, Q. Hou, Y. Li, J. Ren, X. Dai, Z. Yao, Y. Zhou, L. Xiang, H. Du, H. He, N. Wang, K. Jiang, H. Lin, **2018**, *28*, 1706777.

[212] T. Niu, J. Lu, M.-C. Tang, D. Barrit, D.-M. Smilgies, Z. Yang, J. Li, Y. Fan, T. Luo, I. McCulloch, A. Amassian, S. (Frank) Liu, K. Zhao, *Energy Environ. Sci.* **2018**, *11*, 3358.

[213] Z. Wang, Q. Lin, F. P. Chmiel, N. Sakai, L. M. Herz, H. J. Snaith, *Nat. Energy* **2017**, *2*, 17132.

[214] H. Ren, S. Yu, L. Chao, Y. Xia, Y. Sun, S. Zuo, F. Li, T. Niu, Y. Yang, H. Ju, B. Li, H. Du, X. Gao, J. Zhang, J. Wang, L. Zhang, Y. Chen, W. Huang, *Nat. Photonics* **2020**, *14*, 154.

[215] D. S. Lee, J. S. Yun, J. Kim, A. M. Soufiani, S. Chen, Y. Cho, X. Deng, J. Seidel, S. Lim, S. Huang, A. W. Y. Ho-Baillie, *ACS Energy Lett.* **2018**, *3*, 647.

[216] W.-Q. Wu, P. N. Rudd, Q. Wang, Z. Yang, J. Huang, *Adv. Mater.* **2020**, *32*, 2000995.

[217] M. Jung, T. J. Shin, J. Seo, G. Kim, S. Il Seok, *Energy Environ. Sci.* **2018**, *11*, 2188.

[218] M. Chen, Q. Dong, F. T. Eickemeyer, Y. Liu, Z. Dai, A. D. Carl, B. Bahrami, A. H. Chowdhury, R. L. Grimm, Y. Shi, Q. Qiao, S. M. Zakeeruddin, M. Grätzel, N. P. Padture, *ACS Energy Lett.* **2020**, *5*, 2223.

[219] H. Kim, S. U. Lee, D. Y. Lee, M. J. Paik, H. Na, J. Lee, S. Il Seok, *Adv. Energy Mater.* **2019**, *9*, 1902740.

[220] T. Niu, J. Lu, X. Jia, Z. Xu, M. C. Tang, D. Barrit, N. Yuan, J. Ding, X. Zhang, Y. Fan, T. Luo, Y. Zhang, D. M. Smilgies, Z. Liu, A. Amassian, S. Jin, K. Zhao, S. Liu, *Nano Lett.* **2019**, *19*, 7181.

[221] A. H. Proppe, M. Wei, B. Chen, R. Quintero-Bermudez, S. O. Kelley, E. H. Sargent, *J. Am. Chem. Soc.* **2019**, *141*, 14180.

[222] J. Cao, C. Li, X. Lv, X. Feng, R. Meng, Y. Wu, Y. Tang, *J. Am. Chem. Soc.* **2018**, *140*, 11577.

[223] J. J. Yoo, S. Wieghold, M. C. Sponseller, M. R. Chua, S. N. Bertram, N. T. P. Hartono, J. S. Tresback, E. C. Hansen, J. P. Correa-Baena, V. Bulović, T. Buonassisi, S. S. Shin, M. G. Bawendi, *Energy Environ. Sci.* **2019**, *12*, 2192.

[224] Y. Bai, S. Xiao, C. Hu, T. Zhang, X. Meng, H. Lin, Y. Yang, S. Yang, *Adv. Energy Mater.* **2017**, *7*, 1701038.

[225] M. Wei, K. Xiao, G. Walters, R. Lin, Y. Zhao, M. I. Saidaminov, P. Todorović, A. Johnston, Z. Huang, H. Chen, A. Li, J. Zhu, Z. Yang, Y. K. Wang, A. H. Proppe, S. O. Kelley, Y. Hou, O. Voznyy, H. Tan, E. H. Sargent, *Adv. Mater.* **2020**, *32*, 1907058.

[226] Z. Li, M. Yang, J.-S. Park, S.-H. Wei, J. J. Berry, K. Zhu, *Chem. Mater.* **2016**, *28*, 284.

[227] M. Saliba, T. Matsui, J.-Y. Seo, K. Domanski, J.-P. Correa-Baena, M. K. Nazeeruddin, S. M. Zakeeruddin, W. Tress, A. Abate, A. Hagfeldt, M. Gratzel, *Energy Environ. Sci.* **2016**, *9*, 1989.

[228] M. Saliba, M. Saliba, T. Matsui, K. Domanski, J. Seo, A. Ummadisingu, **2016**, *354*, 206.

[229] X. Li, M. Ibrahim Dar, C. Yi, J. Luo, M. Tschumi, S. M. Zakeeruddin, M. K. Nazeeruddin, H. Han, M. Grätzel, *Nat. Chem.* **2015**, *7*, 703.

[230] S. Fu, X. Li, L. Wan, Y. Wu, W. Zhang, Y. Wang, Q. Bao, J. Fang, *Adv. Energy Mater.* **2019**, *9*, 1901852.

[231] J. Yang, C. Liu, C. Cai, X. Hu, Z. Huang, X. Duan, X. Meng, Z. Yuan, L. Tan, Y. Chen, *Adv. Energy Mater.* **2019**, *9*, 1900198.

[232] K. Choi, J. Lee, H. Il Kim, C. W. Park, G.-W. Kim, H. Choi, S. Park, S. A. Park, T. Park, *Energy Environ. Sci.* **2018**, *11*, 3238.

[233] D. Zheng, R. Peng, G. Wang, J. L. Logsdon, B. Wang, X. Hu, Y. Chen, V. P. Dravid, M. R. Wasielewski, J. Yu, W. Huang, Z. Ge, T. J. Marks, A. Facchetti, *Adv. Mater.* **2019**, *31*, 1.

[234] S. Ye, H. Rao, Z. Zhao, L. Zhang, H. Bao, W. Sun, Y. Li, F. Gu, J. Wang, Z. Liu, Z. Bian, C. Huang, *J. Am. Chem. Soc.* **2017**, *139*, 7504.

[235] M. E. Kayesh, K. Matsuishi, R. Kaneko, S. Kazaoui, J. J. Lee, T. Noda, A. Islam, *ACS Energy Lett.* **2019**, *4*, 278.

[236] T. Zhang, L. Xie, L. Chen, N. Guo, G. Li, Z. Tian, B. Mao, Y. Zhao, *Adv. Funct. Mater.* **2017**, *27*, 1603568.

[237] X. Zheng, Y. Deng, B. Chen, H. Wei, X. Xiao, Y. Fang, Y. Lin, Z. Yu, Y. Liu, Q. Wang, J. Huang, *Adv. Mater.* **2018**, *30*, 1803428.

[238] X. Zheng, B. Chen, J. Dai, Y. Fang, Y. Bai, Y. Lin, H. Wei, X. C. Zeng, J. Huang, *Nat. Energy* **2017**, *2*, 17102.

[239] J. Chen, J. Y. Seo, N. G. Park, *Adv. Energy Mater.* **2018**, *8*, 1702714.

[240] S. Yang, J. Dai, Z. Yu, Y. Shao, Y. Zhou, X. Xiao, X. C. Zeng, J. Huang, *J. Am. Chem. Soc.* **2019**, *141*, 5781.

[241] C. Battaglia, A. Cuevas, S. De Wolf, *Energy Environ. Sci.* **2016**, *9*, 1552.

[242] D. Koushik, W. J. H. Verhees, Y. Kuang, S. Veenstra, D. Zhang, M. A. Verheijen, M. Creatore, R. E. I. Schropp, *Energy Environ. Sci.* **2017**, *10*, 91.

[243] Q. Wang, Q. Dong, T. Li, A. Gruverman, J. Huang, *Adv. Mater.* **2016**, *28*, 6734.

[244] F. Wang, A. Shimazaki, F. Yang, K. Kanahashi, K. Matsuki, Y. Miyauchi, T. Takenobu, A. Wakamiya, Y. Murata, K. Matsuda, *J. Phys. Chem. C* **2017**, *121*, 1562.

[245] M. Li, X. Yan, Z. Kang, Y. Huan, Y. Li, R. Zhang, Y. Zhang, *ACS Appl. Mater. Interfaces* **2018**, *10*, 18787.

[246] B. Chaudhary, A. Kulkarni, A. K. Jena, M. Ikegami, Y. Udagawa, H. Kunugita, K. Ema, T. Miyasaka, *ChemSusChem* **2017**, *10*, 2473.

[247] D. Kim, H. J. Jung, I. J. Park, B. W. Larson, S. P. Dunfield, C. Xiao, J. Kim, J. Tong, P. Boonmongkolras, S. G. Ji, F. Zhang, S. R. Pae, M. Kim, S. B. Kang, V. Dravid, J. J. Berry, J. Y. Kim, K. Zhu, D. H. Kim, B. Shin, *Science (80-.)* **2020**, *368*, 155.

[248] T. Supasai, N. Rujisamphan, K. Ullrich, A. Chemseddine, T. Dittrich, *Appl. Phys. Lett.* **2013**, *103*, 183906.

[249] L. Wang, C. McCleese, A. Kovalsky, Y. Zhao, C. Burda, *J. Am. Chem. Soc.* **2014**, *136*, 12205.

[250] Q. Chen, H. Zhou, T.-B. Song, S. Luo, Z. Hong, H.-S. Duan, L. Dou, Y. Liu, Y. Yang, *Nano Lett.* **2014**, *14*, 4158.

[251] C. Roldán-Carmona, P. Gratia, I. Zimmermann, G. Grancini, P. Gao, M. Graetzel, M. K. Nazeeruddin, *Energy Environ. Sci.* **2015**, *8*, 3550.

[252] Y. C. Kim, N. J. Jeon, J. H. Noh, W. S. Yang, J. Seo, J. S. Yun, A. Ho-Baillie, S. Huang, M. A. Green, J. Seidel, T. K. Ahn, S. Il Seok, *Adv. Energy Mater.* **2016**, *6*, 1502104.

[253] T. J. Jacobsson, J. P. Correa-Baena, E. Halvani Anaraki, B. Philippe, S. D. Stranks, M. E. F. Bouduban, W. Tress, K. Schenk, J. Teuscher,

J. E. Moser, H. Rensmo, A. Hagfeldt, *J. Am. Chem. Soc.* **2016**, *138*, 10331.

[254] W. Ke, C. Xiao, C. Wang, B. Saparov, H. S. Duan, D. Zhao, Z. Xiao, P. Schulz, S. P. Harvey, W. Liao, W. Meng, Y. Yu, A. J. Cimaroli, C. S. Jiang, K. Zhu, M. Al-Jassim, G. Fang, D. B. Mitzi, Y. Yan, *Adv. Mater.* **2016**, *28*, 5214.

[255] J. W. Lee, S. G. Kim, S. H. Bae, D. K. Lee, O. Lin, Y. Yang, N. G. Park, *Nano Lett.* **2017**, *17*, 4270.

[256] H. Wang, Z. Wang, Z. Yang, Y. Xu, Y. Ding, L. Tan, C. Yi, Z. Zhang, K. Meng, G. Chen, Y. Zhao, Y. Luo, X. Zhang, A. Hagfeldt, J. Luo, *Adv. Mater.* **2020**, *32*, 2000865.

[257] Q. Jiang, Z. Chu, P. Wang, X. Yang, H. Liu, Y. Wang, Z. Yin, J. Wu, X. Zhang, J. You, *Adv. Mater.* **2017**, *29*, 1703852.

[258] T. A. Berhe, W.-N. Su, C.-H. Chen, C.-J. Pan, J.-H. Cheng, H.-M. Chen, M.-C. Tsai, L.-Y. Chen, A. A. Dubale, B.-J. Hwang, *Energy Environ. Sci.* **2016**, *9*, 323.

[259] J.-W. Lee, S.-G. Kim, S.-H. Bae, D.-K. Lee, O. Lin, Y. Yang, N.-G. Park, *Nano Lett.* **2017**, *17*, 4270.

[260] T. J. Jacobsson, J.-P. Correa-Baena, E. Halvani Anaraki, B. Philippe, S. D. Stranks, M. E. F. Bouduban, W. Tress, K. Schenk, J. Teuscher, J.-E. Moser, H. Rensmo, A. Hagfeldt, *J. Am. Chem. Soc.* **2016**, *138*, 10331.

[261] W. Ke, C. Xiao, C. Wang, B. Saparov, H. Duan, D. Zhao, Z. Xiao, P. Schulz, S. P. Harvey, W. Liao, W. Meng, Y. Yu, A. J. Cimaroli, C. Jiang, K. Zhu, M. Al-jassim, G. Fang, D. B. Mitzi, Y. Yan, *Adv. Mater.* **2016**, *28*, 5214.

[262] D. Kim, H. J. Jung, I. J. Park, B. W. Larson, S. P. Dunfield, C. Xiao, J. Kim, J. Tong, P. Boonmongkolras, S. G. Ji, F. Zhang, S. R. Pae, M. Kim, S. B. Kang, V. Dravid, J. J. Berry, J. Y. Kim, K. Zhu, D. H. Kim, B. Shin, *Science (80-.).* **2020**, *368*, 155.

[263] F. El-Mellouhi, E. T. Bentria, S. N. Rashkeev, S. Kais, F. H. Alharbi, *Sci. Rep.* **2016**, *6*, 30305.

[264] A. M. A. Leguy, Y. Hu, M. Campoy-Quiles, M. I. Alonso, O. J. Weber, P. Azarhoosh, M. Van Schilfgaarde, M. T. Weller, T. Bein, J. Nelson, P. Docampo, P. R. F. Barnes, *Chem. Mater.* **2015**, *27*, 3397.

[265] D. Bryant, N. Aristidou, S. Pont, I. Sanchez-Molina, T. Chotchunangatchaval, S. Wheeler, J. R. Durrant, S. A. Haque, *Energy Environ. Sci.* **2016**, *9*, 1655.

[266] R. Cheacharoen, N. J. Rolston, D. Harwood, K. A. Bush, R. H. Dauskardt, M. D. McGehee, *Energy Environ. Sci.* **2017**, *11*, 144.

[267] S. Emami, J. Martins, D. Ivanou, A. Mendes, *J. Mater. Chem. A* **2020**, *8*, 2654.

[268] S. Zhang, G. Han, *Prog. Energy* **2020**, *2*, 22002.

[269] N. Ahn, K. Kwak, M. S. Jang, H. Yoon, B. Y. Lee, J. K. Lee, P. V. Pikhitsa, J. Byun, M. Choi, *Nat. Commun.* **2016**, *7*, 13422.

[270] Q. Wang, B. Chen, Y. Liu, Y. Deng, Y. Bai, Q. Dong, J. Huang, *Energy Environ. Sci.* **2017**, *10*, 516.

[271] N. Aristidou, I. Sanchez-Molina, T. Chotchuangchutchaval, M. Brown, L. Martinez, T. Rath, S. A. Haque, *Angew. Chemie* **2015**, *127*, 8326.

[272] A. J. Pearson, G. E. Eperon, P. E. Hopkinson, S. N. Habisreutinger, J. T. W. Wang, H. J. Snaith, N. C. Greenham, *Adv. Energy Mater.* **2016**, *6*, 1600014.

[273] A. Farooq, M. R. Khan, T. Abzieher, A. Voigt, D. C. Lupascu, U. Lemmer, B. S. Richards, U. W. Paetzold, *ACS Appl. Energy Mater.* **2021**, *4*, 3083.

[274] Y. Lin, B. Chen, Y. Fang, J. Zhao, C. Bao, Z. Yu, Y. Deng, P. N. Rudd, Y. Yan, Y. Yuan, J. Huang, *Nat. Commun.* **2018**, *9*, 4981.

[275] M. Adil Afroz, N. Ghimire, K. M. Reza, B. Bahrami, R. S. Bobba, A. Gurung, A. H. Chowdhury, P. K. Iyer, Q. Qiao, *ACS Appl. Energy Mater.* **2020**, *3*, 2432.

[276] H. Choi, X. Liu, H. Il Kim, D. Kim, T. Park, S. Song, *Adv. Energy Mater.* **2021**, *11*, 2003829.

[277] Y. Li, J. Shi, J. Zheng, J. Bing, J. Yuan, Y. Cho, S. Tang, M. Zhang, Y. Yao, C. F. J. Lau, D. S. Lee, C. Liao, M. A. Green, S. Huang, W. Ma, A. W. Y. Ho-Baillie, *Adv. Sci.* **2020**, *7*, 1903368.

[278] F. Tan, H. Tan, M. I. Saidaminov, M. Wei, M. Liu, A. Mei, P. Li, B. Zhang, C. S. Tan, X. Gong, Y. Zhao, A. R. Kirmani, Z. Huang, J. Z. Fan, R. Quintero-Bermudez, J. Kim, Y. Zhao, O. Voznyy, Y. Gao, F. Zhang, L. J. Richter, Z. H. Lu, W. Zhang, E. H. Sargent, *Adv. Mater.* **2019**, *31*, 1807435.

[279] Q. Jiang, Y. Zhao, X. Zhang, X. Yang, Y. Chen, Z. Chu, Q. Ye, X. Li, Z. Yin, J. You, *Nat. Photonics* **2019**, *13*, 460.

[280] W.-Q. Wu, P. N. Rudd, Z. Ni, C. H. Van Brackle, H. Wei, Q. Wang, B. R. Ecker, Y. Gao, J. Huang, *J. Am. Chem. Soc.* **2020**, *142*, 3989.

[281] D. J. Kubicki, D. Prochowicz, A. Hofstetter, M. Saski, P. Yadav, D. Bi, N. Pellet, J. Lewiński, S. M. Zakeeruddin, M. Grätzel, L. Emsley, *J. Am. Chem. Soc.* **2018**, *140*, 3345.

[282] N. De Marco, H. Zhou, Q. Chen, P. Sun, Z. Liu, L. Meng, E.-P. Yao, Y. Liu, A. Schiffer, Y. Yang, *Nano Lett.* **2016**, *16*, 1009.

[283] G. Grancini, M. K. Nazeeruddin, *Nat. Rev. Mater.* **2019**, *4*, 4.

[284] H. Ren, S. Yu, L. Chao, Y. Xia, Y. Sun, S. Zuo, F. Li, T. Niu, Y. Yang, H. Ju, B. Li, H. Du, X. Gao, J. Zhang, J. Wang, L. Zhang, Y. Chen, W. Huang, *Nat. Photonics* **2020**, *14*, 154.

[285] T. Niu, J. Lu, X. Jia, Z. Xu, M.-C. Tang, D. Barrit, N. Yuan, J. Ding, X. Zhang, Y. Fan, T. Luo, Y. Zhang, D.-M. Smilgies, Z. Liu, A. Amassian, S. Jin, K. Zhao, S. Liu, *Nano Lett.* **2019**, *19*, 7181.

[286] A. H. Proppe, M. Wei, B. Chen, R. Quintero-Bermudez, S. O. Kelley, E. H. Sargent, *J. Am. Chem. Soc.* **2019**, *141*, 14180.

[287] S. H. Turren-Cruz, A. Hagfeldt, M. Saliba, *Science (80-.).* **2018**, *362*, 449.

[288] J. W. Lee, S. H. Bae, Y. T. Hsieh, N. De Marco, M. Wang, P. Sun, Y. Yang, *Chem* **2017**, *3*, 290.

[289] A. Y. Alsalloum, B. Turedi, X. Zheng, S. Mitra, A. A. Zhumekenov, K. J. Lee, P. Maity, I. Gereige, A. AlSaggaf, I. S. Roqan, O. F. Mohammed, O. M. Bakr, *ACS Energy Lett.* **2020**, *5*, 657.

[290] S. Shahbazi, M.-Y. Li, A. Fathi, E. W.-G. Diau, *ACS Energy Lett.* **2020**, *5*, 2508.

[291] M. Hadadian, J. P. Correa-Baena, E. K. Goharshadi, A. Ummadisingu, J. Y. Seo, J. Luo, S. Gholipour, S. M. Zakeeruddin, M. Saliba, A. Abate, M. Grätzel, A. Hagfeldt, *Adv. Mater.* **2016**, *28*, 8681.

[292] H. Li, L. Tao, F. Huang, Q. Sun, X. Zhao, J. Han, Y. Shen, M. Wang, *ACS Appl. Mater. Interfaces* **2017**, *9*, 38967.

[293] H. Zhang, Y. Wu, C. Shen, E. Li, C. Yan, W. Zhang, H. Tian, L. Han, W. H. Zhu, *Adv. Energy Mater.* **2019**, *9*, 1803573.

[294] Z. Wang, Q. Lin, F. P. Chmiel, N. Sakai, L. M. Herz, H. J. Snaith, *Nat. Energy* **2017**, *2*, 17135.

[295] Y. Lin, Y. Bai, Y. Fang, Z. Chen, S. Yang, X. Zheng, S. Tang, Y. Liu, J. Zhao, J. Huang, *J. Phys. Chem. Lett.* **2018**, *9*, 654.

[296] D. Bi, P. Gao, R. Scopelliti, E. Oveisi, J. Luo, M. Grätzel, A. Hagfeldt, M. K. Nazeeruddin, *Adv. Mater.* **2016**, *28*, 2910.

[297] T. Zhou, H. Lai, T. Liu, D. Lu, X. Wan, X. Zhang, Y. Liu, Y. Chen, *Adv. Mater.* **2019**, *31*, 1901242.

[298] J. Cho, S. Banerjee, *Chem. Mater.* **2018**, *30*, 6144.

[299] Y. Hu, J. Schlipf, M. Wussler, M. L. Petrus, W. Jaegermann, T. Bein, P. Müller-Buschbaum, P. Docampo, *ACS Nano* **2016**, *10*, 5999.

[300] K. Lee, J. Kim, H. Yu, J. W. Lee, C. M. Yoon, S. K. Kim, J. Jang, *J. Mater. Chem. A* **2018**, *6*, 24560.

[301] C. Chen, Z. Song, C. Xiao, R. A. Awni, C. Yao, N. Shrestha, C. Li, S. S. Bista, Y. Zhang, L. Chen, R. J. Ellingson, C.-S. Jiang, M. M. Al-Jassim, G. Fang, Y. Yan, *ACS Energy Lett.* **2020**, *5*, 2560.

[302] X. Jiang, J. Zhang, S. Ahmad, D. Tu, X. Liu, G. Jia, X. Guo, C. Li, *Nano Energy* **2020**, *75*, 104892.

[303] E. H. Jung, N. J. Jeon, E. Y. Park, C. S. Moon, T. J. Shin, T. Y. Yang, J. H. Noh, J. Seo, *Nature* **2019**, *567*, 511.

[304] F. Ansari, E. Shirzadi, M. Salavati-Niasari, T. LaGrange, K. Nonomura, J.-H. Yum, K. Sivula, S. M. Zakeeruddin, M. K. Nazeeruddin, M. Grätzel, P. J. Dyson, A. Hagfeldt, *J. Am. Chem. Soc.* **2020**, *142*, 11428.

[305] Z. Liu, K. Meng, X. Wang, Z. Qiao, Q. Xu, S. Li, L. Cheng, Z. Li, G. Chen, *Nano Lett.* **2020**, *20*, 1296.

[306] T. Zhao, C. C. Chueh, Q. Chen, A. Rajagopal, A. K. Y. Jen, *ACS Energy Lett.* **2016**, *1*, 757.

[307] K. T. Cho, Y. Zhang, S. Orlandi, M. Cavazzini, I. Zimmermann, A. Lesch, N. Tabet, G. Pozzi, G. Grancini, M. K. Nazeeruddin, *Nano Lett.* **2018**, *18*, 5467.

[308] L. Gao, I. Spanopoulos, W. Ke, S. Huang, I. Hadar, L. Chen, X. Li, G. Yang, M. G. Kanatzidis, *ACS Energy Lett.* **2019**, *4*, 1763.

[309] J. J. Yoo, S. Wieghold, M. C. Sponseller, M. R. Chua, S. N. Bertram, N. T. P. Hartono, J. S. Tresback, E. C. Hansen, J.-P. Correa-Baena, V. Bulović, T. Buonassisi, S. S. Shin, M. G. Bawendi, *Energy Environ. Sci.* **2019**, *12*, 2192.

[310] Y. Liu, S. Akin, L. Pan, R. Uchida, N. Arora, J. V. Milić, A. Hinderhofer, F. Schreiber, A. R. Uhl, S. M. Zakeeruddin, A. Hagfeldt, M. Ibrahim Dar, M. Grätzel, *Sci. Adv.* **2019**, *5*, 2543.

[311] Q. Zhou, L. Liang, J. Hu, B. Cao, L. Yang, T. Wu, X. Li, B. Zhang, P. Gao, *Adv. Energy Mater.* **2019**, *9*, 1802595.

[312] H. Kim, M. Pei, Y. Lee, A. A. Sutanto, S. Paek, V. I. E. Queloz, A. J. Huckaba, K. T. Cho, H. J. Yun, H. Yang, M. K. Nazeeruddin, *Adv. Funct. Mater.* **2020**, *30*, 1910620.

Mahdi Malekshahi Byranvand is a researcher at the Forschungszentrum Jülich and Institute for Photovoltaics (IPV) at the University of Stuttgart. Previously, he worked on different parts of perovskite solar cells during his postdoctoral fellowships at Karlsruhe Institute of Technology (KIT), Pohang University of Science and Technology (POSTECH), and Sharif University of Technology. He received his Ph.D. degree in inorganic chemistry from the University of Tehran in 2015, working on photon management in dye-sensitized solar cells. His research interests are currently focused on passivation techniques of perovskite films and perovskite–silicon tandem solar cells in the Prof. Michael Saliba's group.

Michael Saliba is the director of the Institute for Photovoltaics (IPV) at the University of Stuttgart with a dual appointment as the Helmholtz Young Investigator at the Forschungszentrum Jülich, Germany. His research focuses on a deeper fundamental understanding and improvement of the optoelectronic properties of emerging photovoltaic materials with an emphasis on perovskites for a sustainable energy future. Previously, he held positions at TU Darmstadt, University of Fribourg, and EPFL. He obtained his Ph.D. degree from Oxford University. He is a member of the National Young Academy of Germany and the Global Young Academy.